Marchenko
Basic-PlaneWave-MME-3D-MD

Jan Thorbecke, Joeri Brackenhof, Lele Zhang, Gio

April 11, 2024

There are diferent ways to get the source code for the Marche
a tagged snapshot from the GitHub repository. These tagged
The latest tagged version that can be cloned from the reposi

and contains the full package. To get a version with the late
of the most current version

The package extracts into ,the directory with the following sub-director

- FFTlib: basic library for FFT's includes a wrapper for MK
- MDD: Multiple Dimensional Deconvolution $Ax = b$ problems $x = \frac{bA^*}{AA^*}$. solve difere
- corrvir: seismic interferometry (correlation) for pass
- doc: documentation related to the code.
- extrap: recursive wavefeld depth extrapolation, includ
- extrap3d: 3D version of the above.
- fdacrtmc: RTM based on fdelmodc.
- fdelmodc: fnite diference modeling (visco)-acoustic, a
- fdelmodc3D: 3D version for acoustic media.
- fdemmodc: EM fnite diference code.
- marchenko: basic, plane-wave and MME implementations.
- marchenko3D: 3D version of the basic algorithm.
- raytime: eikonal solver.
- raytime3D: 3D eikonal solver.
- utils: basic (pre-) processing and additional programs f
- zfp: ZFP data compression library from Peter Lindstrom.

Besides the Marchenko algorithms the OpenSource package c
manual we will only describe the diferent Marchenko implemen
.

The fle in the ROOT directory contains guidelines how to
briefy explains the diferent code packages and how to r
papers. Section Besides this manual contains a brief (one-sentence) ex
Marchenko source code fles in the source tree of this packag
The code is used by many diferent people and new options are b

1. To compile and link the code you frst have to set the ROOT
which can be found in the directory where you have found th and instructions.

2. Check the compiler and CFLAGS options in the fle Make_inc
are using. The default options are set for a the GNU C-com
g++ compiler is only needed to compile the MDD code. The c
been compiled and tested with several versions of GNU, AM

3. If the compiler options are set in the Make_include fle yo

and the Makefle will execute the commands to compile and
directories.

The compiled FFT and ZFP libraries will be placed in the executables
directory and the include fles of the FFT and ZFP libraries i
To use the executables don't forget to include the pathname

On Linux systems using the bash shell you can put the
setting in , to set it every time you login.
Other useful make commands are:

- : removes all object fles, but leaves libraries and
- : removes also object fles, libraries and execut

The examples and demo scripts make use of SU programs o
make sure that SU is compiled without XDR (-DSUXDR in $CWPROOT/Makefile.co
must be set in compiling SU. The SU output fles of fdelmodc
When the XDR fag is set in SU you have to convert the output fl
in the utils directory: basop, fconv, extendmodel, makemod
SU programs.

If the compilation has fnished without errors and produced
run one of the demo programs by running

in the directory. This demo directory contains many script
diferent possibilities of the modeling program.

- To reproduce the Figures shown in the Geophysics manusc
(Thorbecke and Draganov, 2011) the scripts in Fi
uresPaper directory can be used. Please read the README i
instructions and guidelines.

To clean-up all the produced output fles in the directory
you can run the script in those directories.
An extensive manual of fdelmodc can be found in

If the compilation has finished without errors and produced a
can run one of the demo programs by running a set of scripts t
of the directories or .

- To reproduce the Figures shown in the Geophysics paper
  the scripts in directory can be used. The READ
  directory gives more instructions and guidelines.
- To reproduce the Figures shown in the Scientific Reports
  the scripts in marchenko/demo/Sc
  directory can be used. The README in this directory gives
- To reproduce the Figures shown in the Geophysics paper
  the scripts in directory can be use
  The README_PRIMARIES in this directory gives more instru
- To reproduce the Figures shown in the Geophysics paper
  the scripts in directory can be used. The
  in this directory gives more instructions and guidelines
- To reproduce the Figures shown in the IEEE (under review) p
  the scripts in
  directory can be used. The README in this directory gives

A brief manual about the MME program 'marchenko_primaries'

- To reproduce the Figures shown in the paper the scripts in
  directory can be used. The README in this directory gives

0 DOI reference of this software release
  https://zenodo.org/badge/latestdoi/23060862

1. If the Finite Difference code has helped you in your resear
   your publications:

   Jan Thorbecke and Deyan Draganov, 2011, Geophysics, Vol
   H1–H18, doi: 10.1190/GEO2010-0039.1 Download: pdf

2. If the Marchenko code has helped you in your research pleas

   Jan Thorbecke, Evert Slob, Joeri Brackenhof, Joost van
   Geophysics, Vol. 82, no. 6 (November-December); p. WB29–
   Download: pdf

3. If you used the code to construct homogeneous Green's fun
   related publications:

   Brackenhof, J., Thorbecke, J., and Wapenaar, K., 2019, J
   Earth, Vol. 124, 11,802-11,821. pdf-file

   Wapenaar, K., Brackenhof, J., Thorbecke, J., van der Neut
   Scientific Reports, Vol. 8, 2497. Download: pdf

4 When you are using the marchenko_primaries algorithm dev
the following papers:

Lele Zhang and Evert Slob 2019, Geophysics, Vol. 84, no.
10.1190/GEO2018-0548.1 Download: pdf

Jan Thorbecke, Lele Zhang, Kees Wapenaar and Evert Slob
(March-April); p. xxxx, doi: xxxx Download: pdf

5 When you are using the plane wave versions of marchenko
developed by Giovanni Meles please refer to the following

Meles, G.A., K. Wapenaar, and J. Thorbecke, 2018, Geophy
(1), p. 508–519.

6. If you use the fdacrtmc code of Max Holicki please refer t

Holicki, M., Drijkoningen, G., and Wapenaar, K., 2019, A
decomposition: Geophysical Prospecting, Vol. 67, 32-51 pdf

7. If you use the vmar code of Johno van IJsseldijk please re

Van IJsseldijk, J., van der Neut, J., Thorbecke, J., and W
(2), R135-R143 Download: pdf

-7- A reference to the extrapolation and migration progr

Jan Thorbecke, Kees Wapenaar, Gerd Swinnen, 2004, Geophy
pdf

In this section we describe in detail the implementational as
Marchenko method based on focusing functions. Although the
the treatment of amplitudes, and the initialisation steps o
The input of the method is a reflection response without free
source wavelet. The output of an SRME scheme can (in princip
(smooth) background model is needed to calculate an initia
The Numerical Examples section demonstrates the use of the a
with the Marchenko technique.

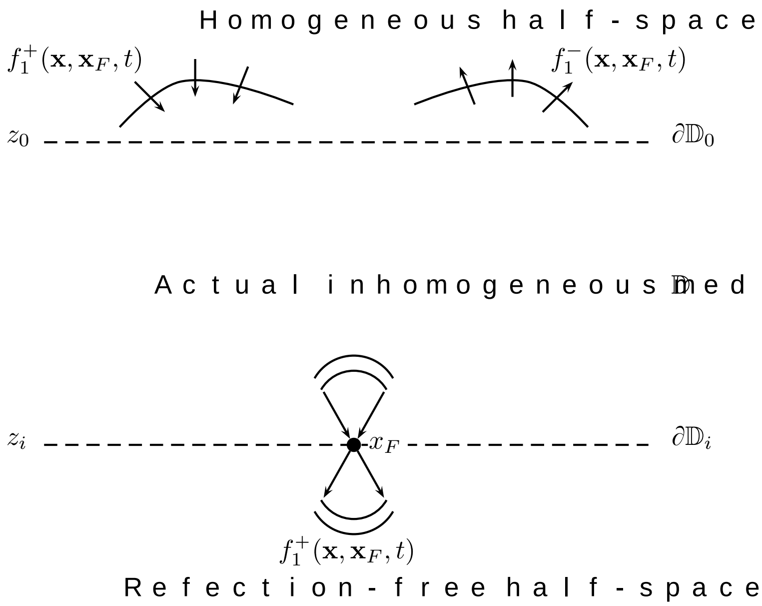

Figure 1: Downgoing and upgoing components of the f_1 focusing function for the 2D wave equation in the truncated medium.

The Marchenko method is briefly introduced here aiming at an
understand the algorithm. The references mentioned in the
the derivation of this method. In an imaginary medium truncated at z_i a focusing function f_1. The truncated medium is identical to the actual medium above z_i and reflection-free below this depth level (Figure 1). The actual and truncated media are reflection-free above the surface $\partial\mathbb{D}_0$. We introduce up- and downgoing parts of the focusing function f_1 (Slob et al., 2014).

$$f_1(\mathbf{x}, \mathbf{x}_F, t) = f_1^+(\mathbf{x}, \mathbf{x}_F, t) + f_1^-(\mathbf{x}, \mathbf{x}_F, t),$$

where $x_F = (x_F, z_i)$ is a focal position on $\partial\mathbb{D}_i$, $\mathbf{x}$ can be a boundary point and t in the me
is time (see Figure 1). In our notation the first argument represents th
argument stands for the focal point. The downgoing part f_1^+ focuses at o
point $\mathbf{x}_F$, and the superscript $-$ in f_1^- represents an upgoing field. Below boundary $\partial\mathbb{D}_i$, f_1^+ continues
as a diverging downgoing field into the reflection-free half-
The $f_1^\pm$ focusing functions are defined to relate the up- and dow
medium with the reflection response at the surface (Wapenaar et al., 2014):

$$G^+(\mathbf{x}_F, \mathbf{x}_R, t) = -\int_{\partial\mathbb{D}_0} \int_{t'=-\infty}^{t} R(\mathbf{x}_R, \mathbf{x}, t-t') f_1^-(\mathbf{x}, \mathbf{x}_F, -t') \mathrm{d}t' \mathrm{d}\mathbf{x} + f_1^+(\mathbf{x}_R, \mathbf{x}_F, -t), \tag{1}$$

$$G^-(\mathbf{x}_F, \mathbf{x}_R, t) = \int_{\partial\mathbb{D}_0} \int_{t'=-\infty}^{t} R(\mathbf{x}_R, \mathbf{x}, t-t') f_1^+(\mathbf{x}, \mathbf{x}_F, t') \mathrm{d}t' \mathrm{d}\mathbf{x} - f_1^-(\mathbf{x}_R, \mathbf{x}_F, t). \tag{2}$$

$R(\mathbf{x}_R,\mathbf{x},t)$ is the reflection response after surface multiple elim the wavelet. The first argument of R is the receiver location, the se location, and the last argument time. R is a measured pressure wavefield at $\mathbf{x}_R$ of a vertical force source F_z, or, via reciprocity, the particle velocity V_z of a point source of volume injection at $\mathbf{x}_R$ (Wapenaar et al., 2014a). This reflection response is related t

$$\frac{\partial R(\mathbf{x}_R,\mathbf{x},t)}{\partial t} = \frac{2}{\rho(\mathbf{x})}\frac{\partial G^s(\mathbf{x}_R,\mathbf{x},t)}{\partial z} \tag{3}$$

with G^s the Green's function of the scattered field only (it does integration boundary $t'=0$ for the time integral in equations (1) and (2) accounts for the causal reflection response $R(\mathbf{x}_R,\mathbf{x},t-t')$. Summing equations (1) and (2) and using source-receiver re the Green's function as (Wapenaar et al., 2017a)

$$G(\mathbf{x}_R,\mathbf{x}_F,t) = \int_{\partial\mathbb{D}_0}\int_{t'=-\infty}^{t} R(\mathbf{x}_R,\mathbf{x},t-t') f_2(\mathbf{x}_F,\mathbf{x},t')\mathrm{d}t'\mathrm{d}\mathbf{x} + f_2(\mathbf{x}_F,\mathbf{x}_R,-t), \tag{4}$$

The Green's function $G(\mathbf{x}_R,\mathbf{x}_F,t)$ represents the response to a virtual point rate at $\mathbf{x}_F$ and pressure receiver at $\mathbf{x}_R$. The focusing function f_2 is defined as

$$f_2(\mathbf{x}_F,\mathbf{x},t) = f_1^+(\mathbf{x},\mathbf{x}_F,t) - f_1^-(\mathbf{x},\mathbf{x}_F,-t). \tag{5}$$

Wapenaar et al. (2014a) introduced $f_2(\mathbf{x}_F,\mathbf{x},t)$ as a focusing function, which has its focus at $\partial\mathbb{D}_0$. Here we merely use f_2 as a compact notation for the combination of the f_1^+ and f_1^-, as defined in equation (5). Note that the time-reversed f_1^- is not upgoing but acts as a downgoing function. Hence, $f_2(\mathbf{x}_F,\mathbf{x},t)$ is a downgoing focusing function which is emitted from the surface at $\mathbf{x}_F$ ... receiver The argument change between equation (5) and $\mathbf{x}_F$ in the left- and right-hand s $f_1^{\pm}$ follows from the same logic in the other arguments a (Wapenaar et al., 2014a). In the Numerical Examples section, f_2 can be back-propagated into the focus $\mathbf{x}_F$ as in Wapenaar et al. (2013) (reciprocal) $f_2(\mathbf{x}_F,\mathbf{x},t)$ and the downgoing wave $p^+(\mathbf{x},\mathbf{x}_F,t)$ is given. Together with p^-, the upgoing reflecti at $\mathbf{x}$ from the focal point $\mathbf{x}_F$. The sum of p^+ and p^- gives also the Green's function (4). The $p^{\pm}$ functions are just a different notation of the Marchenko r Green's functions in a convenient way. The $p^{\pm}$ are therefore used in the compute the Green's function. From an educational point of v understood by using the focusing functions only and we will The above equations, on which the following implementation Other papers derive similar equations (Wapenaar et al., 2013; Slob et al., 2014; Broggini et al., 2015; van der Neut et al., 2015b). The relationship between pressure- and fu is explained in Wapenaar et al. (2014a).

The Marchenko algorithm estimates $f_1^+(\mathbf{x},\mathbf{x}_F,t)$ and $f_1^-(\mathbf{x},\mathbf{x}_F,t)$. However, equations (1) and (2) are by themselves insufficient to determine the unknowns, but onl We can eliminate two unknowns by exploiting the fact that foc different causality properties in the time-space domain. Ba no energy arrives before $t_d(\mathbf{x}_R,\mathbf{x}_F)$, therefore the Green's function $G(\mathbf{x}_R,\mathbf{x}_F,t<t_d(\mathbf{x}_R,\mathbf{x}_F))$ is zero. This also holds for the up- and downgoing Green's fu

$$0 = -\int_{\partial\mathbb{D}_0}\int_{t'=-\infty}^{t} R(\mathbf{x}_R,\mathbf{x},t-t') f_1^-(\mathbf{x},\mathbf{x}_F,-t')\mathrm{d}t'\mathrm{d}\mathbf{x} + f_1^+(\mathbf{x}_R,\mathbf{x}_F,-t), \tag{6}$$

$$0 = \int_{\partial\mathbb{D}_0}\int_{t'=-\infty}^{t} R(\mathbf{x}_R,\mathbf{x},t-t') f_1^+(\mathbf{x},\mathbf{x}_F,t')\mathrm{d}t'\mathrm{d}\mathbf{x} - f_1^-(\mathbf{x}_R,\mathbf{x}_F,t), \tag{7}$$

where $t<t_d(\mathbf{x}_R,\mathbf{x}_F)$ in both equations above.

The combination of equations (6) and (7) is known as the Marchenko equation. The basis of the iterative scheme, which solves f_1^+ and f_1^-. Wapenaar et al. (2014a) using fun the relation

$$f_1^+(\mathbf{x},\mathbf{x}_F,t) = T^{inv}(\mathbf{x}_F,\mathbf{x},t), \tag{8}$$

is used to derive an initial estimate f_1^+ that can start the inversion scheme (8).
$T^{inv}(\mathbf{x}_F,\mathbf{x},t)$ is the inverse of the transmission response of the t
the actual medium between $\partial\mathbb{D}_0$ and $\partial\mathbb{D}_i$, for a source at $\mathbf{x}$ (at $\partial\mathbb{D}_0$) and a receiver at $\partial\mathbb{D}_i$. It is assumed that this inverse transmission T^{inv} can be composed as a direct wave follo
coda (Van der Neut et al., 2015b).

$$f_1^+(\mathbf{x},\mathbf{x}_F,t) = T_d^{inv}(\mathbf{x}_F,\mathbf{x},t) + M^+(\mathbf{x},\mathbf{x}_F,t), \tag{9}$$

where M^+ is the unknown scattering coda and T_d^{inv} the direct arrival of the inverse tr
In equation (9) the inverse of the direct arrival of the transmissio
take the time-reversal of the direct arrival of the Green's $G_d(\mathbf{x},\mathbf{x}_F,-t)$

$$f_1^+(\mathbf{x},\mathbf{x}_F,t) \approx G_d(\mathbf{x},\mathbf{x}_F,-t) + M^+(\mathbf{x},\mathbf{x}_F,t). \tag{10}$$

We thereby introduce an overall scaling error and an ofset t
to transmission losses in $G_d(\mathbf{x},\mathbf{x}_F,-t)$, the time-reversed direct ar
transmission response to a subsurface focal point $\mathbf{x}_F$ can for example be computed fr
macromodel. As mentioned before, $G_d(\mathbf{x},\mathbf{x}_F,t)$ is the direct arrival at t_d, hence $G_d(\mathbf{x},\mathbf{x}_F,t)$ is zero before $t<t_d$. The multiple scattering coda $M^+(\mathbf{x},\mathbf{x}_F,t)$ follows after the first arrival of f_1^+, for $t \leqslant -t_d$. It can also be shown that $t \geqslant +t_d$ (Slob et al., 2014) zero for
Equations (6) and (7) are only valid for $t < t_d$. We therefore define a time-window fu

$$\theta(\mathbf{x}_R,\mathbf{x}_F,t) = \begin{cases} 1 & t < t_d^\varepsilon \\ \frac{1}{2} & t = t_d^\varepsilon \\ 0 & t > t_d^\varepsilon \end{cases}. \tag{11}$$

where t_d^ε is the time of the direct arrival t_d from $\mathbf{x}_F$ to $\mathbf{x}_R$ minus a small positive constant ε to exclude the wavelet in G_d. For example a time-window th
times $t < -t_d^\varepsilon$ to zero and applied to equation (10) mutes $G_d(-t)$, but leaves M^+ intact. In the following we will use the short-hand θ_t for $\theta(\mathbf{x}_R,\mathbf{x}_F,t)$ and the truncated Marchenko pr
is an input parameter, see Appendix A for all input parameters)
tapering in this mute-window to suppress high frequency art
It is further assumed that it is possible to get an estimate G_d of the transmission response. Given the reflection response $R(\mathbf{x}_R,\mathbf{x},t)$ and the direct arrival $G_d(\mathbf{x},\mathbf{x}_F,t)$ from the focal point, the Marchenko algorithm solves for $M^+(\mathbf{x},\mathbf{x}_F,t)$, the coda of $f_1^+(\mathbf{x},\mathbf{x}_F,t)$ and the scattering co
$f_1^-(\mathbf{x},\mathbf{x}_F,t)$.
The iterative solution of the Marchenko equations can now be
with the following initialization of M^+:

$$M_0^+(\mathbf{x}_R,\mathbf{x}_F,t) = 0. \tag{12}$$

The subscript 0 in M_0^+ defines the iteration number. By substituting (10) and (12) into equation (7) we arrive at the initialisation of f_1^-:

$$f_{1,0}^-(\mathbf{x}_R,\mathbf{x}_F,t) = \theta_t \int_{\partial\mathbb{D}_0} \int_{t'=-\infty}^{t} R(\mathbf{x}_R,\mathbf{x},t-t') G_d(\mathbf{x},\mathbf{x}_F,-t') \mathrm{d}t' \mathrm{d}\mathbf{x}. \tag{13}$$

Equation (13) includes the previously defined θ_t. Equations (10) and (6) are now both a function of f_1^+. By combining these equations the (10) is only M^+. The remain
iterative update of M^+ for step $k \geqslant 1$ is given by

$$M_k^+(\mathbf{x}_R,\mathbf{x}_F,-t) = \theta_t \int_{\partial\mathbb{D}_0} \int_{t'=-\infty}^{t} R(\mathbf{x}_R,\mathbf{x},t-t') f_{1,k-1}^-(\mathbf{x},\mathbf{x}_F,-t') \mathrm{d}t' \mathrm{d}\mathbf{x}. \tag{14}$$

Following the assumption in equation (10), that $f_{1,k}^+$ is a direct wavefield plus sca
coda, the update of $f_{1,k}^+$ at step k is given by

$$f_{1,k}^+(\mathbf{x}_R,\mathbf{x}_F,t) = G_d(\mathbf{x}_R,\mathbf{x}_F,-t) + M_k^+(\mathbf{x}_R,\mathbf{x}_F,t). \tag{15}$$

Using equation (7) and the expression for f_1^+ in equation (15), the update of f_1^- at step k is given by

$$f^-_{1,k}(\mathbf{x}_R,\mathbf{x}_F,t) = f^-_{1,0}(\mathbf{x}_R,\mathbf{x}_F,t) + \theta_t \int_{\partial\mathbb{D}_0}\int_{t'=-\infty}^{t} R(\mathbf{x}_R,\mathbf{x},t-t')M^+_k(\mathbf{x},\mathbf{x}_F,t')\mathrm{d}t'\mathrm{d}\mathbf{x}. \quad (16)$$

This completes the definition of the iterative Marchenko sche
are discussed in detail and illustrated with simple numeric

To compute focusing functions f_1 with the Marchenko method two ing

- Reflection data without free-surface multiples $R(\mathbf{x}_R, \mathbf{x}, t)$, ghosts a with sources $\mathbf{x}$ and receivers $\mathbf{x}_R$ over the same surface $\partial\mathbb{D}_0$, and a small enough $\mathbf{x}_R$ sampling fo to avoid spatial aliasing.

- An estimate of the direct arrival between $\mathbf{x}_R$ and the focal point $\mathbf{x}_F$: $G_d(\mathbf{x}_R, \mathbf{x}_F, t)$, and derived from it the direct arrival time $t_d(\mathbf{x}_R, \mathbf{x}_F, t)$. Note that t_d can also be computed by another method, for example an eik

Given these two components the iterative method can be initi method can start.

The initialisation of the method is given by equations (12) and (13). The time-windowed expression $f^-_{1,0}(\mathbf{x}_R, \mathbf{x}_F, t)$ in equation (13) is renamed to:

$$-N_0(\mathbf{x}_R, \mathbf{x}_F, -t) = \theta_t \int_{\partial\mathbb{D}_0} \int_{t'} R(\mathbf{x}_R, \mathbf{x}, t-t') G_d(\mathbf{x}, \mathbf{x}_F, -t') \mathrm{d}t' \mathrm{d}\mathbf{x}. \tag{17}$$

At each iteration, the spatial integration and temporal convolution with R is used to define new focus N_i (as suggested in Wapenaar et al. (2014b)). The N_i terms are used to update the estimates of f^+_1 and f^-_1. Although the N_i terms are strictly not needed to describe the method, they possible to the actual implementation.
For computational efficiency, the temporal convolution with R is implemented in the Fourier spatial integration is carried out by summing the resulting receiver gather. The introduced time-window θ_t zero-window $t < t_d^{\epsilon}$ (17). Applying the mute-window is therefore a crucial and mar without it the method would be incorrect.
Given these initialisations the first step, in equations (14) and (15), can be computed. This first step, $k = 1$, involves two integration-convolutions with R of f^+_1 and f^-_1:

$$\begin{aligned}
M^+_1(\mathbf{x}_R, \mathbf{x}_F, -t) &= \theta_t \int_{\partial\mathbb{D}_0} \int_{t'} R(\mathbf{x}_R, \mathbf{x}, t-t') f^-_{1,0}(\mathbf{x}, \mathbf{x}_F, -t') \mathrm{d}t' \mathrm{d}\mathbf{x} && (18)\\
&= -\theta_t \int_{\partial\mathbb{D}_0} \int_{t'} R(\mathbf{x}_R, \mathbf{x}, t-t') N_0(\mathbf{x}, \mathbf{x}_F, t') \mathrm{d}t' \mathrm{d}\mathbf{x}\\
&= N_1(\mathbf{x}_R, \mathbf{x}_F, -t),\\
f^+_{1,1}(\mathbf{x}_R, \mathbf{x}_F, t) &= G_d(\mathbf{x}_R, \mathbf{x}_F, -t) + M^+_1(\mathbf{x}_R, \mathbf{x}_F, t)\\
&= G_d(\mathbf{x}_R, \mathbf{x}_F, -t) + N_1(\mathbf{x}_F, \mathbf{x}_R, t), && (19)\\
f^-_{1,1}(\mathbf{x}_R, \mathbf{x}_F, t) &= f^-_{1,0}(\mathbf{x}_R, \mathbf{x}_F, t) + \theta_t \int_{\partial\mathbb{D}_0} \int_{t'} R(\mathbf{x}_R, \mathbf{x}, t-t') M^+_1(\mathbf{x}, \mathbf{x}_F, t') \mathrm{d}t' \mathrm{d}\mathbf{x}\\
&= -N_0(\mathbf{x}_R, \mathbf{x}_F, -t) + \theta_t \int_{\partial\mathbb{D}_0} \int_{t'} R(\mathbf{x}_R, \mathbf{x}, t-t') N_1(\mathbf{x}, \mathbf{x}_F, t') \mathrm{d}t' \mathrm{d}\mathbf{x},\\
&= -N_0(\mathbf{x}_R, \mathbf{x}_F, -t) - N_2(\mathbf{x}_R, \mathbf{x}_F, -t), && (20)\\
f_{2,1}(\mathbf{x}_F, \mathbf{x}_R, t) &= G_d(\mathbf{x}_R, \mathbf{x}_F, -t) + N_0(\mathbf{x}_R, \mathbf{x}_F, t) + N_1(\mathbf{x}_R, \mathbf{x}_F, t) + N_2(\mathbf{x}_R, \mathbf{x}_F, t). && (21)
\end{aligned}$$

The first integration-convolution with R in equation (18) is used to update f^+_1, as shown in equation (19). The second integration-convolution (20) updates f^-_1. The update of f_2, introduced in equation (5), includes the results of all R integration-convolutio

The next step ($k=2$) results in the following updates:

$$\begin{aligned}
M_2^+(\mathbf{x}_R,\mathbf{x}_F,-t) &= \theta_t \int_{\partial\mathbb{D}_0}\int_{t'} R(\mathbf{x}_R,\mathbf{x},t-t')f_{1,1}^-(\mathbf{x},\mathbf{x}_F,-t')\mathrm{d}t'\mathrm{d}\mathbf{x} && (22)\\
&= -\theta_t \int_{\partial\mathbb{D}_0}\int_{t'} R(\mathbf{x}_R,\mathbf{x},t-t')\{N_0(\mathbf{x},\mathbf{x}_F,t)+N_2(\mathbf{x},\mathbf{x}_F,t)\}\mathrm{d}t'\mathrm{d}\mathbf{x}\\
&= N_1(\mathbf{x}_R,\mathbf{x}_F,-t)+N_3(\mathbf{x}_R,\mathbf{x}_F,-t),\\
f_{1,2}^+(\mathbf{x}_R,\mathbf{x}_F,t) &= G_d(\mathbf{x}_R,\mathbf{x}_F,-t)+M_2^+(\mathbf{x}_R,\mathbf{x}_F,t)\\
&= G_d(\mathbf{x}_R,\mathbf{x}_F,-t)+N_1(\mathbf{x}_R,\mathbf{x}_F,t)+N_3(\mathbf{x}_R,\mathbf{x}_F,t), && (23)\\
f_{1,2}^-(\mathbf{x}_R,\mathbf{x}_F,t) &= f_{1,0}^-(\mathbf{x}_R,\mathbf{x}_F,t)+\theta_t \int_{\partial\mathbb{D}_0}\int_{t'} R(\mathbf{x}_R,\mathbf{x},t-t')M_2^+(\mathbf{x},\mathbf{x}_F,t')\mathrm{d}t'\mathrm{d}\mathbf{x}\\
&= -N_0(\mathbf{x}_R,\mathbf{x}_F,-t)+\theta_t \int_{\partial\mathbb{D}_0}\int_{t'} R(\mathbf{x}_R,\mathbf{x},t-t')\{N_1(\mathbf{x},\mathbf{x}_F,t)+N_3(\mathbf{x},\mathbf{x}_F,t)\}\mathrm{d}t'\mathrm{d}\mathbf{x}\\
&= -N_0(\mathbf{x}_R,\mathbf{x}_F,-t)-N_2(\mathbf{x}_R,\mathbf{x}_F,-t)-N_4(\mathbf{x}_R,\mathbf{x}_F,-t), && (24)\\
f_{2,2}(\mathbf{x}_F,\mathbf{x}_R,t) &= G_d(\mathbf{x}_R,\mathbf{x}_F,-t)+N_0(\mathbf{x}_R,\mathbf{x}_F,t)+N_1(\mathbf{x}_R,\mathbf{x}_F,t)+\\
&\quad N_2(\mathbf{x}_R,\mathbf{x}_F,t)+N_3(\mathbf{x}_R,\mathbf{x}_F,t)+N_4(\mathbf{x}_R,\mathbf{x}_F,t). && (25)
\end{aligned}$$

From these updates it becomes clear that in equation (23) for f_1^+, G_d and the odd N_i terms of f_2 are used and in equation (24) for f_1^- the even N_i terms of f_2 are used. The function in equation (25) is built up from G_d and both the even and odd N_i.

In the implementation the N_i terms are computed by

$$N_{-1}(\mathbf{x}_R,\mathbf{x}_F,-t) = G_d(\mathbf{x},\mathbf{x}_F,-t'), \tag{26}$$

$$N_i(\mathbf{x}_R,\mathbf{x}_F,-t) = -\theta_t \int_{\partial\mathbb{D}_0}\int_{t'} R(\mathbf{x}_R,\mathbf{x},t-t')N_{i-1}(\mathbf{x},\mathbf{x}_F,t')\mathrm{d}t'\mathrm{d}\mathbf{x}, \tag{27}$$

and used to update the f_1^+, f_1^- and f_2 functions. This makes the algorithm both efficient. In summary, the M_m^+, N_i and the updates for the focusing functions for the mth iteration with $m \geqslant 1$ are simply:

$$M_m^+(\mathbf{x}_R,\mathbf{x}_F,t) = \sum_{l=0}^{m-1} N_{2l+1}(\mathbf{x}_R,\mathbf{x}_F,t), \tag{28}$$

$$f_{1,m}^+(\mathbf{x}_R,\mathbf{x}_F,t) = G_d(\mathbf{x}_R,\mathbf{x}_F,-t)+\sum_{l=0}^{m-1} N_{2l+1}(\mathbf{x}_R,\mathbf{x}_F,t), \tag{29}$$

$$f_{1,m}^-(\mathbf{x}_R,\mathbf{x}_F,t) = -\sum_{l=0}^{m} N_{2l}(\mathbf{x}_R,\mathbf{x}_F,-t), \tag{30}$$

$$f_{2,m}(\mathbf{x}_F,\mathbf{x}_R,t) = G_d(\mathbf{x}_R,\mathbf{x}_F,-t)+\sum_{l=0}^{2m} N_l(\mathbf{x}_R,\mathbf{x}_F,t). \tag{31}$$

In the provided program each computed N_i term is added to the focusing function updates. The implementation is shown in Algorithm 1 and Algorithm 2. The ... in Figure ... f_1^-, ... iteration ... f_1^+, f_2, and N_i are done just before the iteration starts. The N_i updates f_1^-. The even ... and f_1^+ respectively. The Green's function is computed by inserting f_2 of equation (31) into equation (4)

$$\begin{aligned}
G(\mathbf{x}_F,\mathbf{x}_R,t) = f_2(\mathbf{x}_F,\mathbf{x}_R,-t) &+ \int_{\partial\mathbb{D}_0}\int_{t'=-\infty}^{t} R(\mathbf{x}_R,\mathbf{x},t-t')G_d(\mathbf{x},\mathbf{x}_F,-t)\mathrm{d}t'\mathrm{d}\mathbf{x}\\
&+ \sum_{l=0}^{2m}\int_{\partial\mathbb{D}_0}\int_{t'=-\infty}^{t} R(\mathbf{x}_R,\mathbf{x},t-t')N_l(\mathbf{x},\mathbf{x}_F,t')\mathrm{d}t'\mathrm{d}\mathbf{x}. && (32)
\end{aligned}$$

In equation (32) the integration-convolution terms can be recognis

N_i terms. By storing the sum of these unmuted terms the Green's

functions can be calculated as a summation of previously com

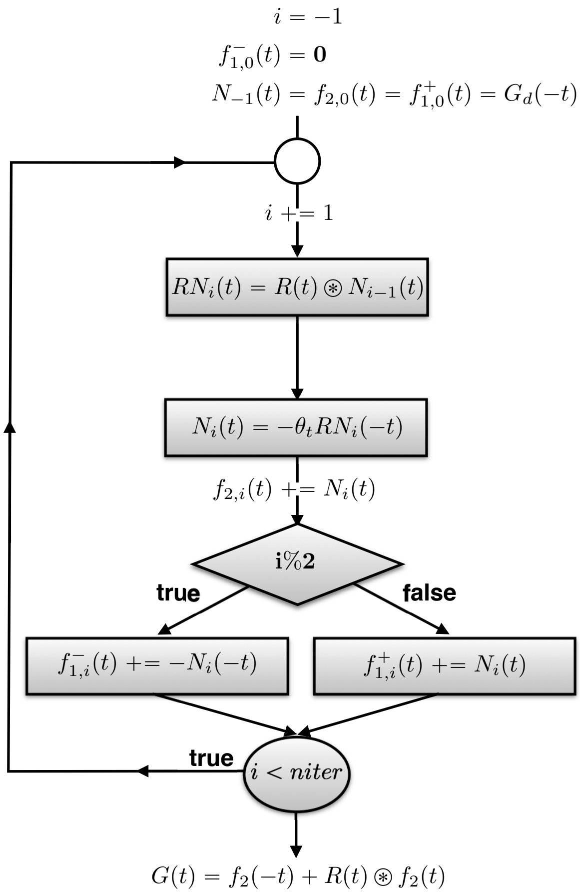

Figure 2: Flowchart of the Marchenko algorithm. In the notation t
a more compact notation. The symbol $\circledast$ represents the integration-convolutio

The program can compute the results of multiple focal points (Nfoc in Algorithm 1) in t
This is convenient for calculating the Marchenko results (e
of interest in one run. The computational advantage is that
only once to compute the results of multiple focal points.
are independent of each other. Hence, the code is OpenMP par
( ).
The function in Algorithm 1 computes the integration-convolution
term N_i with R, in the frequency domain (Fourier $\mathcal{F}$). For the computatio
of only one focal point, loading the required input data in
the computational work. The implementation has additional (1)
to compute the up- and downgoing Green's functions by equations (1) and (2)
computed N_i field (to disk).

```
Main
  Reading SU-style input Data and Allocate arrays
  Initialisation
  Ni(t) = f2p(t) = f1plus(t) = G_d(-t)
  f1min(t) = pmin(t) = 0.0
    iter ← 0   niter
    synthesis(Ref, Ni, iRN)
    Ni(t) = -iRN(-t)
    pmin(t) += iRN(t)
    applyMute(Ni, muteW)
    f2p(t) += Ni(t)
        (iter % 2 == 0)
      f1min(t) -= Ni(-t)

      f1plus(t) += Ni(t)

  Green(t) = pmin(t) + f2p(-t)

synthesis(Ref, Ni, iRN)

  iRN = 0
  ∀l,i: Fop(l,i,ω) = F{Ni(l,i,t)}
    k ← 0   nshots
    #pragma omp parallel for
      l ← 0   Nfoc
        ω ← ω_min   ω_max
        sum(ω) = 0
          i ← 0   nrecv
          sum(ω) += Ref(i,k,ω) * Fop(l,i,ω)

      iRN(l,k,t) = F^-1{sum(ω)}
```

Marchenko algorithm as implemented in the provid

To use the Marchenko method with numerically modeled data i of the refection response are correct. This is certainly als of amplitude scaling is explained frst before discussing th In the summation of N_1 and G_d to compute $f^+_{1,1}$ in equation (19), it is important that the a the measured refection data is accurate. A wrong amplitude of R will result in a wrong $f^+_{1,1}$ and the scheme will not converge. This is illustrated with we introduce a wrong scaling factor b in R to compute $f^+_{1,1}$. Then the frst iterations will c

$$-bN_0(\mathbf{x}_R,\mathbf{x}_F,-t) = \theta_t \int_{\partial\mathbb{D}_0}\int_{t'} bR(\mathbf{x}_R,\mathbf{x},t-t')G_d(\mathbf{x},\mathbf{x}_F,-t')\mathrm{d}t'\mathrm{d}\mathbf{x},$$

$$-b^2N_1(\mathbf{x}_R,\mathbf{x}_F,-t) = \theta_t \int_{\partial\mathbb{D}_0}\int_{t'} bR(\mathbf{x}_R,\mathbf{x},t-t')bN_0(\mathbf{x},\mathbf{x}_F,t')\mathrm{d}t'\mathrm{d}\mathbf{x},$$

$$f^+_{1,1}(\mathbf{x}_R,\mathbf{x}_F,t) = G_d(\mathbf{x}_R,\mathbf{x}_F,-t) + b^2N_1(\mathbf{x}_R,\mathbf{x}_F,t).$$

The update $f_{1,1}^+$ involves a^2 and in each next update the error in $f_{1,m}^+$ in N_{2m+1} the update will grow with b^{2m+2}. A wrong amplitude in G_d is not a problem as the Marchenko equa[tion] the focusing function. An amplitude error can be factored ou[t]

$$
\begin{aligned}
-aN_0(\mathbf{x}_R, \mathbf{x}_F, -t) &= \theta_t \int_{\partial\mathbb{D}_0} \int_{t'} R(\mathbf{x}_R, \mathbf{x}, t-t') aG_d(\mathbf{x}, \mathbf{x}_F, -t') \mathrm{d}t' \mathrm{d}\mathbf{x}, \\
-aN_1(\mathbf{x}_R, \mathbf{x}_F, -t) &= \theta_t \int_{\partial\mathbb{D}_0} \int_{t'} R(\mathbf{x}_R, \mathbf{x}, t-t') aN_0(\mathbf{x}, \mathbf{x}_F, t') \mathrm{d}t' \mathrm{d}\mathbf{x}, \\
af_{1,1}^+(\mathbf{x}_R, \mathbf{x}_F, t) &= aG_d(\mathbf{x}_R, \mathbf{x}_F, -t) + aN_1(\mathbf{x}_R, \mathbf{x}_F, t).
\end{aligned}
$$

van der Neut et al. (2015) introduces an adaptive amplitude-correctio[n] amplitude errors in R by solving the Marchenko equation in an explicit [...] errors can be adjusted by adaptive subtraction of the focus[ing] better suited to apply to noisy data. van der Neut et al. (2015); Staring et al. (2016).
Brackenhoff (2016); Thomsen (2016) have developed estimation methodologie[s] factor b to R. These methods compensate for an R, which is an important main [...] first step to apply the Marchenko method on measured data. Br[...] use of the $G^-(\mathbf{x}, \mathbf{x}_F, t)$ that is identically zero below the deepest reflector [...] $\mathbf{x}_F$ [...]
The following will provide step by step directions how to co[...] amplitudes.

- The reflection data must be deconvolved for the wavelet (McIntosh, 2017). The result of the deconvolution is the reflection response of a zero-phase [wavelet with] frequencies f_{min} and f_{max}. Since we are computing the reflection respo[nse] [...]lution and directly model the reflection response with a s[ource wavelet that has a] spectrum of amplitude 1.0:

$$
s(t) = \int_{f_{min}}^{f_{max}} 1.0 \exp(-j2\pi ft) df \tag{33}
$$

  The implemented flat wavelet spectrum has smooth transit[ions to] and from the maximum, frequency to avoid a very long wave[let. The pro]vided program can generate these waveforms and the provide[d] parameters used to calculate the source wavelet. Note, i[n the com]putation of the source wavelet in the frequency domain on[e] frequency Δf, in the normalization [...] going from frequency to time with the Fou[rier] wavelet used in the example is shown in Figure 3. A shift of 0.3 seconds (paramete[r] in) is added to the source wavelet to make it causal a[...] difference program. In the finite difference modeling of th[e] data is postponed with 0.3 seconds (parameter to reset the peak of the wavelet back at the correct time.

- In the finite-difference program source for modeling $R(\mathbf{x}_R, \mathbf{x}, t)$ a vertical force F_z is [...] manual of the finite-difference modeling program about th[e] [...] The receivers are placed at the same surface as the source[...]

- The amplitude scaling factor, in the finite-difference source F_z with the time signal $s(t)$, is defined in the update of V_z as of particle velocity

$$
V_z(x, z, t + \Delta t) = V_z(x, z, t) - \frac{\Delta P(x, z, t)}{\rho \Delta z} + \frac{\Delta t}{\rho \Delta x^2} s(t). \tag{34}
$$

  The discrete intervals $\Delta t, \Delta x = \Delta z$ are the steps in the finite-difference [...] ρ the density at the injection point of the source [...] $\frac{\Delta P}{\Delta z}$ is the finite-difference [...] of the first derivative [...] z of the pressure field P.

- To compute R, from the Green's functions calculated by the fini[te-difference program a factor] -2 is needed (e.g. Wapenaar et al. (2012)). This factor -2 is included in [the] program when it reads in R the reflection response

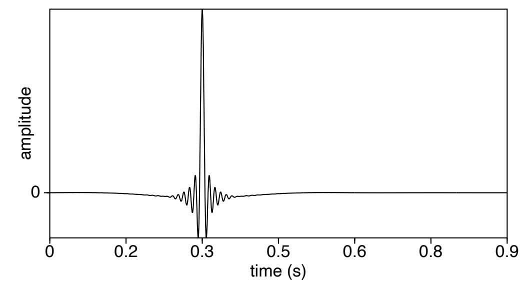

a) Source wavelet R for modeling

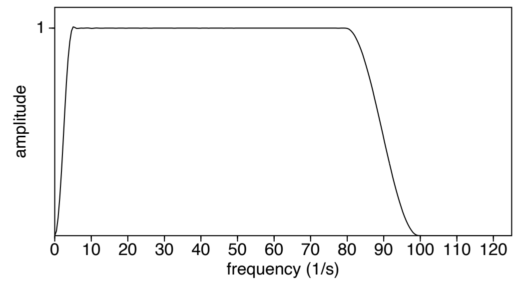

b) Amplitude spectrum of source wavelet.

Figure 3: Source wavelet with a fat frequency spectrum between f_{min} (= 5 Hz) and f_{max} (= 80 Hz) used to model the refection response.

- The time convolution of R is implemented by a forward Fourier transfo… quency domain, multiplication in the frequency domain, a… main. In the numerical implementation of the convolution a factor Δt … with Δx for the integration over x, must be included as well. Together wit… factor $\frac{1}{N}$ of discrete Fourier transformations when going f… time, with N the number of time samples, the scale factor to co… space integration in the frequency domain becomes:

$$\frac{\Delta x \Delta t}{N}.$$

The Marchenko algorithm is illustrated with a 2-dimensiona… 4. The numerical modeling is carried out with a finite-difference … Thorbecke and Draganov, 2011) that is also included in the software package. The i… the refection response $R(x_R, x, t)$ is approximately a sinc-function with a fa… as shown in Figure 3.
The full reflection matrix $R(x_R, x, t)$, for a fixed-spread geometry, can be const… modeled shot (Figure 4c), since the model contains no lateral variatio… geometry ranges from -2250 to 2250 meter with 5 meter distan… The 5 meter distance is chosen to avoid spatial aliasing. We… the time to compute the reflection response R in a laterally varying medium is too … for the desired reproducibility of the examples in this pap… not make any assumption about the medium and can handle late… demo directory of the Marchenko program contains also an exa… ( ).
The transmission response, recorded at the surface, is shown in Figure 4d. For a sou… has been modeled with a zero-phase Ricker source wavelet s(t… that the chosen source wavelet of G_d be zero-phase, otherwise the time rev… algorithm would not work properly and the Marchenko scheme w… to choose a source wavelet that decreases rapidly in time. T…

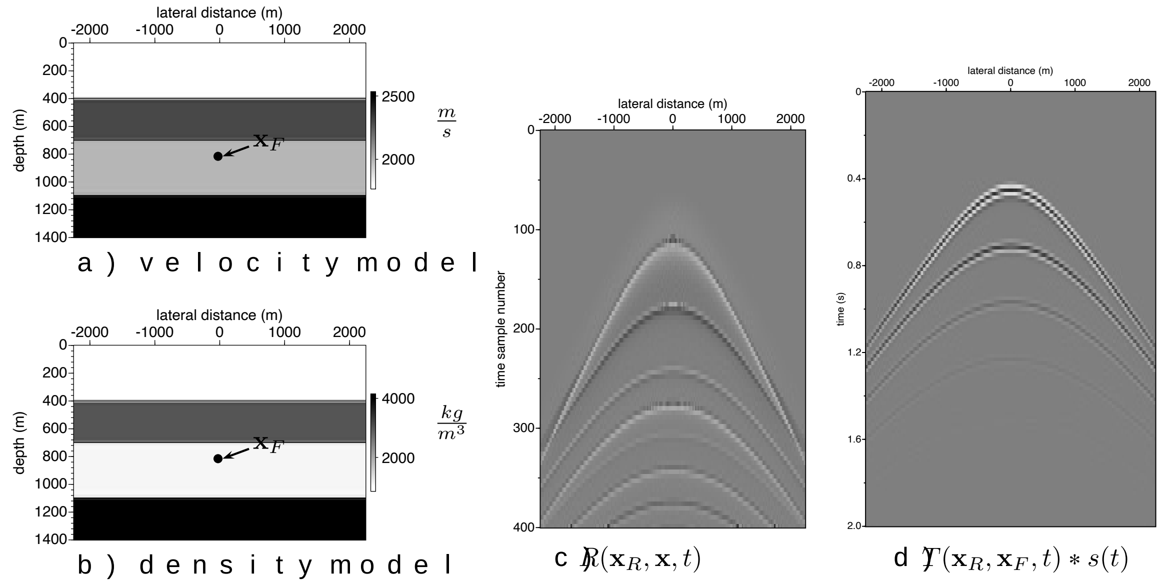

Figure 4: Four layer model with velocity (a) and density (b) contr... $\mathbf{x}(x=0,z=0)$ and receivers $\mathbf{x}_R(x=x_R,z=0)$ (c), and the transmission respons... $\mathbf{x}_F(x=0,z=900)$ (d). Note that the source wavelet ... R (c) is given by ... (3) ... of Figure ... (d) is modeled with a Ricker wavelet with a peak at 25 Hz.

between the direct arrival and the first reflection ... (10). In case of ... overlap ... defined window function θ (equation (11)) ... cuts through the overlapping events ... is not retrieved correctly.

The initialisation $f^-_{1,0}$ (equation (17)) is computed ... first step ... Figure 5. Each trace ... in $R(\mathbf{x}_R,\mathbf{x},t)$ is convolved with $G_d(\mathbf{x}_R,\mathbf{x}_F,-t)$, ... $G_d(\mathbf{x}_R,\mathbf{x}_F,-t)$ shown in Figure 5 only contains the time-reversal of the full transmission ... 4. By making use of ... shift invariance $R(\mathbf{x}_R,\mathbf{x},t)=R(\mathbf{x}_R-\mathbf{x},0,t)$, the time-convolution result is integrated (s... $\mathbf{x}_R$) and results in one trace at position $\mathbf{x}$ ... N_0 ...

In $-N_0(\mathbf{x},\mathbf{x}_F,-t)$ the dotted lines indicate the cut-of boundaries o... $\theta(\mathbf{x},\mathbf{x}_F,t)$. To suppress wrap-around events (from positive times ... window $\theta(\mathbf{x},\mathbf{x}_F,t)$, as introduced in equation (11), is symmetrized. Hence $\theta(\mathbf{x},\mathbf{x}_F,t)$ from here is zero for $t>t_d^\varepsilon$ and $t<-t_d^\varepsilon$, and unity for $-t_d^\varepsilon<t<t_d^\varepsilon$. For deep focal points o... also extend the time axis by padding zeros at the end of the a... wrap-around events in the time domain. In the Appendix the tr... in more detail.

The events before the top dotted line and the events after th... remaining events originate from the two refectors above the ... detailed explanation of the diferent events in the Marchenko ... Van der Neut et al. (2015). Staring (2016) give a similar explanation in case free-surf... Marchenko method. This is the initial ... f_1^- ... for the next step to comput... f_1^+, given in equations (18) and (19).

The computation of $f^+_{1,1}$ involves the same time convolution and spatial ... illustrated in Figure 6. The result of the integration, $-N_1(\mathbf{x},\mathbf{x}_F,-t)$, is ... according to equation (19), time reversed, multiplied with -1 and ... $\theta(\mathbf{x},\mathbf{x}_F,t)$ to get the first estimate $f^+_{1,1}$. Note, that the lower (causal) part of $\theta(\mathbf{x},\mathbf{x}_F,t)$ ... the window at direct ... time. This event at the direct arrival time t_d ... update of the Green's ... adjust the amplitude of the direct arrival ... Van der Neut et al. (2015). The Green's f... update of the direct arrival in the Green's function is expl...

Figure 7 shows the results of the first 4 iterations of the Marchen... the results of each convolution and integration N_i with R ... focus ... (all with the same clipping factor) ... N_i becomes smaller ...

next iteration.

The trace in the fifth column is a comparison between the ref[erence] the computed Green's function (dotted black). In these trac[es] that some events are weakened by subsequent iterations: The the reference Green's function.

To get a better understanding of the computation of the Gree[n] discussed in more detail. The initial G_d (equation (26)) of the metho[d] computed according to (32). The equation is (

$$
\begin{aligned}
f_{2,0}(\mathbf{x}_F, \mathbf{x}_R, t) &= G_d(\mathbf{x}_R, \mathbf{x}_F, -t) \\
G_0(\mathbf{x}_R, \mathbf{x}_F, t) &= G_d(\mathbf{x}_R, \mathbf{x}_F, -t) + \int_{\partial \mathbb{D}_0} \int_{t'=-\infty}^{t} R(\mathbf{x}_R, \mathbf{x}, t-t') G_d(\mathbf{x}, \mathbf{x}_F, -t) \mathrm{d}t' \mathrm{d}\mathbf{x} \\
&\quad + N_0(\mathbf{x}_R, \mathbf{x}_F, -t)
\end{aligned}
\tag{35}
$$

Note that in (35) the result of the first integral R is not muted with θ_t convoluti[on]. The initial estimate of the Green's function is thus built u[p]

1. The direct arrival of the transmission response ($G_d(\mathbf{x}_R, \mathbf{x}_F, -t)$).
2. The integration R-convolution with G_d, the result of the (unmuted) top left pane[l] of Figure 7.
3. A θ_t muted and multiplied by -1 version of the integration R-convolution with G_d: $N_0(\mathbf{x}_R, \mathbf{x}_F, -t) = -f^-_{1,0}(\mathbf{x}_R, \mathbf{x}_F, t)$, the second panel in the top row of Figure 7.

It is important to note that the result of the combination o[f] $f^-_{1,0}(t)$ (the events within the black-dotted lines) from the unmuted R with G_d. This is the same as the inverse of θ_t. To get the first estimate of the Green's function $G_d(\mathbf{x}_R, \mathbf{x}_F, -t)$ is added to this result and gives the top right panel of Figure 7. In the next iteration we have

$$
\begin{aligned}
f_{2,1}(\mathbf{x}_F, \mathbf{x}_R, t) &= G_d(\mathbf{x}_F, \mathbf{x}_R, -t) + N_0(\mathbf{x}_F, \mathbf{x}_R, t) \\
G_1(\mathbf{x}_F, \mathbf{x}_R, t) &= G_0(\mathbf{x}_R, \mathbf{x}_F, t) + \int_{\partial \mathbb{D}_0} \int_{t'=-\infty}^{t} R(\mathbf{x}_R, \mathbf{x}, t-t') N_0(\mathbf{x}, \mathbf{x}_F, t) \mathrm{d}t' \mathrm{d}\mathbf{x} \\
&\quad + N_1(\mathbf{x}_R, \mathbf{x}_F, -t)
\end{aligned}
\tag{36}
$$

Compared to the previous iteration two new terms are added:

1. The integration R-convolution with N_0, the (unmuted) panel for $i=1$ in Figure 7.
2. The θ_t muted, time reversed, multiplied by -1 result of the integration R-convolution with N_0: $N_1(-t)$.

The combination of these two terms results in the subtractio[n] from the unmuted integration R-convolution of N_0.

Each next iteration follows this same pattern: by θ_t (and θ^ϵ_d) the events wi[thin] to update f_1 or the focusing function, the events (set by θ_t and θ^ϵ_d) are used to update the Green's function. Application of the θ_t time window for the focusing function Green's function.

There is one important remark to make: for the T^{inv}_d, the focusing function $f^\dagger_1$ is not updated, whereas the direct arrival in the Green's function G_d is updated. In the first iterati[on] (Figure 7) the direct arrival in G_0 is the same as G_d. In the second iteration (Figure 7) the amplitude of the direct arrival is corrected by $-N_1(-t)$ just below the e[vents] the black-dotted line of the mute window. This $-N_1(-t)$ was positioned at the direct arrival and decreases th[e] Van der Neut et al. (2015). In the plotted trace G_0 the amplitude of the direct arrival (dotted line) is mu[ch] In G_1 the amplitudes of the direct arrival between reference a[nd] much closer. We do not expect that the scheme with $T^{inv}_d \approx G_d$ will arrive at the correct amplitudes; in order to achieve accurate amplit[udes] had to be used G_d. There is an offset dependent scaling factor b

computed Green's function. Thorbecke et al. (2013) showed that this estimate of the d
not have to be precise and can be based on a macro model. The r
of the computed Green's function is correct and shown in the
in Figure 7.

The iterative corrections of the amplitude of the Green's fu
mission losses. The result is that at $t = t_d$ the upgoing field amplitude that is r
to the local refection coefficient at x_f (Slob et al., 2014). In the next section we wi
good this correction is, when focusing function f_2 is emitted into the medi
Broggini et al. (2014) use the energy before the direct arrival in the
convergence of the scheme. In the provided Marchenko progra
give the user the freedom to choose the number of iterations c
term $\sqrt{\sum_{x,t} N_i^2(x,t)}$) is computed and printed for each iteration and ca
In each next iteration this energy should become smaller. Th
in Figure 8.

A comparison with the reference Green's function and the Ma
8 iterations is shown in Figure 9. The difference with the reference Green's f
middle part of the picture at $x = 0$. A small amplitude mismatch increases s
ofset. Closer to the edge of the acquisition (± 2250 m) the difference with the ref
larger, because the full Fresnel zone is not included in the
present at earlier times, are also not captured. Beyond ~ 1.5 s, the limit
the presence of higher wavenumbers becomes smaller, and th
decreases. To suppress artefacts from limited acquisition
the initial focusing operator and/or the refection respons
efects on suppressing these artefacts. Depending on the sp
the fnite aperture efect could slightly be attenuated. In
the non-tapered part adjacent to the tapered region and fn
usually smaller, amplitude mismatch is caused by the use of
transmission responses C_d (equation 10) instead of the inverse.

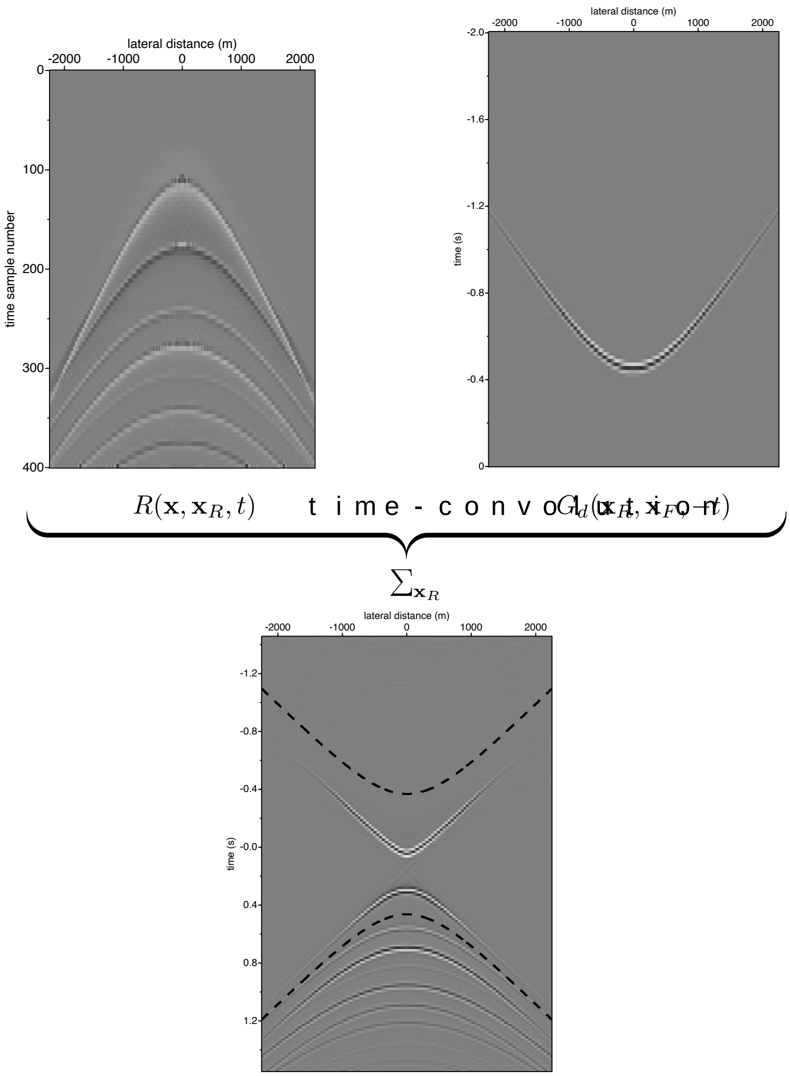

$-N_0(\mathbf{x},\mathbf{x}_F,-t)$

Figure 5: Initialisation step to compute $f^-_{1,0}(\mathbf{x},\mathbf{x}_F,t) = -N_0(\mathbf{x},\mathbf{x}_F,-t)$. After applying the time $\theta(\mathbf{x},\mathbf{x}_F,t)=\theta_t$ only events between the dotted lines of N_0. The mute window is applied to mute the wrap-around events of the temporal convolution for $t<0$ is only a practical solution and not needed from the theory. Note the panels; positive time for $R(t)$, negative for $G_d(-t)$ and negative and positive for $N_0(-t)$.

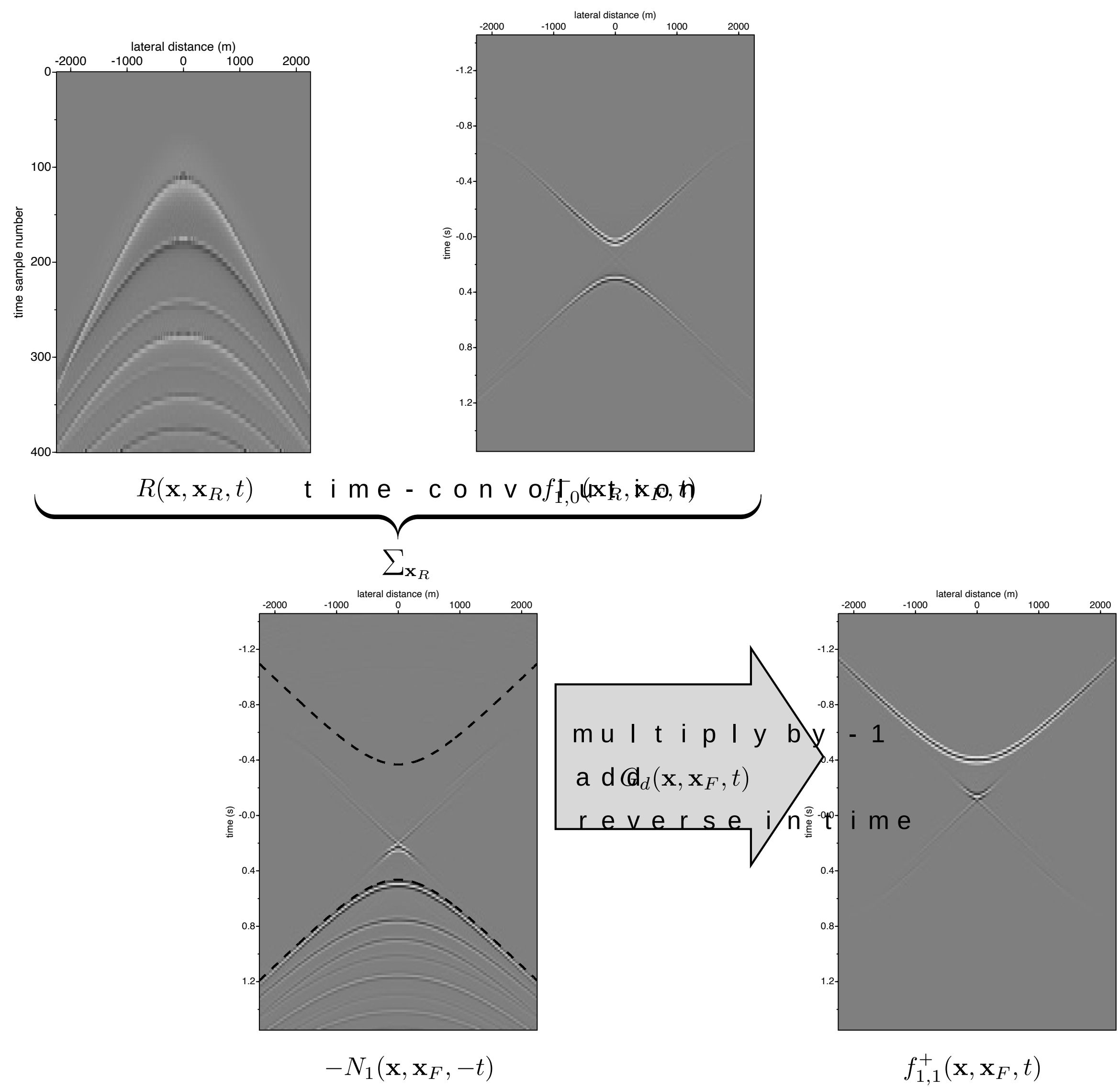

Figure 6: First iteration to compute $f^+_{1,1}(\mathbf{x},\mathbf{x}_F,t)$ from $f^+_{1,0}(\mathbf{x}_R,\mathbf{x}_F,t)$. In the summation of G_d with N_1 it is important that the amplitudes of R are correct.

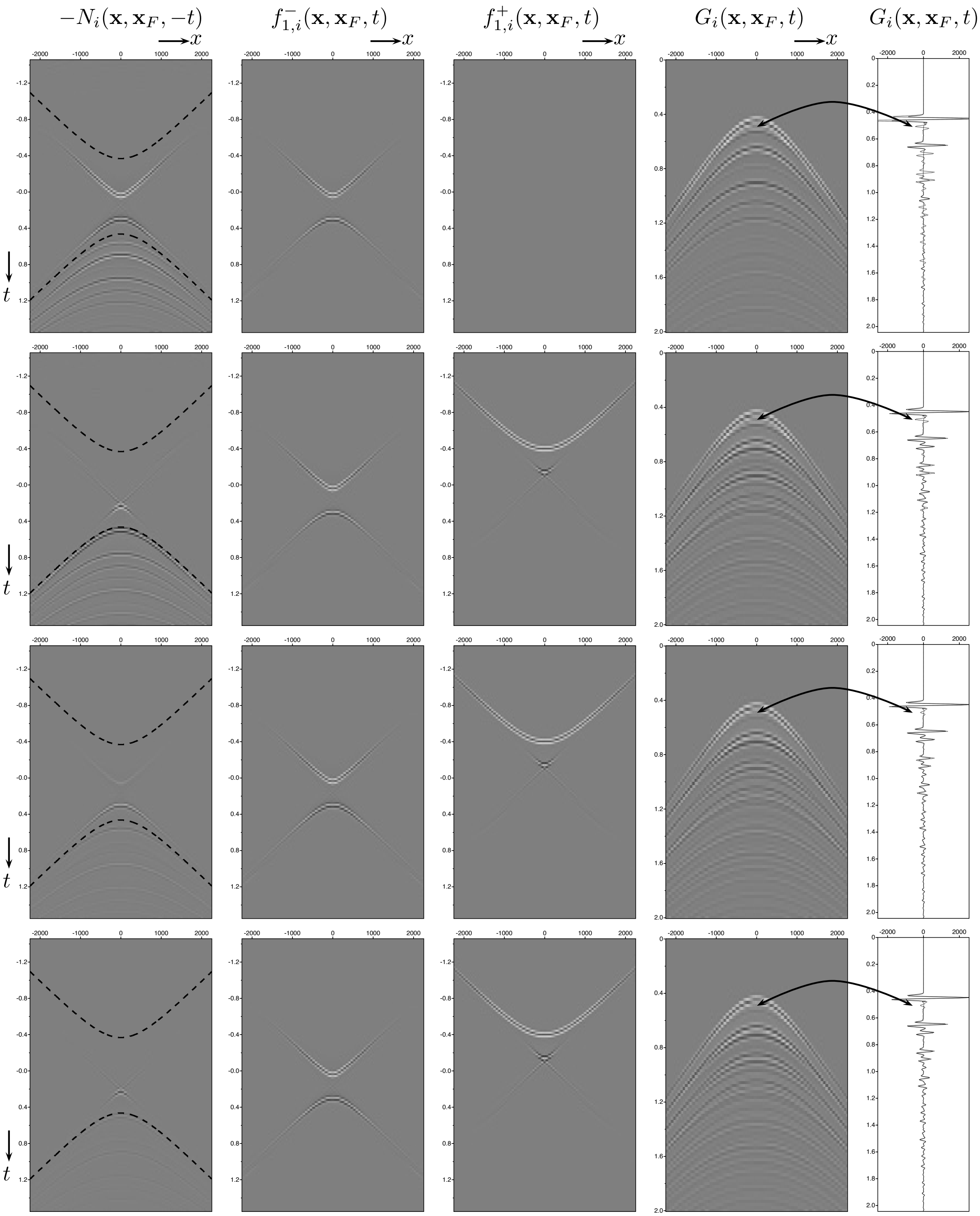

Figure 7: Four successive iterations of the Marchenko method. Th
not belong to the Green's function are weak and $f^-_{1,i}$ (the 2nd column) only ch
from $i = 1$ to $i = 2$, while $f^+_{1,i}$ (the 3rd column) changes from $i = 0$ to $i = 1$ and from $i = 2$ to $i = 3$.
The clip level of N_i and G_i is the same for all panels. Labels of the horiz
same for all panels, and are shown for the top and left panels

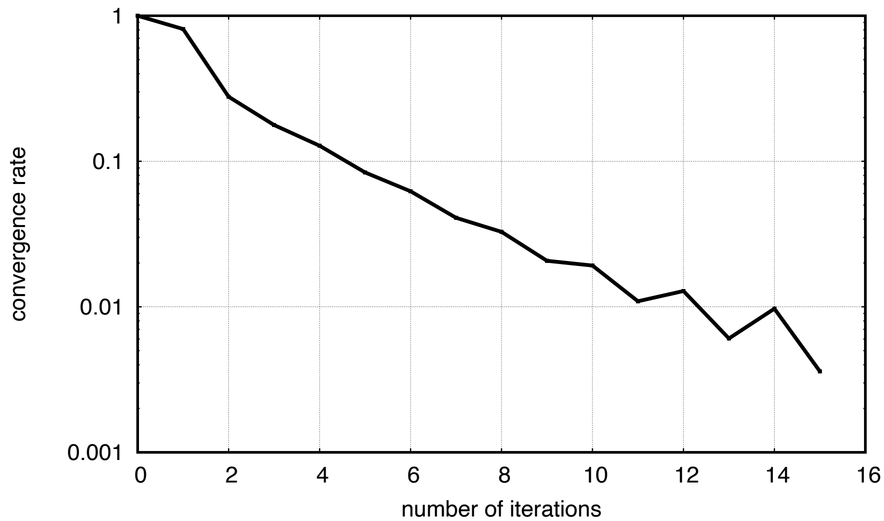

Figure 8: Logarithmic convergence rate of the example for 16 iterations. The bumps at the end of the curve are caused by limited aperture
magnitude smaller than the main events.

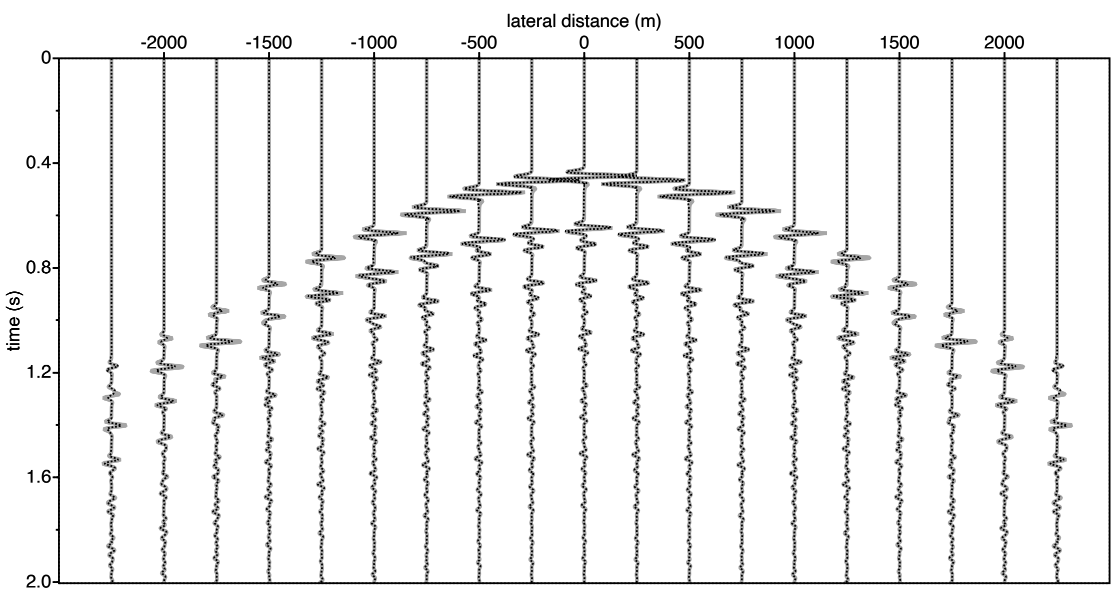

Figure 9: Comparison of the Marchenko computed Green's function
Green's function: solid-gray trace in the background is the
function computed with the Marchenko method.

One of the properties of the focusing function $f_2(\mathbf{x}_F, \mathbf{x}, t)$ (5) is that it will focus at $t=0$ at the focal point $\mathbf{x}_F$. This property can be demonstrated by emitting $f_2(\mathbf{x}_F, \mathbf{x}, t)$ from $\partial\mathbb{D}_0$ into the medium and show that it has a focus at $\mathbf{x}_F$ at $t=0$ (Slob et al., 2014; Wapenaar et al., 2017). If the transmission losses are correctly taken into account all internal multiples will be cancelled at $t=0$. The left column of Figure 10 shows snapshots at $t=-0.30, -0.15, -0.03, -0.02$, and 0. The snapshot at $t=0$ indeed shows only a focus at the focal point. In the snapshots at $t=-0.03, t=-0.02$ it is observed that events internal multiples have opposite amplitude and travel towards $t=0$. The second column of Figure 10 shows snapshots at positive times, after the $t=0$. After $t=0$ the focussed and dimmed events separate again and c

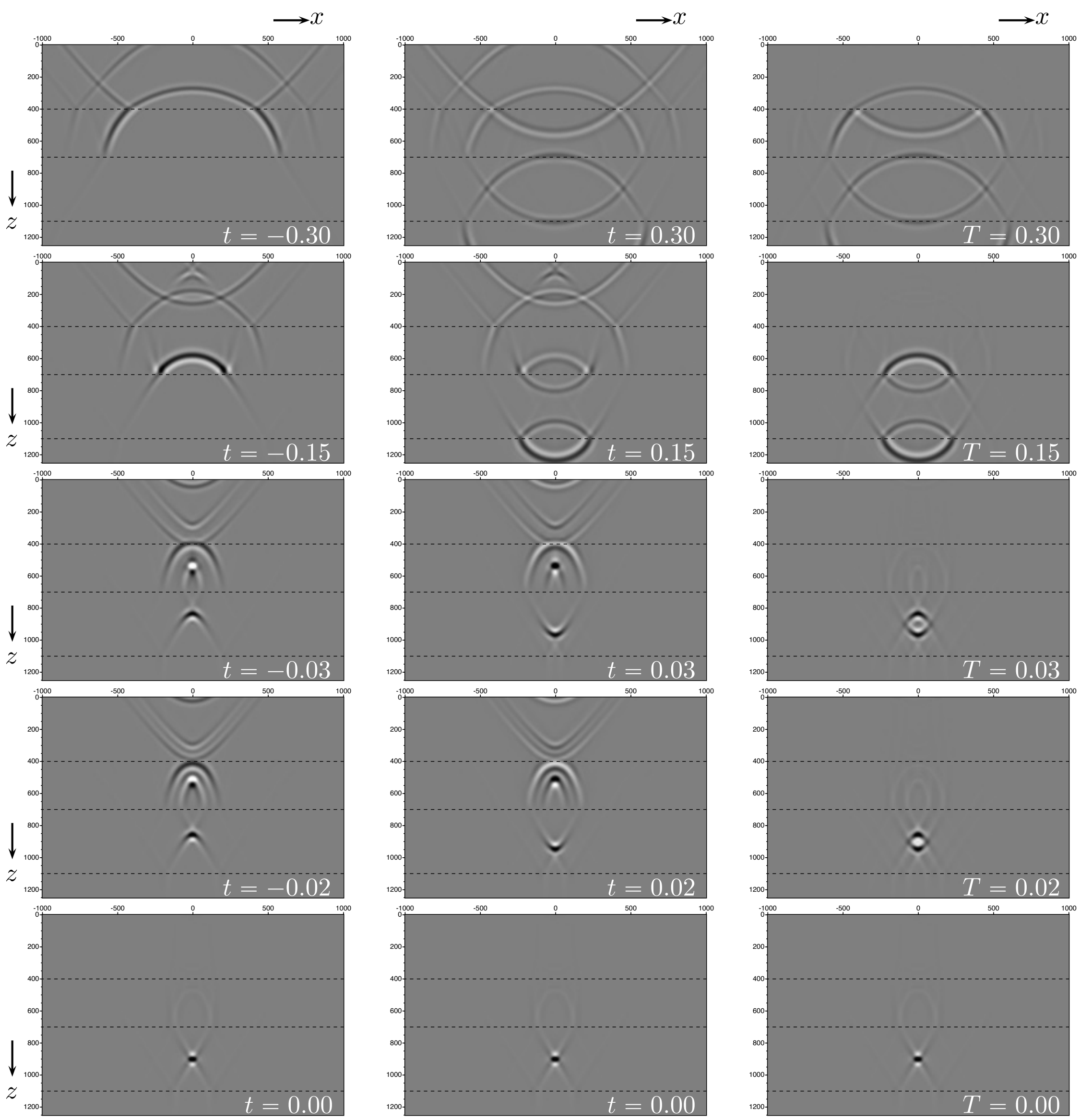

Figure 10: Snapshots of propagation of f_2 through the actual medium. The left column shows snapshots at a-causal times, the middle column snapsh shows the addition of the acausal snapshots at negative tim at positive times (T). Labels of the horizontal and vertical axes ar shown for the top and left panels.

Adding the snapshots at negative times to the correspondin
snapshots of the homogeneous Green's function (Wapenaar et al., 2016) with a virtual source at $\mathbf{x}_F$.
The third column in Figure 10 shows these combined snapshots, where the s
negative times are summed, and represent the causal part of
snapshots can be interpreted as the response of a virtual sou
$\mathbf{x}_F$.

marchenko

The self-doc of the program is shown by typing on the command line without any
You will then see the following list of parameters:
If you are not considering special cases, the default values
parameters have to be changed from their default values to g
The provided marchenko source-code package contains two ma

- : picks the first arrival time from a transmission respo
- : solves for the focusing functions in the Marchen
  functions

The program tracks the first arrival from a transmission res
Its main use is to separate the direct arrival (G_d) from the multiples in the transmis
coda (M^+). In the examples provided the transmission response
modeling and the direct arrival needs to be separated from
component $G_d(t)$ from $T(t)$ in Figure 4. The program is not needed if a method is u
eikonal solver) that computes the direct arrival G_d of the program direc
is the input of the program. The different parameters are shown in the
self-documentation of the program:

```
fmute - mute in time domain file_shot along curve of maximum amplitude i

fmute file_shot= {file_mute=} [optional parameters]

Required parameters:

  file_mute= ................ input file with event that defines the mut
  file_shot= ................ input data that is muted

Optional parameters:

  file_out= ................ output file
  above=0 .................. mute after(0), before(1) or around(2) the
  ........................ options 4 is the inverse of 0 and -1 the inv
  shift=0 .................. number of points above(positive) / below(n
  check=0 .................. plots muting window on top of file_mute: ou
  scale=0 .................. scale data by dividing through maximum
  hw=15 .................... number of time samples to look up and down
  smooth=0 ................. number of points to smooth mute with cosine
  verbose=0 ................ silent option; >0 display info
```

If is not provided, will be used instead to pick the first arr
The option is explained in Figure 11 and separates in different ways the dir (t_d)
from the coda. The and options have also a truncation point a
time-axis, with the time reversal t_d, to mute wrap-around events introduced b
discrete Fourier transform. Note that the lower end of the t
The option defines a pass t_d and window convenient to select the
the transmission response in case the first arrival also cont
To find the first arrival time a simple tracking algorithm is implem
position equal to the source position the algorithm searche
assumed that this is the first arrival time at the source posi
true and it is therefore always good to verify in the created output t
if the program has tracked the correct direct arrival time.

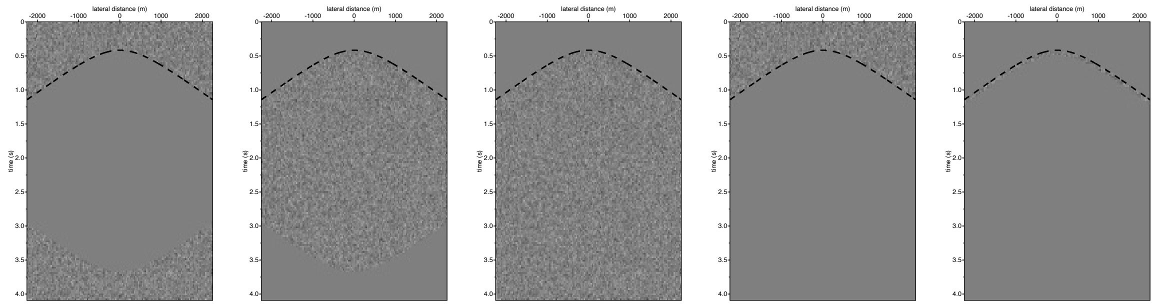

Figure 11: The different options of the parameter in the and programs, illustra
with a shot panel consisting of noise.

maximum (j_{max}) in the source trace i, the algorithm looks in the neighbour trace $i \pm 1$ for the maximum ce
It only searches for this maximum in a restricted time windo
trace is searched in the time window $j_{max} - n < t_{i-1} < j_{max} + n$, where n is a number of sample
given as input parameter. If there are head-waves present t
direct arrival, so it is good practice to choose a small n (4 - 8 samples).

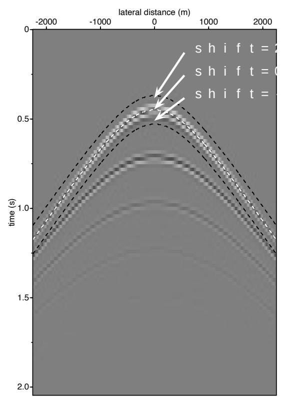

Figure 12: The parameter in the and programs.

The option represents t_d^ϵ and is needed to include the width of the
window. Figure 12 shows the effect of setting a negative or positive s
of the wavelet. With the option a positive shift will mute the dire
will preserve the direct arrival.
The parameter defines a transition zone (in samples) going fro
Using a few time-samples (3-5) for the smooth transition zon
direction of the taper, going from 1 to 0, is away from $\pm t_d$.
The program has the following parameters and options:

```
MARCHENKO - Iterative Green's function and focusing functions retrieva

marchenko file_tinv= file_shot= [optional parameters]

Required parameters:

  file_tinv= ............... direct arrival from focal point: G_d
  file_shot= ............... Reflection response: R

Optional parameters:

 INTEGRATION
  tap=0 .................... lateral taper focusing(1), shot(2) or both
```

```
   ntap=0 .................. number of taper points at boundaries
   fmin=0 .................. minimum frequency in the Fourier transform
   fmax=70 ................. maximum frequency in the Fourier transform
 MARCHENKO ITERATIONS
   niter=10 ................ number of iterations
 MUTE-WINDOW
   above=0 ................. mute above(1), around(0) or below(-1) the
   shift=12 ................ number of points above(positive) / below(n
   hw=8 .................... window in time samples to look for maximum
   smooth=5 ................ number of points to smooth mute with cosine
   plane_wave=0 ............ enable plane-wave illumination function
   src_angle=0 ............. angle of plane source array
   src_velo=1500 ........... velocity to use in src_angle definition
 REFLECTION RESPONSE CORRECTION
   tsq=0.0 ................. scale factor n for t^n for true amplitude r
   Q=0.0 ......,............ Q correction factor
   f0=0.0 .................. ... for Q correction factor
   scale=2 ................. scale factor of R for summation of Ni with G
   pad=0 ................... amount of samples to pad the reflection ser
   reci=0 .................. 1; add receivers as shots 2; only use recei
   countmin=0 .............. 0.3*nxrcv; minumum number of reciprocal tr
 OUTPUT DEFINITION
   file_green= ............. output file with full Green function(s)
   file_gplus= ............. output file with G+
   file_gmin= .............. output file with G-
   file_f1plus= ............ output file with f1+
   file_f1min= ............. output file with f1-
   file_f2= ................ output file with f2 (=p+)
   file_pplus= ............. output file with p+
   file_pmin= .............. output file with p-
   file_iter= .............. output file with -Ni(-t) for each iteratio
   rotate=1 ................ 1: t=0 at nt/2 (middle) 0: t=0 at sample 0 f
   verbose=0 ............... silent option; >0 displays info
```

The number of iterations required for convergence depends o of events in the model; a complex model will need more iterat between 8 and 20. An automatic stopping criterion could be b N_i. This stopping criterion is not implemented to give the u iterations.

To suppress artefacts from a limited acquisition aperture, focusing ope)rand/o(r the refecti)on.Inresponexpe(rience these t limited efects on suppressing the fnite-acquisition relate

The mute-window parameters have the same meaning as in the

The temporal convolution of events at positive times in the R be shifted forward in time. Events at negative times in R will Marchenko method it is important that these backward shifte focal points some events can be shifted to negative times. in the frequency domain, we make use of the periodic propert negative times wrap-around to the end of the discrete time a The reason to symmetrise the time window θ_t is to suppress unwanted time wrap-ar time-wrap-around efects can also be avoided by padding zero R traces long, where the last samples are zeros. The padding to the t traces of R. Adding extra time samples will lead to longer comput use a symmetrised time window to suppress the unwanted efect

The parameter can be useful when the modeled data does not represents the previously computed function of the refection response ally, when the fle-name is defned, output results of computed Green

Defning writes for each iteration $-N_i(-t)$ (for i in the update term of Algorithm 1) before applying the mute window. By setting the energy of the update term is printed out for each iteration and can be used

The code to reproduce all fgures in this paper can be found in fle in that directory explains in detail how to run the s varying) model can be found in the directory. This example usually take hours to complete the refection data modeling on a personal

In addition to the Marchenko programs, the package also cont
ence modeling code, that is used to model all data for the exa (Thorbecke and Draganov, 2011). The directory contains programs to calculate a grid
source wavelets as well as programs for basic processing step
In the next subsections all the parameters will be described
how to use them.

The parameter verbose prints messages and produces additional f
the programs. Table 1 shows the kind of messages and the extra files pri
. Those messages and files contain extra information for
different setting of the verbose parameter are:

setting	messages printed to stdout
0	no messages only warnings
1	data information, source, receiver, paramete
2	+ iteration convergence
3	+ mute-window, OpenMP info
4	+ shot gather processing
>4	

Table 1: The files and messages produced by different values o

The demo directory contains scripts which demonstrate the di
In the subsections below most demo script are explained and

In this section, we describe the implementation of both Mar Transmission-compensated Marchenko Multiple Elimination eliminate internal multiple reflections without the need fo Only a reflection response without source wavelet and free-s as input. The paper is organised as follows: In the theory se MME and T-MME schemes. In the implementation section the pr step and this section provides a user's first step with the MM of the algorithm is illustrated with a simple three-reflecto This simple model is chosen to keep the number of events limi can be followed more easily. The method is not limited to sim to complicated 3D media as shown in Zhang and Slob (2019) for example.

In this section we give a brief overview of the theory of both surface is located at $\partial\mathbb{D}_0$. The surface reflection response $R(\mathbf{x}_0, \mathbf{x}'_0, t)$ is measured with the source and receiver positions $\mathbf{x}'_0$ and $\mathbf{x}_0$, which is free from free-surface rela and source wavelet. The time is denoted t.

As presented in Zhang et al. (2019), we give the equations of the Marchenko Mul scheme as

$$R_t(\mathbf{x}'_0, \mathbf{x}''_0, t = t_2) = R(\mathbf{x}'_0, \mathbf{x}''_0, t = t_2) + \sum_{m=1}^{\infty} M_{2m}(\mathbf{x}'_0, \mathbf{x}''_0, t = t_2, t_2), \tag{37}$$

with

$$\begin{aligned} M_{2m}(\mathbf{x}'_0, \mathbf{x}''_0, t, t_2) = &\int_{t'=0}^{+\infty} \int_{\partial\mathbb{D}_0} R(\mathbf{x}'''_0, \mathbf{x}'_0, t') H(t - t' - \varepsilon) \mathrm{d}\mathbf{x}'''_0 \mathrm{d}t' \times \\ &\int_{t''=0}^{+\infty} \int_{\partial\mathbb{D}_0} R(\mathbf{x}_0, \mathbf{x}'''_0, t'') H(t' - t + t_2 - t'' - \varepsilon) \times \\ &\quad M_{2(m-1)}(\mathbf{x}_0, \mathbf{x}''_0, t - t' + t'', t_2) \mathrm{d}\mathbf{x}_0 \mathrm{d}t'', \end{aligned} \tag{38}$$

and initialization

$$M_0(\mathbf{x}'_0, \mathbf{x}''_0, t, t_2) = -(H(t + t_2 - \varepsilon) - H(t + \varepsilon)) R(\mathbf{x}'_0, \mathbf{x}''_0, -t), \tag{39}$$

where R_t denotes the retrieved dataset without internal multip t_2 H the Heaviside function, which is used to apply the offset $(\varepsilon, t_2 - \varepsilon)$ in the equations. The constant ε is a small positive value which can b time-duration in practice. The M_0 initialization is the time-reversed shot at shot position $\mathbf{x}'_0$ for times $(\varepsilon, t_2 - \varepsilon)$. The left-hand side of equation 37 R_t is the same shot record, but without internal multiples (Zhang and Slob, 2019a). We fix t_2 as constant and independent of the source and receiver positions in the r is carried out over the receiver coordinate for both integra The second term in the right-hand side of equation 37 predicts internal multiple r Equation 39 indicates that the measured reflection response is the in equation 37. To retrieve a dataset without internal multiples at time t, this process must be repeated for all times t_2.

Equation 38 contains the terms that correct for the internal multi[ples in] $R(\mathbf{x}_0', \mathbf{x}_0'', t)$. To better explain the right-hand side of equation 38 we divide the expression into two pa[rts]

$$M_{2m}(\mathbf{x}_0', \mathbf{x}_0'', t, t_2) = \int_{t'=0}^{+\infty} \int_{\partial \mathbb{D}_0} R(\mathbf{x}_0''', \mathbf{x}_0', t') H(t - t' - \varepsilon) \times \\ M_{2m-1}(\mathbf{x}_0''', \mathbf{x}_0'', t - t', t_2) \mathrm{d}\mathbf{x}_0''' \mathrm{d}t', \tag{40}$$

$$M_{2m-1}(\mathbf{x}_0''', \mathbf{x}_0'', t - t', t_2) = \int_{t''=0}^{+\infty} \int_{\partial \mathbb{D}_0} R(\mathbf{x}_0, \mathbf{x}_0''', t'') H(t' - t + t_2 - t'' - \varepsilon) \times \\ M_{2(m-1)}(\mathbf{x}_0, \mathbf{x}_0'', t - t' + t'', t_2) \mathrm{d}\mathbf{x}_0 \mathrm{d}t''. \tag{41}$$

Equation 40 is a time domain convolution of R with M integrated over the spatial coordinate $\mathbf{x}_0'''$, which is the receiver position $\mathbf{x}_0'$. Equation 41 is a time domain correlation of R with M integrated over the spatial coordinate $\mathbf{x}_0$, which is the receiver position $\mathbf{x}_0'''$. The Heaviside function in equation 40 is to exclude negative times $t - t' < \varepsilon$ and only use the causal part of M_{2m-1}. In equation 41 the function $M_{2(m-1)}$ contains non-zero values for $t_2 - \varepsilon$. The ... contribute to the integral and $M_{2(m-1)}$ the Heaviside ... the integration $t'' + t - t' > t_2 - \varepsilon$. Note that equations 40 and 41 perform very simil[ar] operations (they differ by a sign change) and are implemented ... 38 this function is applied two times. The convolution terms a[re] ... function and the correlation terms are the odd numbered oper[ations]. To better explain the method and for illustration purposes the M ... 40 is defined as the field:

$$k_{1,i}^{-}(\mathbf{x}_0', \mathbf{x}_0'', t, t_2) = R(\mathbf{x}_0', \mathbf{x}_0'', t, t_2) - \sum_{m=1}^{i} \int_{t'=0}^{+\infty} \int_{\partial \mathbb{D}_0} R(\mathbf{x}_0''', \mathbf{x}_0', t') H(t - t' - \varepsilon) \times \\ M_{2m-1}(\mathbf{x}_0''', \mathbf{x}_0'', t - t', t_2) \mathrm{d}\mathbf{x}_0''' \mathrm{d}t'. \tag{42}$$

We can evaluate equation 42 at $t \geqslant t_2 - \varepsilon$ and the equation can be further split as follows

$$k_{1,i}^{-}(\mathbf{x}_0', \mathbf{x}_0'', t, t_2) = \begin{cases} v_{1,i}^{-}(\mathbf{x}_0', \mathbf{x}_0'', t, t_2) & t < t_2 - \varepsilon \\ u_{1,i}^{-}(\mathbf{x}_0', \mathbf{x}_0'', t, t_2) & t \geqslant t_2 - \varepsilon \end{cases}, \tag{43}$$

where v_1^- and u_1^- are similar to the projected Green's function and ... Marchenko scheme in van der Neut and Wapenaar (2016). The minus superscript in 42 and 43 refers to upgoing wavefields at $\mathbf{x}_0'$. To solve the MME equation 37 ... v_1^- ... compensation is not needed. The M ... terms at $t \geqslant t_2 - \varepsilon$ are used to solve the Marchenko e[quation] ... compute at t_2 a u_1^-. The solution of the MME scheme is v_1^- at $t = t_2$ collected fro[m] ... Similarly for the summation of the terms in equation 41, a following function is defined

$$k_{1,i}^{+}(\mathbf{x}_0', \mathbf{x}_0'', t, t_2) = \int_{t'=0}^{+\infty} \int_{\partial \mathbb{D}_0} R(\mathbf{x}_0', \mathbf{x}_0, -t') v_{1,i}^{-}(\mathbf{x}_0, \mathbf{x}_0'', t - t', t_2) \mathrm{d}t' \mathrm{d}\mathbf{x}_0. \tag{44}$$

$$v_{1,i}^{+}(\mathbf{x}_0''', \mathbf{x}_0'', t, t_2) = \sum_{m=1}^{i} \int_{t''=0}^{+\infty} \int_{\partial \mathbb{D}_0} R(\mathbf{x}_0, \mathbf{x}_0''', t'') H(t' - t + t_2 - t'' - \varepsilon) \times \\ M_{2(m-1)}(\mathbf{x}_0, \mathbf{x}_0'', t + t'', t_2) \mathrm{d}\mathbf{x}_0 \mathrm{d}t'', \tag{45}$$

Equation 44 (a) can be further split in the time domain as follows;

$$k_{1,i}^{+}(\mathbf{x}_0''', \mathbf{x}_0'', t, t_2) = \begin{cases} v_{1,i}^{+}(\mathbf{x}_0''', \mathbf{x}_0'', t, t_2) & t < t_2 - \varepsilon \\ u_{1,i}^{+}(\mathbf{x}_0''', \mathbf{x}_0'', t, t_2) & t \geqslant t_2 - \varepsilon \end{cases}, \tag{46}$$

where v_1^+ is similar to the projected focusing function in the reg[ular scheme of] van der Neut and Wapenaar (2016). v_1^+ and the multiple annihilator is created and t[he] ... numerical examples 4 ... only $\varepsilon < t_2 - \varepsilon$ ... The plus superscript in 44 refers to downgoing wavefields. To solve the MME Marchenko ... v_1^+ ... defined for illustration purposes to explain the mechanism o[f] ...

Time t_2 is the instant two-way travel-time where the solution o
The primary reflection for every time t_2 is collected in $\bar{v}_1$. This is a computational e
way, since only one sample is collected in the output. Never
implemented without any human interaction or model informa
one sample around t_2, and it can take bigger time steps, but the num
around t_2 must take into consideration the frequency bandwidth o
by examples in the detailed discussion of the implementatio
algorithm.
In this MME scheme the primary is collected from the origina
removes all overlapping internal multiples from earlier re
the physical reflection amplitude as present in the data.

Both internal multiple reflections and transmission losses
the Transmission-compensated Marchenko ... Zhang et al. (2019) ... eliminat
The equation is given by

$$R_r(\mathbf{x}_0', \mathbf{x}_0'', t = t_2) = R(\mathbf{x}_0', \mathbf{x}_0'', t = t_2) + \sum_{m=1}^{\infty} \bar{M}_{2m}(\mathbf{x}_0', \mathbf{x}_0'', t = t_2, t_2), \qquad (47)$$

with

$$\begin{aligned} \bar{M}_{2m}(\mathbf{x}_0', \mathbf{x}_0'', t, t_2) = & \int_{t'=0}^{+\infty} \int_{\partial \mathbb{D}_0} R(\mathbf{x}_0''', \mathbf{x}_0', t') H(t - t' + \varepsilon) \mathrm{d}\mathbf{x}_0''' \mathrm{d}t' \times \\ & \int_{t''=0}^{+\infty} \int_{\partial \mathbb{D}_0} R(\mathbf{x}_0, \mathbf{x}_0''', t'') H(t' - t + t_2 - t'' + \varepsilon) \\ & \bar{M}_{2(m-1)}(\mathbf{x}_0, \mathbf{x}_0'', t - t' + t'', t_2) \mathrm{d}\mathbf{x}_0 \mathrm{d}t'' \end{aligned} \qquad (48)$$

and

$$\bar{M}_0(\mathbf{x}_0', \mathbf{x}_0'', t, t_2) = -(H(t + t_2 + \varepsilon) - H(t + \varepsilon)) R(\mathbf{x}_0', \mathbf{x}_0'', -t), \qquad (49)$$

where R_r denotes the retrieved dataset without internal multip
primary reflections. The truncation window in equation 48 is different from the window in equation 38, ... window in
which guarantees that the second term in equation 47 on the right-hand side both ... internal
reflections and transmission losses. In the primary reflection equation 48 ...
$\bar{M}_{2(m-1)}$ does not have a contribution for values of $t'' - t + t' > t_2 + \varepsilon$ ... in equation 41 ... equation
t_2 is now part of the integration and $\bar{M}_{2m}$ ... is defined in equation 49 ...
measured reflection response is the only input to solve the T
The primary reflection is, different than $\bar{v}_1$ in the MME scheme, ...
transmission compensation. The matrices $\bar{k}_1$, $\bar{v}_1$ ... are no longer ... $\bar{M}_{2m}$ ... of a
scheme is applied for every time instant t_2 and has the same advantages and disadva
scheme. In the T-MME scheme the amplitude of the primary is a
because it is the only way to predict and attenuate internal
We come back to this remark in the explanation of Figure 13
Both MME and T-MME schemes use the measured reflection response R as input. The reflect
response R needs to be deconvolved for the source-wavelet and the
must be removed. The output of a surface-related multiple el... Verschuur et al. (1992) ...
scheme can meet these requirements. Diffracted and refracte
schemes and a detailed analysis about limitations can ... Zhang et al. (2019).

The basic Marchenko algorithm (MME) ... is explained in Algorithm 2. The arrays ...
stored in C-order; the last (most right) addressed dimensi
dimensions of these arrays ... [...] ... function ca
regular (...) brackets. The data input of the algorithm is R the measured

Main

Read SU-style input parameters

Initialization, reading of input parameters and allocat

READ($R[N_{shots}, i\omega, N_{recv}]$)

$DD[N_{recv}, it] = \mathcal{F}^{-1}\{R^*[j, i\omega, N_{recv}]\}$

$ii \leftarrow istart$ $iend$

$$M_0[N_{recv}, it] = \begin{cases} 0 & 0 < it < n_t - ii + n_\varepsilon \\ -DD[N_{recv}, it] & n_t - ii + n_\varepsilon \leqslant it < n_t \end{cases}$$

$k^-_{1,0}[N_{shots}, it] = DD[N_{recv}, n_t - it]$

$v^+_{1,i}[N_{shots}, it] = 0$

$i \leftarrow 0$ n_i

synthesis(R, M_i, RM_i)

$M_{i+1}[N_{shots}, it] = RM_i[N_{shots}, n_t - it]$

(i % 2 == 0)

$M_{i+1}[N_{shots}, it] = 0; \quad ii - n_\varepsilon < it < n_t$

$v^+_{1,i+1}[N_{shots}, it] = v^+_{1,i}[N_{shots}, it] + M_{i+1}[N_{shots}, it]$

$k^-_{1,i+1}[N_{shots}, it] = k^-_{1,i}[N_{shots}, it] - M_{i+1}[N_{shots}, n_t - it]$

$M_{i+1}[N_{shots}, it] = 0; \quad 0 < it < n_t - ii + n_\varepsilon$

$R_t[j, N_{shots}, ii] = k^-_{1,n_i}[N_{shots}, ii]$

Basic Marchenko algorithm, without transmission [...] mented in the provided source code. The integer ii, that runs from sample number $istart$ to $iend$, represents $t = it * \Delta t$. The number of recorded time samples is n_t, the time sample position of the source is $\varepsilon = n_\varepsilon * \Delta t$ and time sample ii represents $t_2 = ii * \Delta t$. The number of receivers N_{recv} and number of shots N_{shots}. The loop represents the number of Marchenko iterations n_i. Note that the samples $n_t - it$ represent negative time $-t$.

reflection data must be properly pre-processed as explained in Brackenhoff (2016). The pre-processing must take care of the following:

- Elimination of free-surface multiples. Note that there is also a very similar Marchenko algorithm [...] multiples Ravasi (2017). [...] discusses a redatuming algorithm Singh et al. (2015) [...] similar [...] and requires a smooth model. Zhang and Slob (2019) [...] while all multiples [...] does not need any model information.
- Sufficient (i.e. alias free) sampling in the spatial receiver [...] Note, there are Marchenko-based methods that can fill in m[...] under the assumption that the [...] Wapenaar and van IJsseldijk (2020) [...]
- Compensate for dissipation.
- Shot amplitude regularization.
- Deconvolution for source wavelet.

Following Algorithm 2, the pre-processed reflection data is read from disk [...] $\mathcal{F}\{...\}$) to the frequency domain ($i\omega$) and all shots and receivers are stored [...] step in the algorithm and the only significant data read. One [...] (j) where we want to suppress the internal multiples from, is se[...] step. This shot record is transformed back to time, (R^*) [...] DD in time reversed [...]

frst loop in the algorithm loops over the selected number of
internal multiples. Typically this represents all samples
the number of samples to the frst refection event in the sel
ii the iterative Marchenko algorithm is executed. The larges
in Thorbeck et al. (2017) is that time-truncation along the frst arriva
subsurface) is replaced by a constant time-truncation and t
needed anymore. The initial M_0 is formed from the shot record which we
would like to attenuate (DD). M_0 is a copy of the time-reversed sh
equation (39) and set to zero from the $n_t - ii + n_\epsilon$ sample, where n_t is the total number
of samples in the shot record. n_ϵ takes the extra samples of time duratio
to exclude a possible ii. The initial $k^-_{1,0}$ is a time complete (no time-m
is carried out) copy of the shot record that still contains a
With these two initializations the iterations of the Marche
updated feld M_i is computed by RM_i. This integration process is ca
produces the output RM_i, as explained in more detail below. Depend
i, being odd or even, diferent time muting on RM_i and two components are use
an update M_{i+1}. For even iterations the time samples between $ii - n_\epsilon$ and n_t are set to zero and for
iterations the time samples between 0 and $ii + n_\epsilon$ are set to zero. Only $k^-_{1,i}$ is updated with thi
the unmuted M_{i+1}. In this update $k^-_{1,i}$ internal multiples are attenuated. This i
update represents (37) where equation M_{2m} points at the fact one even and one odd
the implemented Marchenko algorithm, $2m-1$ and equation (42) since the notatio
In the regular redatuming Marchenko algorithm (Thorbeck et al., 2017) the truncation windows
the frst arrival time of a focal point in the subsurface. In
rithm, the focal point is projected on the surface and the t
constant time. The fat time window has the big advantage th
data-informed. Meles et al. (2020) demonstrate that in the application of
algorithm to dipping plane waves a time truncation consiste
Depending on the position of strong refectors typically, 10
time sample ii in the selected shot record. The presence of strong re
convergence slow at large times (20). This is the reason, as shown in Figure, higher-or
are attenuated with even v^-_1 and that are removed again later whe
multiple is fnally removed by a converged multiple attenuato
all multiples are removed and hence all earlier higher-orde
Once the iterations are fnished for ii the output of v^-_1 is stored in sample
sample ii in the multiple free R_t, the fnal output of the program that re
shot record with attenuated internal multiples. It is a com
equations for each sample ii in the shot records. A faster algorithm (10-20x) implem
Algorithm 2.
In Algorithm 3, after the Marchenko equations for $ii-1$ are solved the next time sample ii
is initialized with the result $ii-1$ (Zhang and Slob, 2020). The idea is that to re
the internal multiples at the next time sample there is no n
multiples that were already removed in the previous time-sa
attenuated multiples need to be attenuated plus one (or a fe
new time sample only the multiples have to be removed that we
deviation from the previous results and usually 2 iteratio
the next time sample. In the fast algorithm the initial M_0 is the diference be
(DD) and $k^{-(ii-1)}_{1,n_i}$; the already estimated internal multiples at $ii-1$. The initial $k^-_{1,0}$ is from t
is the previous result $k^{-(ii-1)}_{1,n_i}$. With these initializations RM_i contains only a small
correction, since it is based on a converged previous resul
get the complete internal multiple M_{i+1}, DD is added to RM_i (Zhang and Slob, 2020).
In this fast algorithm only one pair of even-odd iterations i
could solve the equations only one time and use that result t
models of numerically modeled data this works fne indeed. Ho
of numerically modeled data and on feld data we have to do a fu
and the speed-up of the faster algorithm is limited to one o
we would advise to begin with the basic algorithm and then ve

speed-up the computations. The reason for this limited use
data-sets and a large number of iterations, artifacts, for
get amplifed. The primary refections will still converge,
in the algorithm and can diverge. In the iterative scheme ea
computed result based on for example 30 iterations. With 10
and can cause artifacts being amplifed to signal level.
In the algorithm we solve the Marchenko equation for ii. From the theory we know
the first event in ii is a primary refector (all multiple refectio
before ii are removed by the scheme). Hence, in a number of samples
of internal multiples. We can make the Marchenko scheme ii result for
samples (n_ε at a time), since that is the time resolution we are a
ii. This can speed-up the code by (n_ε typically 20). This is similar to the fa
without making any iterations and directly use the previous

```
Main
  Read SU-style input parameters
  Initialization, reading of input parameters and allocat
  READ( R[N_shots, iω, N_recv] )
  DD[N_recv, it] = F^{-1}{R*[j, iω, N_recv]}
  ii ← istart   iend
    k^-_{1,0}[N_shots, it] = k^{-,(ii-1)}_{1,n_i}[N_shots, it]
    M_0[N_shots, it] = { 0                                                    0 < it < n_t - ii + n_ε
                       { DD[N_shots, n_t - it] - k^-_{1,0}[N_shots, n_t - it]   n_t - ii + n_ε ⩽ it < n_t
    i ← 0   n_i
      synthesis( R, M_i, RM_i )
      M_{i+1}[N_shots, it] = RM_i[N_shots, n_t - it]
      ( i % 2 == 0 )
        M_{i+1}[N_shots, it] = 0;   ii - n_ε < it < n_t

        M_{i+1}[N_shots, it] = M_{i+1}[N_shots, it] - DD[N_recv, it]
        k^-_{1,i+1}[N_shots, it] = -M_{i+1}[N_shots, n_t - it]
        M_{i+1}[N_shots, it] = 0;   0 < it < n_t - ii + n_ε

    R_t[j, N_shots, ii] = k^-_{1,n_i}[N_shots, ii]
```

Faster Marchenko algorithm that uses $ii-1$ previous resu
($k^{-,(ii-1)}_{1,n_i}$) as input for the current time instant ii.

The synthesis process is shown in Algorithm 4 and computes the second integrant in the
equation 3.8. The synthesis function is a straightforward matrix
data are stored in such a way that the most inner loop, that s
shot, is contiguous in memory. To speed-up the computationa
the outer N_{shots} loop. An alternative implementation of the synthes
loop the outer loop and use a BLAS function to compute the matrix-vector
implementation will also be eﬀ cient when all shots are compu
matrix function becomes the kernel of the synthesis process
the integration is carried out over the number of receivers
at the shot position. Thus N_{shots} output traces are computed.
From a computational point of view the transmission compens
the MME algorithm, except for the application of the time-t
the wavelet (n_ε) is applied in the opposite time direction for the T

synthesis($R[N_{shots}, i\omega, N_{recv}), M[N_{shots}, it], RM[N_{shots}, it]$)

$Fop[i\omega, N_{shots}] = \mathcal{F}\{M[N_{shots}, it]\}$
$RM[N_{shots}, t] = 0$
#pragma omp parallel for
$k \leftarrow 0$ N_{shots}
$i\omega \leftarrow \omega_{min}$ ω_{max}
$i \leftarrow 0$ N_{recv}
$sum[i\omega] = sum[i\omega] + R[k, i\omega, i] * Fop[i\omega, i]$

$RM[k, it] = \mathcal{F}^{-1}\{sum[i\omega]\}$

Marchenko synthesis kernel with $i\omega = i * \Delta\omega \; (= \frac{2\pi}{n_t * \Delta t})$.

of n_ε in the MME algorithm take into account the possible overlap of the events ... instant it in the initialization M_i. Suppose that it is the two-way traveltime ... refector (13a). The reflection of the M_i ... in the MME algorithm (Figure 13a), but in $\bar{M}_i$ ... in the T-MME algorithm (Figure 13b). In the T-MME algorithm the event at instant it ... updated in the MME algorithm the r... from the original shot $\bar{v}_1^-$. When there is ... between two ref... then there is no diference between the MME and T-MME (Figure 13c) ... the MM... scheme.

To get to the T-MME scheme ... Algorithm ... in the ... $-n_\varepsilon$ ... time ... $-n_\varepsilon$. The R_t ... R_r that contains the transmission compensated pr...

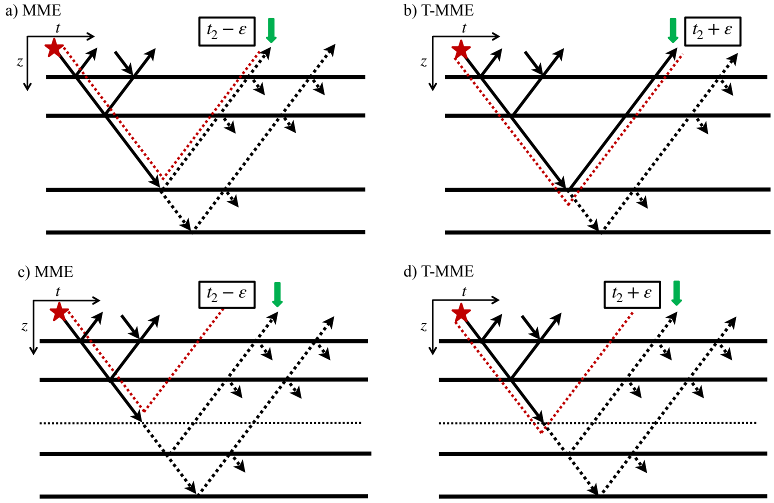

Figure 13: Comparison of the MME and and T-MME schemes. Figures a ... t_2 equal to the two-way traveltime of the third refector. The ... a red dotted line. The dotted lines ... M_i ... in M_i, after application of the time window. Figures c) and d)

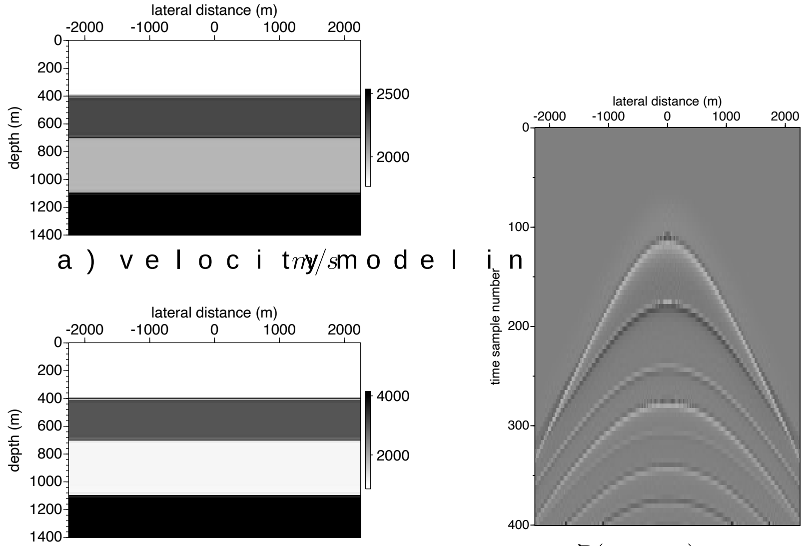

a) velocity model in m/s

b) density model in kg/m^3

c) $R(\mathbf{x}_R, \mathbf{x}, t)$

Figure 14: Four layer model with velocity (a) and density (b) par[ameters] ... position $\mathbf{x}_i = (x = 0, z = 0)$ and receiver $\mathbf{x}_R = (x = x_R, z = 0)$ (c). The source wavelet in R has a flat frequency spectrum from 5 to 90 Hz.

The Marchenko algorithm is illustrated with a 1.5-dimension[al] ... 14. The numerical modeling is carried out with a finite-difference ... (Thorbecke and Draganov, 2011) that is also included in the software package. The ... the reflection response $R(\mathbf{x}_0'', \mathbf{x}_0', t)$ is approximately a sinc-function with a f[lat spectrum] between f_{min} and f_{max} ($5 - 90$ Hz) to represent a deconvolved source wavel[et] ... program for $R(\mathbf{x}_0'', \mathbf{x}_0', t)$ a source of vertical force is chosen. The re[ceivers are at] $z = 0$ and measure the pressure field. A fixed spread ... -2250 to 2250 m ... distance between the 901 sources ... 5 m. The receiver positions ... interval of 4 ms and 1024 recorded time samples.

Figure 15 demonstrates the first iteration ... M_1 for time sample number 276 (t = 1.100 s). Time sample 276 corresponds to the zero- ... third reflector. In this first step a shot record R ... shot record. In our example we ... $R_0(\mathbf{x}_R, x = 0, t)$ ... shot record; Before the correlation is carried out the selected shot rec[ord] ... $276 - n_\varepsilon$, multiplied by -1 and time reversed $M_0(t)$ in equation 39 ... Figure 15 the shot record is convolved with a Ricker wavelet to redu[ce] ... (deconvolved) wavelet R (Figure 15 ...). The number n_ε ... $n_\varepsilon = 20$ samples excludes the reflection from ... M_0 ... Figure 15 middle ... R (Figure 15a, where we used source receiver reciprocity) ... $M_0(-t)$ (Figure 15b) correlated to give the result ... The events in Figure 15 ... the first and second reflector ... first internal multiple between the first and second reflector ... the auto-correlation of the ... $t = 0$ ... at the bottom of the panel). Note that the long train of events ... 15 can interfere with events at the end of the time axis. To o[vercome] ... pad the time axis with zeros before the transformation to th[e] ... computed.

The correlation result is time ... 15 ... three events in Figure 15 ... originate from correlation with the ...

the first three events ($\mathbf{r_1}, \mathbf{r_2}, \mathbf{m_1}$) in the shot record. According to [41] to obtain integr…
an output M_1 the traces in Figure [15] are summed together. The stationary …
in Figure [15] give a contribution in the result of the summation. Be…
events (both in time and space) give unwanted contributions …
The integration result is set to zero for samples larger than $276 - n_\varepsilon$ and at … par…
(the middle M_1 trace shown in Figure [15]). In Figure [15] the truncation appears to be a…
but that is the result of the [15] shift upward in time with the arrival tim…
truncation $276 - n_\varepsilon$ is indicated with a dotted line. There are two…
a few linear artifacts. The first hyperbolic event originates from $\mathbf{r_2^*.r_1}$ and …
$\mathbf{m_1^*.r_2}$, and the second hyperbolic event from the $\mathbf{c_2} = \mathbf{m_1^*.r_1}$ internal …
The linear events are unwanted artifacts due to truncation a…
taper at the truncation boundaries in time and space.

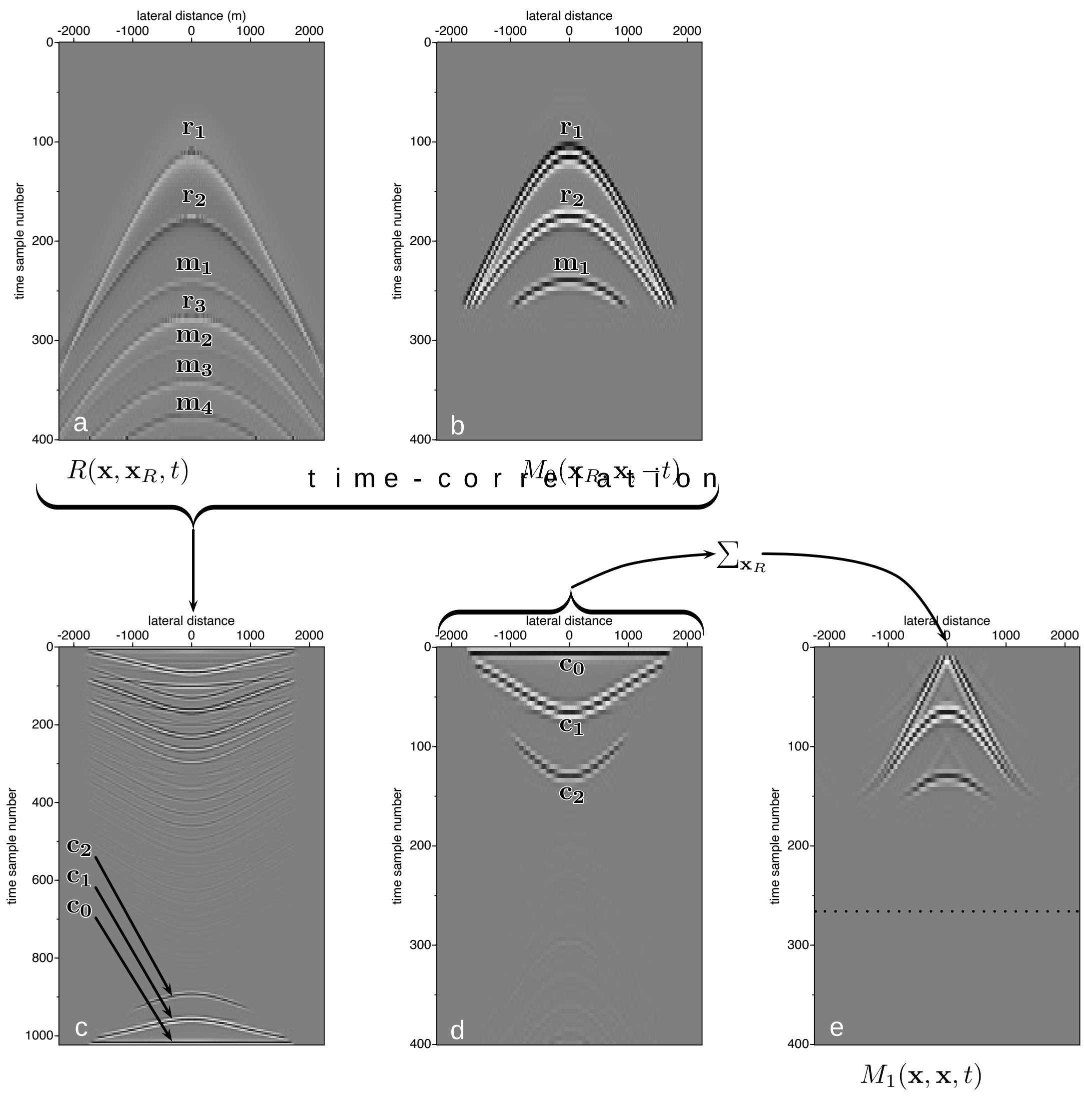

Figure 15: Computational steps to compute M_1 from M_0 at time sample number 276. The m…
record R is shown in (a); time $276 - n_\varepsilon$, and convolved with a Ricke…
it gives M_0 (b). Time-correlation of (a) with (b) gives (c). Af…
time window again gives (d). The traces in (d) are summed to…
events above sample $276 - n_\varepsilon$ will end-up in the middle trace of M_1 (e). The mute window t_ε samples later
than $t = 0$ is needed to mute the autocorrelation of the first event m_i in the … refector m_l and … 'th multiple. In (c) the labeled correlated ev… $\mathbf{c_0} = \mathbf{r_1^*.r_1} + \mathbf{r_2^*.r_2} + \mathbf{m_1^*.m_1}$,
$\mathbf{c_1} = \mathbf{r_2^*.r_1} + \mathbf{m_1^*.r_2}$, and $\mathbf{c_2} = \mathbf{m_1^*.r_1}$.

Figure 16 demonstrates the computation of M_2 from M_1 (Figure 15) for the second iteration according to equation 40 with $m = 1$. The reflection data (Figure 16a) are convolved with M_1 (Figure 16b) that contains three main events: a_1 and two correlation artifacts c_1 and c_2. The results (Convolving M_1 with the middle shot record R gives Figure 16c. The hyperbolic events are now back at the same times as reflection events in the sho M_1 also convolves with R and introduces many (mostly linear) artifact reversed in time (Figure 16d). After the integration in equation 40 over the lateral coordin x_R becomes the middle M_2 (Figure 16e). Most of the linear artifacts are re to the destructive interference in the integration. $a_2 = r_1.a_1$ in M_2. The only th first term in the sum of equation 37 is now computed in M_2. The last events in M_2, the time re presented in Figure 16, will already attenuate the multiple event m_1.

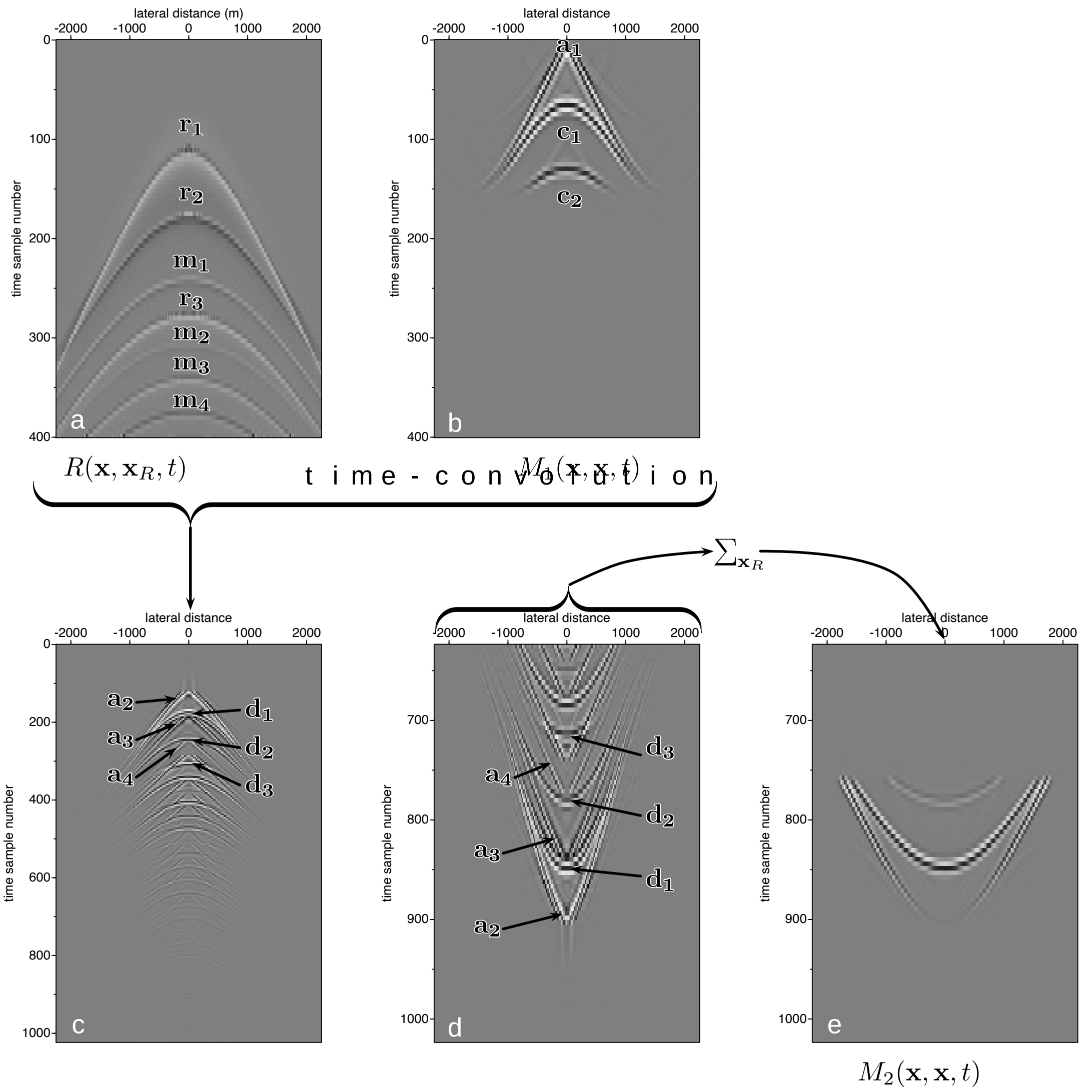

Figure 16: Computational steps to compute $M_2(\mathbf{x},\mathbf{x},t)$ from M_1 at time sample number 276. Th shot record R is shown in (a) and M_1 truncated after sample 276 (Figure 15) is comput (b). Time-convolution of (a) with (b) gives (c). After time- again gives (d). The traces in (d) are summed together and o $n_t - 276 + n_\varepsilon$ end-up in the middle of M_2 (e). The labeled events r_l indicate the l'th reflec the l'th multiple m_l and a_n the n'th artifact. The labeled events in (a) are from the R and from the M_1 (b) are $\mathbf{a_2} = \mathbf{r_1}.\mathbf{a_1}, \mathbf{a_3} = \mathbf{r_2}.\mathbf{a_1}, \mathbf{a_4} = \mathbf{m_1}.\mathbf{a_1}, \mathbf{d_1} = \mathbf{r_1}.\mathbf{c_1}, \mathbf{d_2} = \mathbf{r_1}.\mathbf{c_2} + \mathbf{r_2}.\mathbf{c_1}$ and $\mathbf{d_3} = \mathbf{r_2}.\mathbf{c_2} + \mathbf{m_1}.\mathbf{c_1}$.

To compute M_i (in general odd number i), M_{i-1} ... updates are shifted backward lation) with the time ... M_0. To compute the ... M_2 (events numbered up to M_i) ... M_1, ... s to events are shifted forward (convolution) in time. The even... the scheme. Each event M_i ... v_1^+, ... and ... updated ... M_i and k_1^-. The updates ... scheme reverts the time-axis for each iteration, hence the ... switches also. These time windows ... 276 ... shown in Figure 17 ... these time window... smooth cosine shaped transition zone is used to reduce the t...

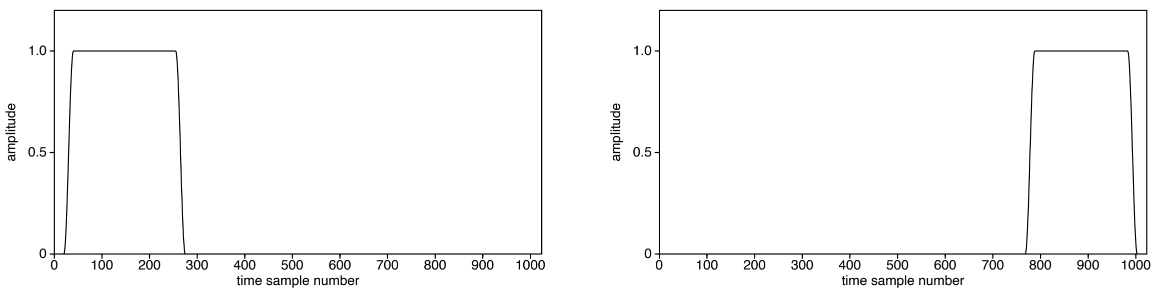

a) Time-window for even iteration number   b) Time-window for odd iteration number

Figure 17: Time-window functions in the Marchenko scheme with a ... zone. This transition zone has $0.5n_\varepsilon$ samples and ... n_ε ... sampling ...

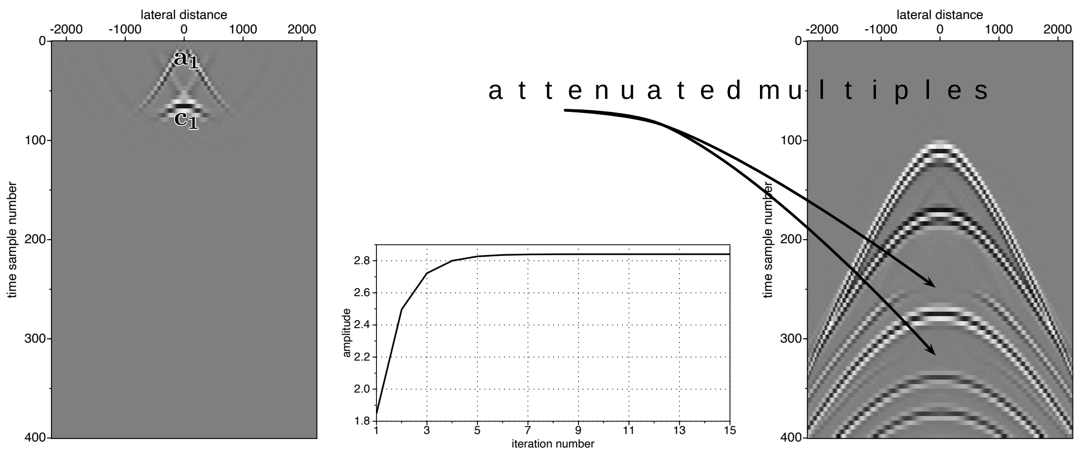

a) $v_{1,1}^+(t)$ b) Convergence of c_1 c) $k_{1,30}^-(t)$

Figure 18: Creation of the event c_1 that (almost) annihilates all the internal m... first and second reflector ... a_1 ... of $v_{1,1}^+(t)$ ... Picture a) s... Marchenko iteration ... $ii = 200$ sample number ... The convergence of the maximum c_1 is shown as function of the iteration count ... Figure c) shows $k_{1,30}^-(t)$ after 30 iterations.

The results in Figure 18 are partial solutions of the Marchenko equati... $ii = 200$. After applying the time window to M_0, ... zero ... $200 - n_\varepsilon$ ... the samples i... no internal multiple reflect... M_0. The time ... between sample 0 and ... sample 2... m_2 and m_1, but not see Figure 15. In the first iteration v_1^+ ... according to equation 44 ... extra event (Figure 18a) c_1 is created to correct for the amplitude of k_1^-. Note that the time window in Figure 18a appears to be around sample 80, but thi... applied ... M_0 is shifted by the correlation to negative times and ti... event c_1 converges to the amplitude that can annihilate the ampl... converged v_1^+ and the reflection data ... equation 40 ... all multiples aris...

between the first and second reflector will [37]. The scheme in this method
without ever having 'seen' r_1 and r_2 the multiple, a reflection event that
all the internal multiples between the [18], the first $k^-_{1,30}(t)$ columns. The ar
computed according to equation [42], the multiples that are already p
are only partly removed because r_2 is only used as a sample of 200 and Repeat
scheme for samples larger than 200 r_1 and r_2 will attenuate all the angles of the
offsets for all internal multiples between r_1 and r_2.

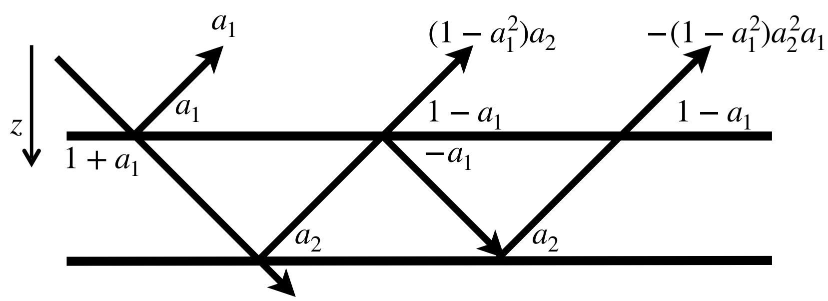

Figure 19: Sketch of the ray-paths and reflection and transmissio
velocity and variable density model. The local reflection co
a_1 and a_2 respectively.

For the investigation of the v_1^+ amplitudes, for the sake of argum
reflection coefficient is a constant [15]. The primary reflections co
a_1, a_2 for respectively $\mathbf{r}_1, \mathbf{r}_2$. We consider the first [18] columns of the truncation in Figure
200 that only creates v_1^+. We determine that after sufficient i
in v_1^+ has converged to an amplitude that can cancel the first-or
multiples related to the M_0 event. For simplicity, r_1, r_2 have reflectio
amplitude:

$$r_1^a = a_1, \tag{50}$$

$$r_2^a = (1-a_1^2)a_2. \tag{51}$$

Figure [19] gives a sketch of the reflection paths and reflection and t
reflector case. According to equation [41], M_0 is correlated with R and integrated
over the receiver coordinate. After applying the time window, M_1
$\mathbf{c}_1 = \mathbf{r}_2^*.\mathbf{r}_1$ in Figure [19] with amplitude:

$$c^a_{1,1} = a_1(1-a_1^2)a_2. \tag{52}$$

The second subscript in $c^a_{1,1}$ indicates the iteration number R in. The next is
iteration (according to equation [40]) after time windowing, $\mathbf{r}_1.\mathbf{c}_1$ remains only as the event
of the reflection of the second reflector with amplitude

$$c^a_{1,2} = a_1^2(1-a_1^2)a_2. \tag{53}$$

In each next iteration, alternating equation [41] and [40], the multiple is attenuated with a_1
in general for iteration i we have

$$c^a_{1,i} = (a_1)^i(1-a_1^2)a_2. \tag{54}$$

Summation of all iterations $c^a_{1,i}$ gives the final amplitude of the multiple in c_1
v_1^+. The initialization of v_1^+ and the summation of the odd terms lead

$$\begin{aligned}\sum_{i=0}^{n_i} c^a_{1,1+2i} &= \sum_{i=0}^{n_i}(a_1)^{1+2*i}(1-a_1^2)a_2,\\ &= a_1a_2 - a_1^3a_2 + a_1^3a_2 - a_1^5a_2 + a_1^5a_2 - a_1^7a_2 + \ldots \\ &\approx a_1a_2.\end{aligned} \tag{55}$$

Application of v_1^+ to the data creates multiple events u_1^- as shown in Figure 18. The
The first-order internal multiple from the first and second c_1 in Figure 18a, the multi
amplitude $a_1 a_2$, will meet each other in time just below the first re
annihilator cancels the first-order downgoing internal mult
To be able to cancel the first downgoing internal multiple the
as that event. The first m_1 in Figure 15 has the amplitude

$$m_1^a = -(1-a_1^2)a_2^2 a_1. \tag{56}$$

After convergence of the scheme c_1 is convolved with the reflector
$\mathbf{r}_2$ or R in the next iteration and m_1 has the same amplitude as m_1^a

$$\begin{aligned} c_1^a r_2^a &= a_1 a_2 . r_2^a, \\ &= (1-a_1^2)a_2^2 a_1. \end{aligned} \tag{57}$$

This result is added to the data m_0, as shown in Figure 18 and equation
37. Furthermore, $\mathbf{c}_1$ convolution with m_1 after the annihilator of the seco
$\mathbf{c}_1$ will automatically annihilate all higher-order multiples
To complete the amplitude analysis, the $\bar{n}_1^-$ (from the equation
equation 43 for the T-MME scheme) can be computed from equation 48 and according to
the even amplitude 54. The time $\bar{a}_1$ is at the time of reversed shot D
in Algorithm 2). Summation of $c_{1,i}^a$ at the time of the second reflect
final amplitude for the second reflector in $\bar{v}_1^-$

$$\begin{aligned} a_2 =& (1-a_1^2)a_2 + \sum_{i=1}^{n_i} a_1^{2*i}(1-a_1^2)a_2 \\ =& a_2 - a_1^2 a_2 + a_1^2 a_2 - a_1^4 a_2 + a_1^4 a_2 - a_1^6 a_2 + \ldots \\ \approx& a_2. \end{aligned} \tag{58}$$

This shows that the transmission compensation is implemented in v_1^-
in the T-MME scheme. The approximation sign is due to a limit
implementation.
Figure 20 is obtained in the same way as Figure 18, but with high contrast layers. T
layers is the same as used in Figure 18, but the density contrast between the la
from a factor 3 (1000-3000) to 10 (500-5000). Compared to Figure 18
this high contrast means the higher-order terms will have large
media and require more iterations for convergence.

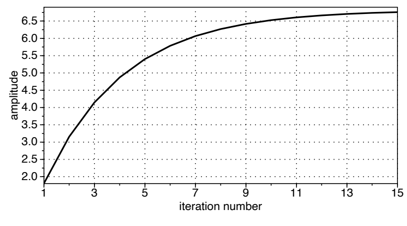

Figure 20: Convergence of the maximum amplitude c_1 in Figure 18a) after the annihilation of
all the internal multiples between the first and second refle

The first few iterations of M_i are shown in Figure 21. The truncation time is
at sample 276 and a first-order multiple of the second layer i M_0
after time-truncation. For higher numbers of iterations th
indicating that the scheme converges. All the updates show
amplitude of the events change during the iterations.

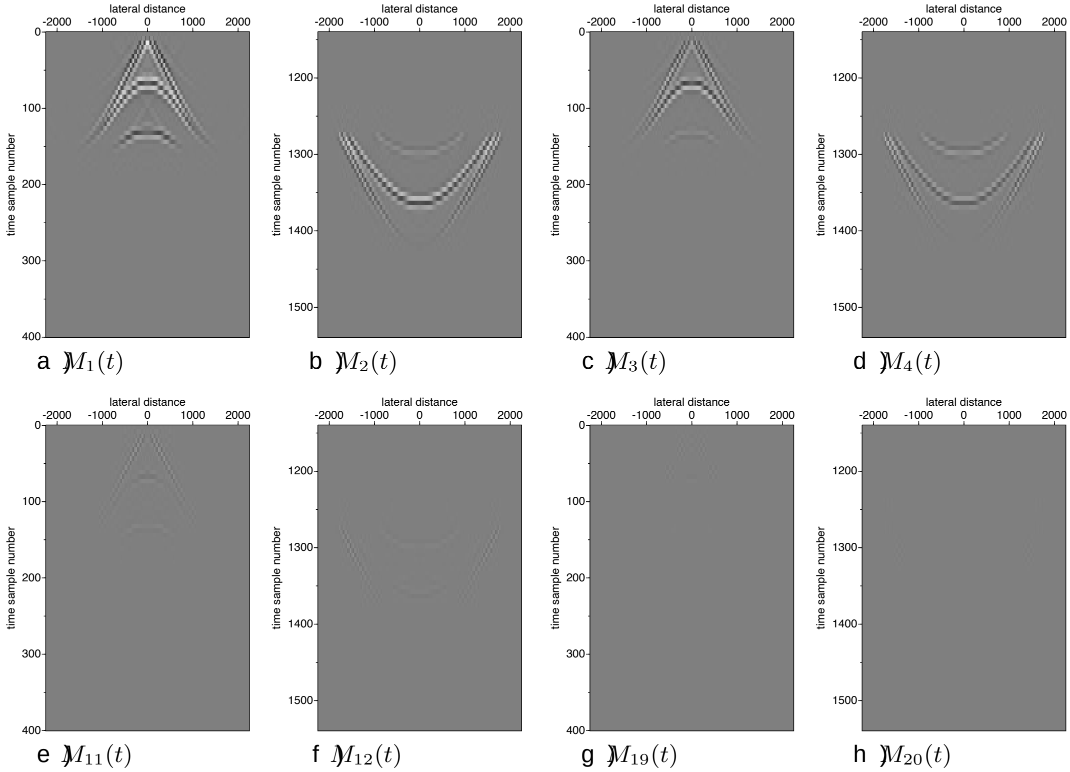

Figure 21: M_i fields for a focal time sample $i = 276$, the zero-offset arrival of the t
figures are plotted with the same clipping factor.

In the odd iterations $k^-_{1,i}(t)$ is the function computed with equation 4.2, updated with $M_i(t)$ the second and four selected iterations 22. After the first iteration Figure shows all order multi with incorrect amplitudes. In the following iterations the because the removal of the first-order multiple improves. Af (indicated with arrows) have further attenuated 22 and are not 22. The higher-order multiples do not have to be removed by a_1^+, but are removed automatically by removing the first-order multiple.

In Figure 22 one can observe that the first internal multiple (po attenuated beyond $276 - n_\varepsilon + 1$, but is not yet completely attenuated b $276 - n_\varepsilon$. The first $276 - n_\varepsilon$ samples below v_1^-, where the information on attenuation is constructed, with $276 - n_\varepsilon + 1$ samples forward from u_1^-, where the multiple is a attenuated. The constant-time cross-section $k^-_{1,i}$ at sample 276 is stored in the final output R_i at sample 276 of u_1^- part (between samples of k_1^- related 276 reflector) has its local reflection coefficient u_1^- amplitude at sample 276 with the physical amplitude with two-way transmission effects.

In Figure 23 the Marchenko equations are solved for different time investigation of g_1^- changes for larger sample numbers. It is observed also before i and beyond i related to internal multiples are a corresponds to the arrival time of the 23 and 23 direct reflector. The sample 276 and we do not observe a change in the number of events. Ho 23 a) to 276 (Figure 23 f) one can see that the multiple, arriving in tim reflector, gets more and more attenuated at larger and larger fast algorithm, to compute the solution in the next time sam a few iterations are sufficient to solve for the multiple atte

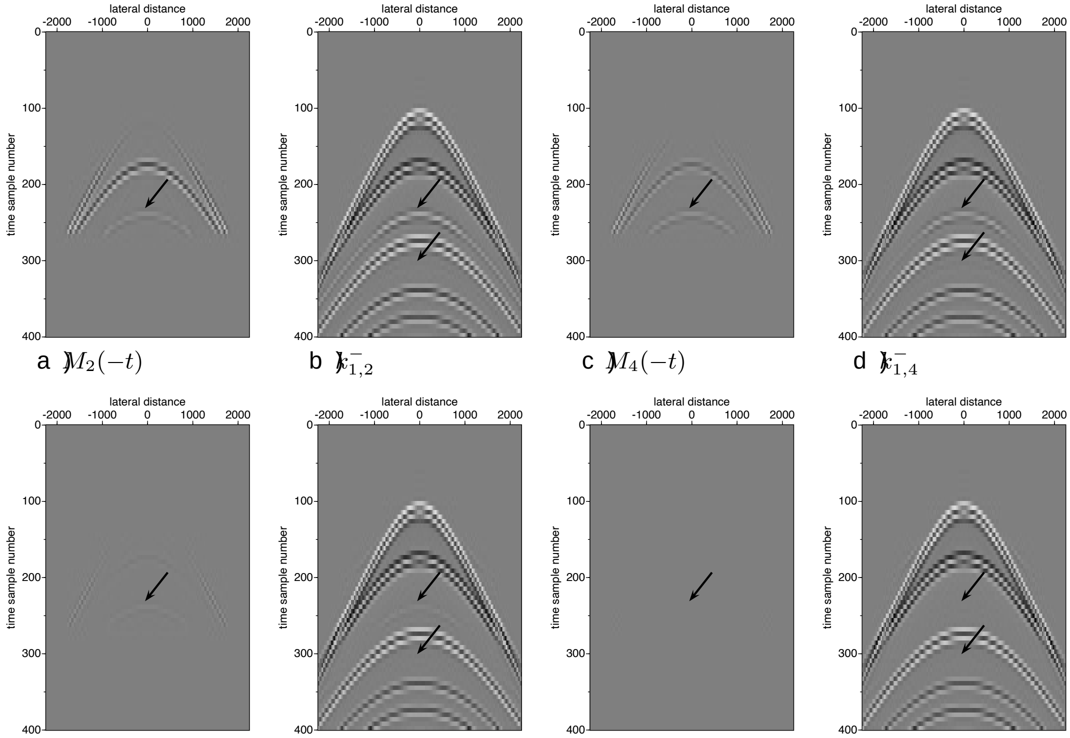

a) $M_2(-t)$ b) $k_{1,2}^-$ c) $M_4(-t)$ d) $k_{1,4}^-$

e) $M_{10}(-t)$ f) $k_{1,10}^-$ g) $M_{20}(-t)$ h) $k_{1,20}^-$

Figure 22: Updates of $k_{1,i}^-$ for a focal time at sample $t_2 = 276$ after i iterations. The arrow ind…
frst and second-order internal multiple between the frst an…

time m passes the arrival time of the third refector, a non-phy…
Figure 23a and 23b) appears just below the arrival time of the second re…
the annihilator a_1^+ that compensates all internal multiples creat…
refector. The cancelation of the internal multiples (Figures 23a and 23b), is obse…
all internal multiples related to the third refector are car…
Figure 24a and 24b sketches of the situation when the focal time at depth $\hat{z}$ is …
or below the third refector, respectively. The event that c…
the second refector (Figure 24a) coincides in travel time with the re…
refector and also compensates for the transmission loss of …
internal multiples related to the third refector (Figure 24a) are compe…
which coincides with the refection time of the third refecto…
refector (upward red arrow) and creates the non-physical re… (Figures 23a-23b)
pointed with an arrow.

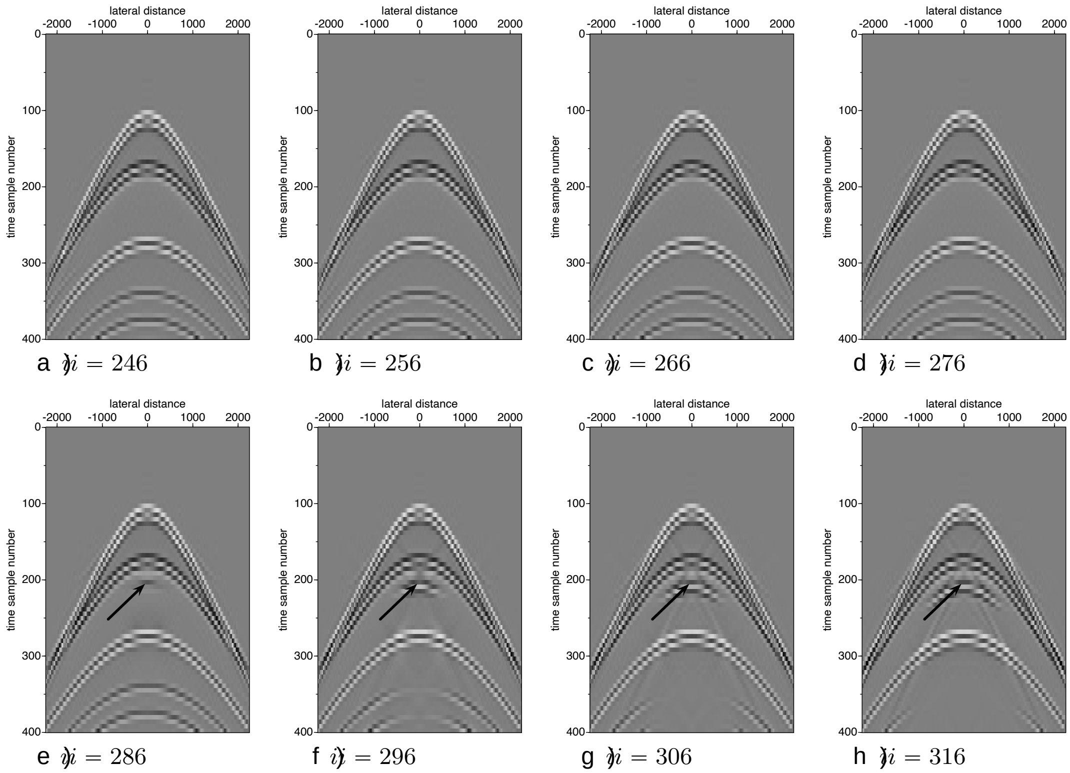

Figure 23: After 32 iterations with k_1 $i = 246$ to $i = 316$ with time steps of 10 sampl
From each panel a constant-time i cross section is selected as
multiple-free data. The arrows point to an event that compen
the second and third refector.

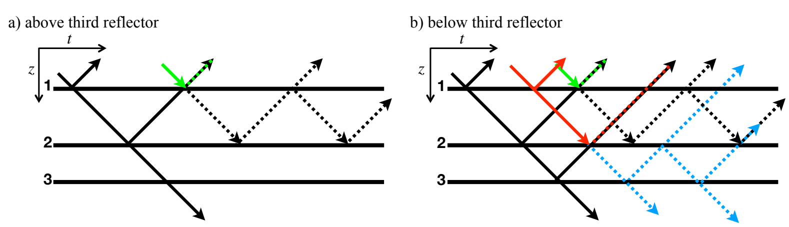

Figure 24: Compensation of internal multiples by events (colou
Marchenko method, applied for a point above (a) and below (b
are numbered from top to bottom.

Figures 25–25 show the same pictures as in Figures 21–28 show the same as Fig
22, 22, 22, 22, but now with the T-MME scheme (Zhang et al., 2018). The T-MME scheme for t
sample 276 includes the refection of the third reflector $276 + n_\varepsilon$. The factor, si
extra refector introduced in $\bar{M}_i$ ... $\bar{k}^-_{1,i}$ ... the non-physical primary,
second refector, is clearly visible in 25 ... after 2021 (at time instant F
instant 296). The diference is that in the T-MME scheme $t_2 + \varepsilon$ (sample 276 + 8) t
and the value at t_2 (time sample 276) $\bar{v}^-$ is exactly the right refection coe ci
in the fnal data output $R_r[276]$, while in the MME scheme ... truncation at $t_2 - \varepsilon$ starts a
(sample 296 - 8) at t_2 (time sample 296) $\bar{u}^-$ is the correct value for the ph
and is stored in the $R_t[296]$ data output (
In the example for the MME scheme 58 we have shown (in equation ... the second refector $\bar{v}_1^-$ from its physical amplitude to its loca
amplitude. It is exactly this feature that T-MME exploits.
arrival time of a refector there is a decision to be made whe
Setting the truncation time $t_2 - \varepsilon$ at t_2 is correctly $\bar{u}_1^-$ obtained. Changing the
truncation time $t_2 - \varepsilon$ to $t_2 + \varepsilon$, the time t_2 is correctly $\bar{v}_1^-$ obtained. In
is the time duration of the source wavelet that allows us to $t_2 - \varepsilon$ ...
is introduced in $\bar{v}_1^-$ and $\bar{u}_1^-$ is correct, whereas by taking $t_2 + \varepsilon$ ... $\bar{v}_1^-$ and $\bar{u}_1^-$ will
be correct at t_2.
The transmission compensated (T-MME) scheme retrieves pri
e cients, while in the regular (MME) scheme the primary ref
e cients that include transmission losses. The local refec
for a horizontally layered medium, but in laterally varying (Zhang et al.,
2019). The only computational diference between the T-MME and
time-truncation window.

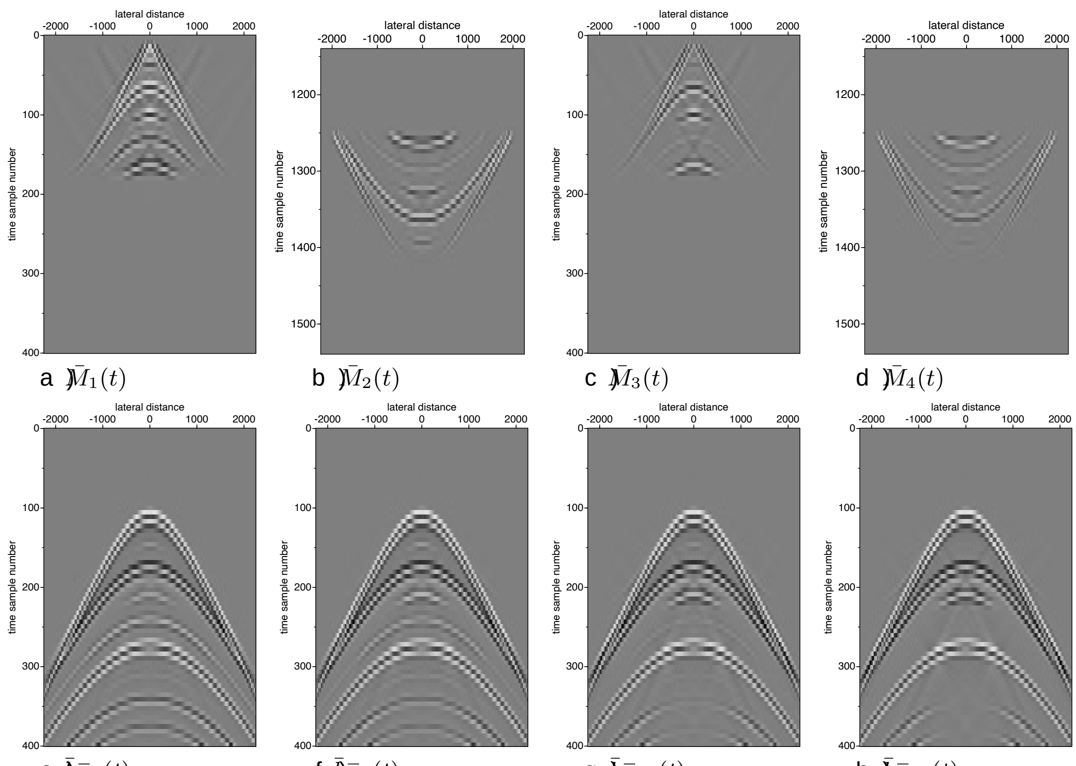

a) $\bar{M}_1(t)$ b) $\bar{M}_2(t)$ c) $\bar{M}_3(t)$ d) $\bar{M}_4(t)$

e) $\bar{k}^-_{1,2}(t)$ f) $\bar{k}^-_{1,4}(t)$ g) $\bar{k}^-_{1,10}(t)$ h) $\bar{k}^-_{1,20}(t)$

Figure 25: Panels (a)-(d) show the $\bar{M}_i$ for a focal time $t_2 = 276$ with the transmissi
compensated scheme T-MME after $i = 1, 2, 3, 4$ iterations. Panels (e)-(h) show t $\bar{k}^-_i$ for
focal time $t_2 = 276$ with the transmission compensated scheme T-MME after $i = 2, 4, 10, 20$
iterations. All fgures are plotted with the same clipping fa

marchenko_primaries

The program has the following parameters and opti

```
MARCHENKO_primaries - Iterative primary reflections retrieval

marchenko_primaries file_tinv= file_shot= [optional parameters]

Required parameters:

  file_shot= ............... Reflection response: R

Optional parameters:

 INTEGRATION
  ishot=nshots/2 ........... shot number(s) to remove internal multiple
  file_tinv= ............... shot-record to remove internal multiples
  file_src= ................ optional source wavelet to convolve select
 COMPUTATION
  tap=0 .................... lateral taper R_ishot(1), file_shot(2), o
  ntap=0 ................... number of taper points at boundaries
  fmin=0 ................... minimum frequency in the Fourier transform
  fmax=70 .................. maximum frequency in the Fourier transform
  plane_wave=0 ............. model plane wave
  src_angle=0 .............. angle with horizontal of plane source arra
  src_velo=1500 ............ velocity to use in src_angle definition
  t0=0.1 ................... time shift in plane-wave source wavelet fo
 MARCHENKO ITERATIONS
  niter=22 ................. number of iterations to initialize and res
  niterec=2 ................ number of iterations in recursive part of t
  niterskip=50 ............. restart scheme each niterskip samples with
  istart=20 ................ start sample of iterations for primaries
  iend=nt .................. end sample of iterations for primaries
 MUTE-WINDOW
  shift=20 ................. number of points to account for wavelet (ep
  smooth=shift/2 ........... number of points to smooth mute with cosine
 REFLECTION RESPONSE CORRECTION
  tsq=0.0 .................. scale factor n for t^n for true amplitude r
  Q=0.0 ......,............. Q correction factor
  f0=0.0 ................... ... for Q correction factor
  scale=2 .................. scale factor of R for summation of Mi with M
  pad=0 .................... amount of samples to pad the reflection ser
 OUTPUT DEFINITION
  file_rr= ................. output file with primary only shot record
  file_dd= ................. output file with input of the algorithm
  file_iter= ............... output file with -Mi(-t) for each iteratio
          ............... M0.su=M0 : initialisation of algorithm
          ............... RMi: iterative terms
          ............... k1min.su: k1min terms
  file_vplus= .............. output file with v+
  file_vmin= ............... output file with v-
  file_uplus= .............. output file with u+
  file_umin= ............... output file with u-
  file_update= ............. output file with updates only => removed in
  T=0 ...................... :1 compute transmission-losses compensate
  verbose=0 ................ silent option; >0 displays info


 author  : Lele Zhang & Jan Thorbecke : 2020
```

Defning writes for each iteration $-M_i(-t) = RM_i(t)$ the term in Algorithm
1 before applying the mute window. $k_{1,i}$ This is $v^{+}_{1,i}$ after the update. B
setting the option to 2 the energy of the focusing update term
and can be used to monitor the convergence of the scheme. When
the program writes the updates (= estimated primaries) can be p
useful when the (modeled) data does not have the correct amp
The parameter enables the fast algorithm when it is set large
value is run with iterations. If set to a value >1 the fast algorithm i
efect and the next iterations use iterations. After iterations

the scheme uses the full iterations to avoid possible cumulative num

amplifed artefacts. The scheme continues with iterations and t

itself. By setting the scheme does not do any new iterations in t

uses the result of the previous iteration. This setting will work to

≈ samples and is possible due to limited bandwidth of the d

The parameter is a switch to enable the T-MME algorithm. The

use plane-waves as input s Meles et al. (2018, 2020) as explained i

The commands to reproduce all fgures in this paper can be fou

The README_PRIMARIES in that directory explains in detail h

plicated (lateral varying) model can be found. This example

take several hours to compute the refection data and is not d

Besides the new Marchenko primaries removal program the pac

fnite diference modeling code, that is used to model all da

(Thorbecke and Draganov, 2011) and the standard Marchenko algorithm (Thorbecke et al., 2017). The

directory contains programs to calcula

and programs for basic processing steps.

This is mainly a copy of publication in Computers & Geosciences

Seismic imaging is a technique to image geological structur
wavefelds measured at the surface of the earth. The measured
activated and controlled sources such as air-guns or vibra
source of the wavefeld can originate from earthquakes, ocea
as tra c. The primary refection of a geological structure,
propagating wavefeld, is of main interest and is used to com
geological structure, wavefelds are partly refected upwar
Between two strong refecting structures, the wavefeld can
generate so called internal multiples. These multiple refe
surface and di cult to distinguish from primary refection
migrated from time to depth and construct an image of the su
recognized as such, they will get imaged being primary refec
multiples distort the actual image of the subsurface; the d
structures that are positioned along with the primary refe
important to recognize these multiple refections, and if po
This removal can be performed at diferent stages of the proc

subsurface. The internal multiples can be directly remove
redatuming step or after the imaging step. For removal after
imaged multiples is subtracted from the image to obtain an i
discuss a method for removing internal multiples during the
Besides internal multiples that are refected between bound
free-surface-related multiples. These multiples are gene
bounce back into the subsurface by the surface of the earth.
this paper. They are assumed to be removed prior to the remov
The Marchenko algorithm can eliminate internal multiples fr (Slob et al., 2014;
Behura et al., 2014). In this algorithm the up- and down-going focus
in the subsurface, are key to the method. The goal of the Ma
and down-going parts of the focusing functions from the ref
so-called Marchenko equations. This set of equations can b (Wapenaar
et al., 2014; Thorbecke et al., 2017) or a direct method (van der Neut et al., 2015; Ravasi, 2017).
The Marchenko method has found many diferent applications,
monitoring (van IJsseldijk et al., 2023), adaptive subtraction of Marchenko est (Staring
et al., 2018), homogeneous Green's functions (Brackenhoff et al., 2019), and direct multip
elimination on target (Zhang and Slob, 2020b). In this paper, a particularly e
of the Marchenko method for imaging by plane-waves is highl
this method are discussed in more detail.
Meles et al. (2018) show that besides focal-points, focal-planes ca
equations. Meles et al. (2020) build on the Marchenko Multiple Elimination
Zhang and Slob (2019) and introduce the plane-wave MME method. The ma
wave-based Marchenko method is that with a minimal efort of
wave), for each depth level (or time instant for MME), a multi
3D applications, the plane-wave Marchenko method is comput
multiple-free (Brackenhoff et al., 2022). A single plane-wave can be sufficient
image if the subsurface interfaces are near-fat. Multiple p
are needed for subsurface interfaces with varying dips, or g
the subsurface (Almobarak et al., 2021). The Marchenko algorithm for the foc
similar to the focal-point algorithm. The initial point-fo
replaced by a time-reversed direct plane-wave response. T
time windows to separate the Green's functions from the foc
to hold for a plane wave are the same as for a point source; a
the direct and later arrivals. In this paper, we discuss in d
the Marchenko plane-wave method, discuss the implementatio
applications on numerically modeled and feld data.
The software accompanied by this paper contains scripts and
examples presented in this paper. The code can also be foun (Thorbecke
et al., 2017; Thorbecke and Brackenhoff, 2020) where the most recent updated vers
developments are available. To reproduce the fgures and per
Seismic Unix (Cohen and Stockwell, 2016) is required.
Most pictures in this section of the manual can be reproduced

The Marchenko method is introduced by two coupled equations
and downgoing focusing functions and Green's functions) we
us to suppress internal multiples by using the up- and downg
refection data from the acquisition surface ($\mathbb{D}_0$) to a focal level in the subsurfa
step, the internal multiples of the overburden are suppress
acquisition boundary $\mathbb{D}_0$. The refection response $R(\mathbf{x}_R, \mathbf{x}_S, t)$, a scaled version of the Gree
without the direct wave (Wapenaar et al., 2021), is measured with sources and rece
$\mathbf{x}_S$ and $\mathbf{x}_R$ on this boundary. The recording time is denoted by t. This reflection response
contain free-surface related multiple refections neither a
required to remove the free-surface multiples and the direc

the measured reflection data.

The up- and downgoing parts f_1^- and f_1^+ of the focusing function are related to the decomposed Green's functions $G^{-,+}$ and $G^{-,-}$ in the actual medium and with the re... at the surface Wapenaar et al. (2014). The focusing functions have a focal point $\mathbf{x}_A$. This focal point serves as a virtual source for the Green's functions. The superscripts of the decomposed Green's function refer to the up- (−) and downgoing (+) direction of the virtual source $\mathbf{x}_A$. The leftmost superscript (−) indicates upgoing propagation at the receiver locations. The relation between the two unknown ... Green's functions is given by Wapenaar et al. (2014) via the following two equations (

$$G^{-,+}(\mathbf{x}_R,\mathbf{x}_A,t)+f_1^-(\mathbf{x}_R,\mathbf{x}_A,t)=\int_{\mathbb{D}_0}\int_{t'=0}^{\infty}R(\mathbf{x}_R,\mathbf{x}_S,t')f_1^+(\mathbf{x}_S,\mathbf{x}_A,t-t')\mathrm{d}t'\mathrm{d}\mathbf{x}_S, \quad (59)$$

$$G^{-,-}(\mathbf{x}_R,\mathbf{x}_A,t)+f_1^+(\mathbf{x}_R,\mathbf{x}_A,-t)=\int_{\mathbb{D}_0}\int_{t'=0}^{\infty}R(\mathbf{x}_R,\mathbf{x}_S,t')f_1^-(\mathbf{x}_S,\mathbf{x}_A,t'-t)\mathrm{d}t'\mathrm{d}\mathbf{x}_S. \quad (60)$$

In the compact operator notation of Van der Neut et al. (2015), equations 59 and 60 are written as

$$G^{-,+}+f_1^-=Rf_1^+, \quad (3)$$

$$G^{-,-}+f_1^{+\star}=Rf_1^{-\star}, \quad (4)$$

where $\star$ denotes the time-reverse. These two equations contain ... and two focusing functions. The only known in these equations is R. Wapenaar et al. (2013) use the reasoning that the Green's function and ... certain circumstances, be separated in time. Wapenaar et al. (2014). Therefore, a t... $\Theta(t)$ is defined that passes the focusing function and removes t... side of equations 3 and 4. For point-sources that radiate in all directi... for both the up- and downgoing traveling waves. Up- and down... propagate at opposite dipping angles; hence, two time windo... These time windows remove all events that arrive at later ti... virtual source $\mathbf{x}_A$ to the receiver positions $\mathbf{x}_R$ at $\mathbb{D}_0$, including the direct wave ... results in the following two equations that only have two un... $f_{1,d}^+$ is known)

$$f_1^-=\Theta_bRf_1^+, \quad (5)$$

$$f_1^{+\star}-f_{1,d}^{+\star}=\Theta_aRf_1^{-\star}, \quad (6)$$

where $f_1^+=f_{1,m}^++f_{1,d}^+$, with $f_{1,d}^+$ the direct f_1^+, and $f_{1,m}^+$ all events that arrive before ... arrival t_d. The separation of $f_{1,d}^+$ and $f_{1,m}^+$ can be successfully applied whe... overlapping reflection events with the direct response. In o... requires additional steps (Zhang et al., 2019). The time windows (Wapenaar et al., 2021) are defined as

$$\Theta_b(t)=\theta(t_b-t), \quad (7)$$

$$\Theta_a(t)=\theta(t_a-t), \quad (8)$$

where $\theta(t)$ denotes a tapered Heaviside step function. Note that ... time t_a and onset t_b. In the point-source case, $t_b=t_d-\varepsilon=t_a$, which makes equation 8 equal to equation 7, with the window $\theta(t_d-\varepsilon-t)$. The ε takes into account the finite l... band-limited wavelet and ensures that the direct wave is rem... (Broggini et al., 2014). Epsilon is typically chosen as half the dominan... To illustrate the application of the time windows, a virtua... in the laterally varying (Figure 26) model (Meles et al., 2018). Figure 27 shows the focusing functions and Green's functions of ... functions (indicated with a dashed line). Figure 27a represents the le... hand side of equation 3 and the time window. Figure 27b represents the time window separates the $f_{1,m}^+$ from $G^{-,-}$ and represents the left-hand side of 4. The convolution/correlation in the right-hand sides of equations 3 and 4 ...

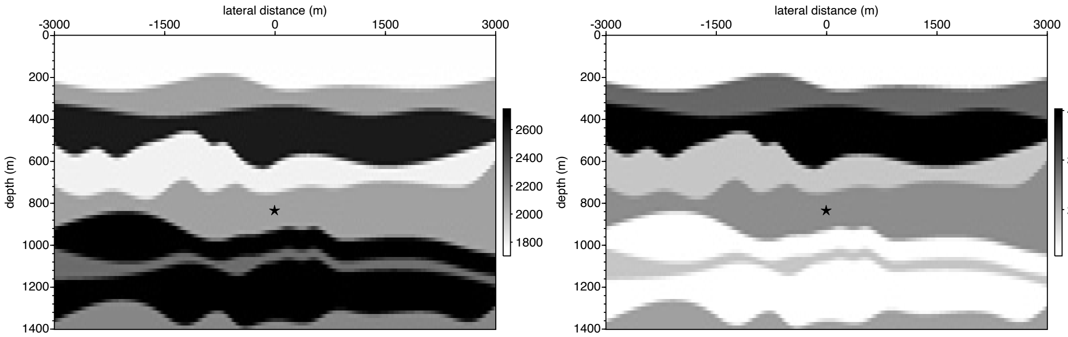

a) velocity model in m/s b) density model in kg/m^3

Figure 26: Multi layer model with velocity (a) and density (b) pa
point-source is marked with a ⋆.

frequency domain, and a discrete Fourier transform in time
data into the frequency domain. The discrete Fourier transf
a periodicity equal to the number of time samples (n_t). Given this periodicity in time
occurring in n_t, i.e. wrap-around into negative times. The time windows 7 and 8 d
pass all events earlier than $t = t_a$ and will also pass these time wrap-arou
these wrap-around events a time window is also implemented 27,
see that the focusing functions also include events at negat
earlier than $-t_a = -t_a + \varepsilon$. Hence, the cutoff point of the time window at n
$-t_a$. The implemented time windows become

$$\Theta_b'(t) = \theta(t_b - t) - \theta(-t_b - t), \tag{9}$$

$$\Theta_a'(t) = \theta(t_a - t) - \theta(-t_a - t), \tag{10}$$

and the time windows at negative times, to suppress time wra
lines in Figure 27. There is no guarantee that this time window suppr
windows are not sufficient to suppress the wrap-around, zeros
To solve the unknown focusing functions in 5 and 6 for the coupled equat
The iterative method Behura et al. (2014); Wapenaar et al. (2014) starts with $f^+_{1,d}$ as the
initial solution of f_1^+ and solves 5 for f_1^- and substitute the solution 6 to output f_1^+ in equat
This process is repeated until the updates to the focusing f
algorithm to solve the Marchenko equations 28. The iterative scheme is shown in Figure (
iteration count at 0 for the initial solution 5 and then the scheme
equation 6. Thorbecke et al. (2017) explain in more detail the implementation
Depending on the application it is not always needed to sol
Staring (2018) the results of the first iteration are used to predi
subtraction method is used to suppress the predicted multip
to solve the coupled equations. Van der Neut et al. (2015) and Ravasi (2017)
Meles (2018) show that plane-wave $\tilde{f}_1^\pm$ focusing functions and associated plane-wave
functions $\tilde{G}^{-,+}$ and $\tilde{G}^{-,-}$ can be obtained by integrating an appropriate se
tion f_1^+ and f_1^-, each involving the solution of a Marchenko equatio
quantities for focusing functions and Green's functions. T Wapenaar et
al. 2021; Brackenhoff et al. 2022 are defined by the following integration

$$\tilde{f}_1^\pm(\mathbf{x}, \mathbf{p}_A, t) = \int_{\mathbb{D}_A} f_1^\pm(\mathbf{x}, \mathbf{x}_A, t - \mathbf{p} \cdot \mathbf{x}_{H,A}) d\mathbf{x}_A, \tag{11}$$

with $\mathbf{p} = (p_1, p_2)$ and p_1 and p_2 horizontal ray parameters and $\mathbf{p}_A = (\mathbf{p}, x_{3,A})$ the ray parameter o
the plane-wave. $\mathbb{D}_A$ is the surface $\mathbb{D}_A$ at the depth level at which focusing
plane-wave Green's functions are defined by a similar integr $\mathbf{x}_{H,A} = (x_{1,A} - x_{1,c}, x_{2,A} - x_{2,c})$,
and $(x_{1,c}, x_{2,c})$ is the rotation point of the plane-wave. The rotatio
lateral extent of the plane-wave. This $t = 0$ at the point of the plane-wave
By making this choice, $t = 0$ of the time-axis in the computed plane-wave Gr

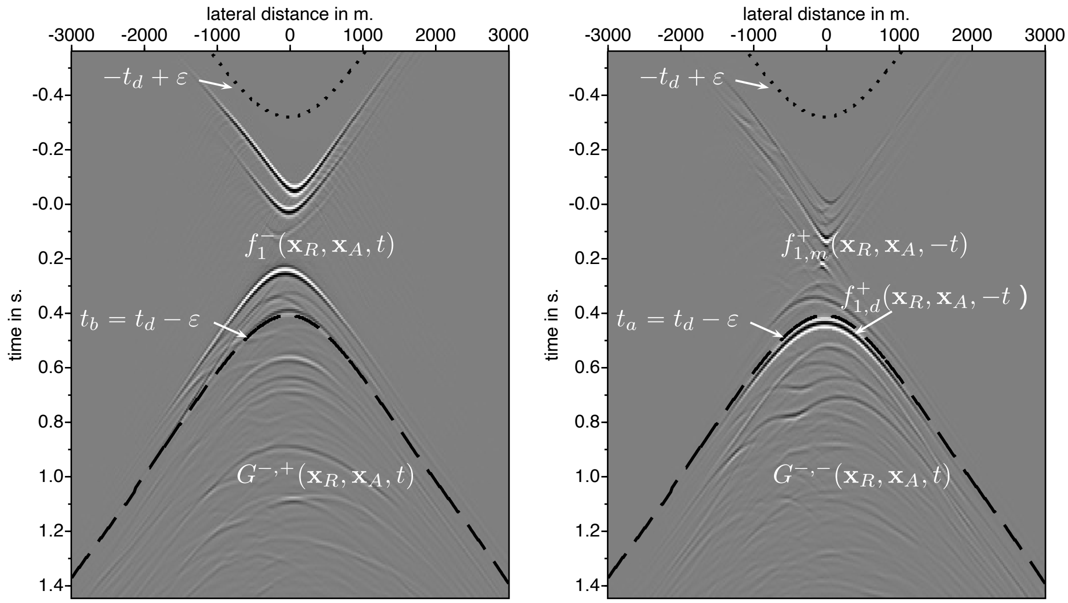

a) Separation of $G^{-,+}$ and f_1^-

b) Separation of $G^{-,-}$ and f_1^{+*}

Figure 2.7: Illustration of the time window function to separate t
function. The dashed black lines indicate the separation li
white arrows. The dotted line indicates the time window that

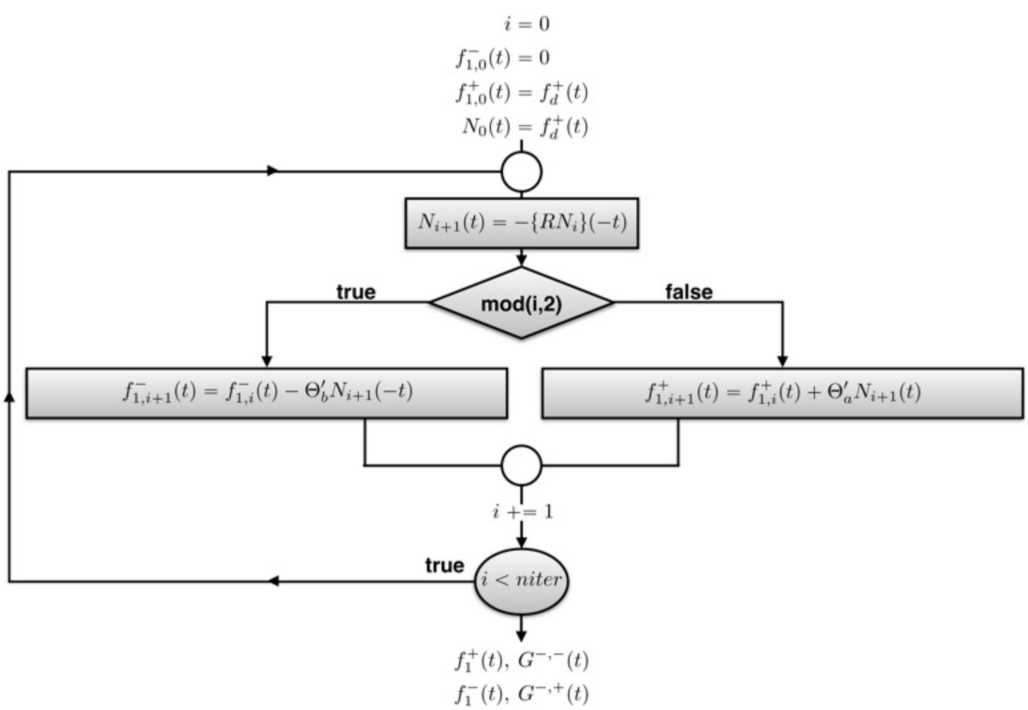

Figure 2.8: Flow chart of the Marchenko algorithm. The down-going (f_1^+) and up-going (f_1^-) functio
are alternately updated. The scheme is finished after a pre-
chosen between 10-20 iterations.

is the same as in the point-source Marchenko solutions with
plane-wave.

Note that the plane-wave integration in equation 11 creates a time-reversed wavefield $\tilde{P}(\mathbf{x},\mathbf{p}'_A,-t)$ gives

$$\tilde{P}(\mathbf{x},\mathbf{p}'_A,-t) = \int_{\mathbb{D}_A} P(\mathbf{x},\mathbf{x}_A,-(t-\mathbf{p}\cdot\mathbf{x}_{H,A}))d\mathbf{x}_A, \quad (12)$$

with $\mathbf{p}'_A = (-\mathbf{p}, x_{3,A})$, a plane-wave dipping opposite to the plane-wave ... $\mathbb{D}_A$ with a homogeneous velocity $\mathbf{p}\cdot\mathbf{x}_{H,A}$ are time shifts that are linear to the distance from the rotation point.

Applying the same integral to the focusing functions results in the plane-wave representations of equations 3 and 4 (Meles et al., 2018).

$$\tilde{G}^{-,+}(\mathbf{x}_R,\mathbf{p}_A,t) + \tilde{f}_1^{-}(\mathbf{x}_R,\mathbf{p}_A,t) = \{R\tilde{f}_1^{+}\}(\mathbf{x}_R,\mathbf{p}_A,t), \quad (13)$$

$$\tilde{G}^{-,-}(\mathbf{x}_R,\mathbf{p}'_A,t) + \tilde{f}_1^{+\star}(\mathbf{x}_R,\mathbf{p}_A,t) = \{R\tilde{f}_1^{-\star}\}(\mathbf{x}_R,\mathbf{p}_A,t). \quad (14)$$

Applying a time window that separates the Green function fr
equations with two unknowns ($\tilde{f}^{+}_{1,d}(\mathbf{x}_R,\mathbf{p}_A,t)$ is known) remain:

$$\tilde{f}_1^{-}(\mathbf{x}_R,\mathbf{p}_A,t) = \tilde{\Theta}_b\{R\tilde{f}_1^{+}\}(\mathbf{x}_R,\mathbf{p}_A,t), \quad (15)$$

$$\tilde{f}_1^{+\star}(\mathbf{x}_R,\mathbf{p}_A,t) - \tilde{f}_{1,d}^{+\star}(\mathbf{x}_R,\mathbf{p}_A,t) = \tilde{\Theta}_a\{R\tilde{f}_1^{-\star}\}(\mathbf{x}_R,\mathbf{p}_A,t) \quad (16)$$

with $\tilde{f}_1^{+\star} = \tilde{f}_{1,m}^{+\star} + \tilde{f}_{1,d}^{+\star}$, where $\tilde{f}_{1,d}^{+\star}$ is the direct arrival of the plane-wave with
by $(\mathbf{p}, x_{3,A})$, and $\tilde{f}_{1,m}^{+\star}$ contains the events that arrive before $\tilde{t}_d$, where $\tilde{t}_d$ is the direc
first arrival time of a plane-wave with $(\mathbf{p}, x_{3,A})$. Note that the Green
functions in 13 and 14 contain plane-waves with opposite dipping $\mathbf{p}_A$ and
$\mathbf{p}'_A$. To separate $\tilde{G}^{-,+}(\mathbf{x}_R,\mathbf{p}_A,t)$ from $\tilde{f}_1^{-}(\mathbf{x}_R,\mathbf{p}_A,t)$ the direct arrival $\tilde{t}_d$, the first arriv
of $\tilde{G}^{-,+}(\mathbf{x}_R,\mathbf{p}_A,t)$, is required. For the estimation of $\tilde{t}_d$ and $\tilde{t}'_d$, our choice is the sa
Wapenaar (2021). This choice of $\tilde{t}_d$ uses the same $'$ as the propagation angle $\mathbf{p}_A$ of
the upgoing Green's functions $\tilde{G}^{-,+}(\mathbf{x}_R,\mathbf{p}_A,t)$ and $\tilde{G}^{-,-}(\mathbf{x}_R,\mathbf{p}'_A,t)$. Note that the defined arri
$\tilde{t}'_d$ has the same arrival time of an upward propagating plane-wave $(x_{3,A})$ with angle $\mathbf{p}'_A$.

The time window $\tilde{\Theta}_b(t)$ removes $\tilde{G}^{-,+}(\mathbf{x}_R,\mathbf{p}_A,t)$ from equation 13. The first non-zero contri
$\tilde{G}^{-,+}(\mathbf{x}_R,\mathbf{p}_A,t)$ is at time $t_b = \tilde{t}_d - \varepsilon$. The time window $\tilde{\Theta}_a(t)$ removes $\tilde{G}^{-,-}(\mathbf{x}_R,\mathbf{p}'_A,t)$ and $\tilde{f}^{+\star}_{1,d}(\mathbf{x}_R,\mathbf{p}_A,t)$
from equation 14, hence all events at times $t_a = \tilde{t}'_d - \varepsilon$ are set to zero. Similar to the
scheme these time windows are implemented with an additiona
time wrap-around and are given by

$$\tilde{\Theta}'_b(t) = \theta(\tilde{t}_d - \varepsilon - t) - \theta(-\tilde{t}'_d + \varepsilon - t), \quad (17)$$

$$\tilde{\Theta}'_a(t) = \theta(\tilde{t}'_d - \varepsilon - t) - \theta(-\tilde{t}_d + \varepsilon - t). \quad (18)$$

Similar to 27, Figure 29 shows the plane-wave focusing functions and
left-hand side of equations 13 and 14, and the window functions separating the
depth of the plane-waves is chosen at 800 m. In the following section
these two time window functions are discussed in more detai
implementation of the Marchenko algorithm are explained.

The plane-wave method is illustrated with two numerical ex
variant medium. In two dimensions the downward propagating $\tilde{f}^{+}_{1}(\mathbf{x},\mathbf{p}_A,t)$
in equation 11 defines a plane-wave at $\mathbb{D}_A$ with the dip angle α: $p_1 = \frac{\sin(\alpha)}{c}$. In the first
numerical example we assume a medium with a horizontally layered ... show
Figure 30a and b. Figure 31 shows $\tilde{f}^{+}_{1}(\mathbf{x}_R,\mathbf{p}_A,t)$, for a focal plane at a depth of 900 m
angles: 31a with an angle of 0 degrees and Figure 31c with an angle of 3 degrees.
31b and 31d the focus function is shown for receivers at the foca

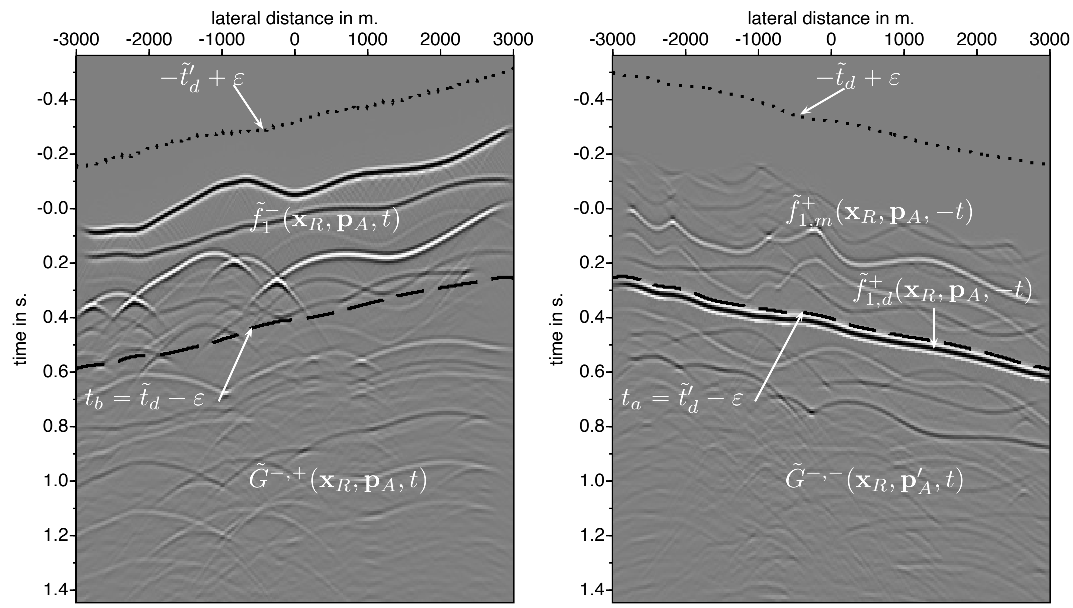

a) Separation of $\tilde{G}^{-,+}(\mathbf{p}_A)$ and $\tilde{f}_1^-(\mathbf{p}_A)$.

b) Separation of $\tilde{G}^{-,-}(\mathbf{p}'_A)$ and $\tilde{f}_1^{+\star}(\mathbf{p}_A)$.

Figure 29: Illustration of the time window function to separate th
focusing function. The dashed black lines indicate the separ
with white arrows. The dotted line indicates the time window

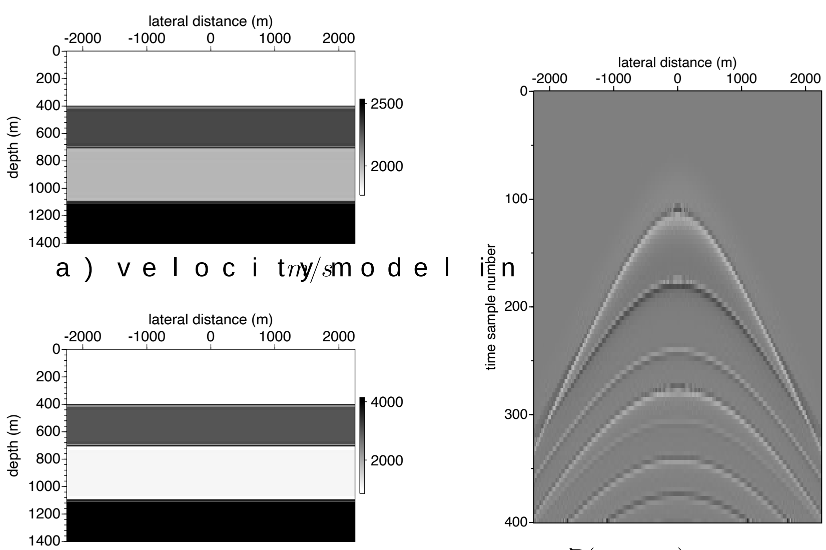

a) velocity model in m/s

b) density model in kg/m^3

c) $R(\mathbf{x}_R, \mathbf{x}, t)$

Figure 30: Two dimensional four layer model with velocity (a) and
source record, with source position $\mathbf{x} = (x_1 = 0, x_3 = 0)$ and receivers at $\mathbf{x}_R = (x_1 = x_R, x_3 = 0)$ (c).
The source wavelet R has a flat frequency spectrum from 5 to 90 Hz.

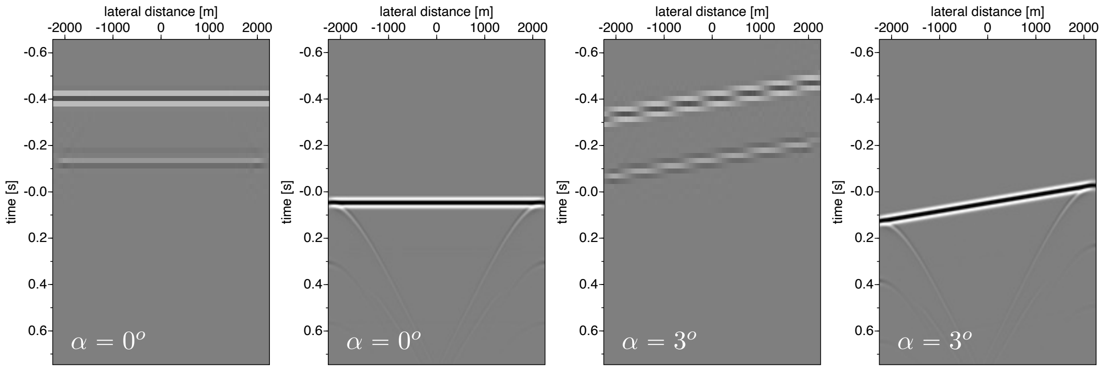

a) depth $x_3 = 0$ m b) depth $x_3 = 900$ m c) depth $x_3 = 0$ m d) depth $x_3 = 900$ m

Figure 3.1: Time recordings of the plane-wave focusing function $\tilde{f}_1^+(\mathbf{x}_R, \mathbf{p}_A, t)$ with a focal depth of ... meter measured with a depth $x_3 = 0$ and $x_3 = 900$ meter in the truncated medium for ... plane-wave propagation angles (0 and 3 degrees). At the end- ... are present due to the limited lateral extent of the constru...

focal-point Marchenko method, the medium for the plane-wave ... below the focal level. The $\tilde{f}_1^+(\mathbf{x}, \mathbf{p}_A, t)$ has a focus at time $t = \mathbf{p} \cdot \mathbf{x}_{H,A}$. For a dipping plane-wave this time focus occurs ... 3.1a and 3.1c show ... the computed $\tilde{f}_1^+(\mathbf{x}_R, \mathbf{p}_A, t)$ at the surface (0 m depth) and includes an extr... that compensates for the multiples generated between the fr... respectively. The compensation of multiples ... Zhang and Slob ... (2019). The focus functions 3.1b and 3.1d ... however ... event, the do... present at the surface is compensated by the reflected event ... To illustrate this compensation effect of $\tilde{f}_1^+(\mathbf{x}, \mathbf{p}_A, t)$ in a ... 3.1 ... of the focu... propagating into the truncated medium (that is homogeneous ... are shown in Figure 3.2 for the same angles of 0 and 3 degrees ... Figure ... snapshots of the superposition of $\tilde{f}_1^+(\mathbf{x}_R, \mathbf{p}_A, t)$ ... wave $\tilde{f}_1^-(\mathbf{x}_R, \mathbf{p}_A, t)$. The snapshots of a plane-wave with an angle of 3 d... 3.2. At 0.05 seconds ... 3.2 ... $t = 0$ ... are two upward traveling ... from the interfaces at 400 and 700 meter ... $\tilde{f}_1^+(\mathbf{x}_R, \mathbf{p}_A, t)$ ... two downg... snapshots 3.2 ... $t = 0.00$ s) 3.2 and ... $t = 0.05$ s) show that the second dow... traveling event coincides at the first interface (at 400 m dep... interface (at 700 m depth) and these events compensate each ... the pictures. The fourth snapshot show that after this comp... the reflectors at 400 and 700 m depth have vanished and only on... reflected wavefield (from the reflector at 700 m depth) are re... upward traveling multiples ... $\tilde{f}_1^+(\mathbf{x}_R, \mathbf{p}_A, t)$ ... of the Marchenko e... illustration in Figure 3.2 demonstrates that the internal multiple compe... the plane-wave Marchenko method.

In Figure 3.3 the experiment is repeated in the 2.6 ... The focal-plane ... chosen at 800 m depth, just below the fourth reflector. The s... events $\tilde{f}_1^\pm(\mathbf{x}_R, \mathbf{p}_A, t)$ compensate the upgoing events at interfaces an... internal multiples.

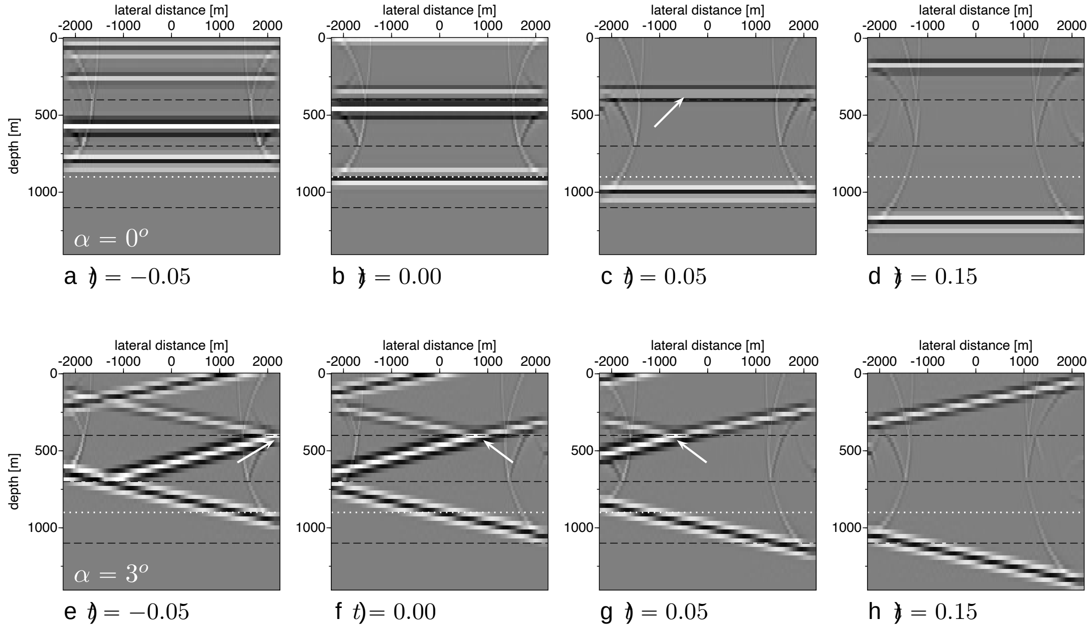

Figure 3.2: Time snapshots of $\tilde{f}_1^+(\mathbf{x}_R, \mathbf{p}_A, t) + \tilde{f}_1^-(\mathbf{x}_R, \mathbf{p}_A, t)$ at two diferent plane-
propagation angles. Note the difraction efects at the edge
indicates the focal depth of the plane-wave.

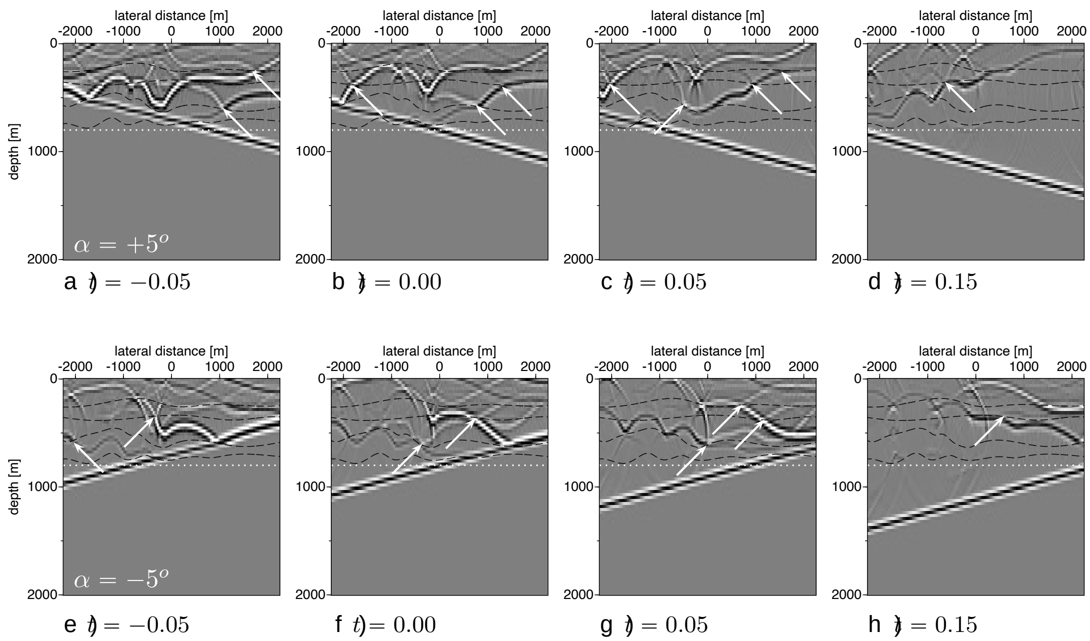

Figure 3.3: Time snapshots of $\tilde{f}_1^+(\mathbf{x}_R, \mathbf{p}_A, t) + \tilde{f}_1^-(\mathbf{x}_R, \mathbf{p}_A, t)$ in model of Figure 2.6
two diferent plane-wave propagation angles. Note that there
from edges on the interfaces. The white dotted-line indica
arrows indicate positions at a refector where an up-going re
is compensated by a down-going event from the focusing funct

To start the iterative Marchenko scheme $\tilde{f}^+_{1,d}(\mathbf{x}_R,\mathbf{p}_A,t)$ is required; the plane-wave ... a plane-wave response from a focal-plane in the subsurface. ... in a macro model estimated from the reflection data. The compu... the first arrival times to get the time $\tilde{f}^+_{1,d}(\mathbf{x}_R,\mathbf{p}_A,t)$. As a first example it is made for a horizontal (zero-degree) plane-wave defined a... model of Figure 26 (same model as in Meles et al., 2018).

Figure 34a shows the forward modeled plane-wave response of a hor... receivers at the surface. The first arrival, 34b, is the time-reversal of the plane-wave ... of the input $\tilde{f}^+_{1,d}(\mathbf{x}_R,\mathbf{p}_A,t)$ of the Marchenko scheme. The computed down-... functions, after 16 iterations of equations 15 and 16 ... the results in e... 13 and 14, are shown in 34c and 34d respectively and give the expected response... Marchenko mute-line $\tilde{\Theta}_{a,b}$ (as used in equations 17 and 18), to separate the Green's fu... the focusing functions, $t=0$ is ... $\tilde{y}_d = \tilde{m}_d$. This is the same time symme... use for the Marchenko point-source algorithm.

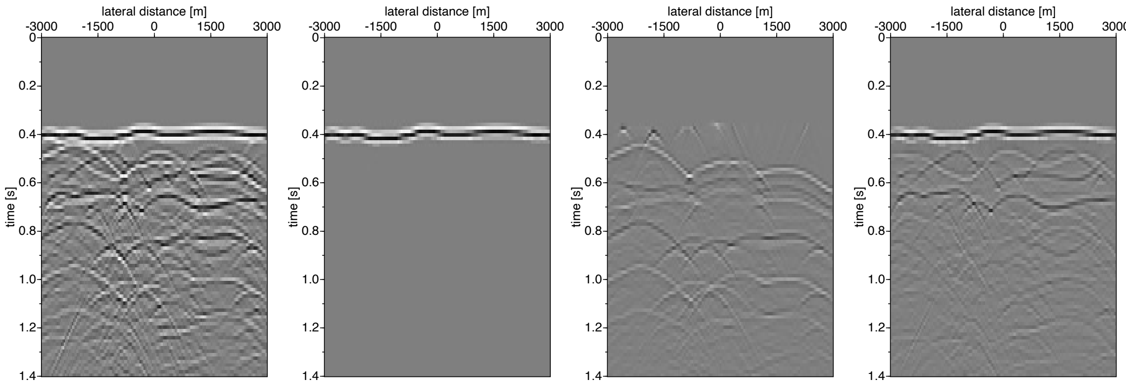

a) $\tilde{G}(\mathbf{x}_R, \mathbf{p}_A, t)$ b) $\tilde{f}^{+\star}_{1,d}(\mathbf{x}_R, \mathbf{p}_A, t)$ c) $\tilde{G}^{-,+}(\mathbf{x}_R, \mathbf{p}_A, t)$ d) $\tilde{G}^{-,-}(\mathbf{x}_R, \mathbf{p}'_A, t)$

Figure 34: Results of the plane-wave Marchenko scheme for a hori[zontal plane-wave] $\mathbf{p}_A = (0, x_{3,A})$. Adding the up- and downgoing Green's functions of c and d, t[...] algorithm, gives the same wavefeld as the directly forward m[...] with the same clipping factor.

The Marchenko algorithm for dipping plane-waves follows th[...] waves. As indicated by equations 17 and 18 the Marchenko time windows have to be d[...] for dipping plane-waves. For horizontal plane-waves the imp[...] $t = 0$ and $\tilde{\Theta}'_a = \tilde{\Theta}'_b$. This does not hold anymore for dipping plane-wav[es]. Figure 35 is an example of time windows that are designed for a dipping plane-wave of +5[...] one for the even iterations (Figure 35a), using equation 15, and one for the odd iteration[s] reverse angle (Figure 35b) and equation 16. To design these windows for a pos[...] first arrival time for a plane-wave at the same depth level wi[...] In the following we explain in more detail what is expressed [in] 15 and 16. The plane-wave Marchenko scheme starts with forward m[...] plane-wave at depth. This modeled wavefield is presented in Figure 37a, where the depth of the plane-wave is chosen at 800 m. The direct arrival is selected [...] 37b. The time reverse of this field $\tilde{f}^{+}_{1,d}(\mathbf{x}_R, \mathbf{p}_A, t)$, $\tilde{f}^{+}_{1,d}(\mathbf{x}_R, \mathbf{p}_A, t)$ is, together with t[he] reflection data R, the input of the plane-wave Marchenko scheme.

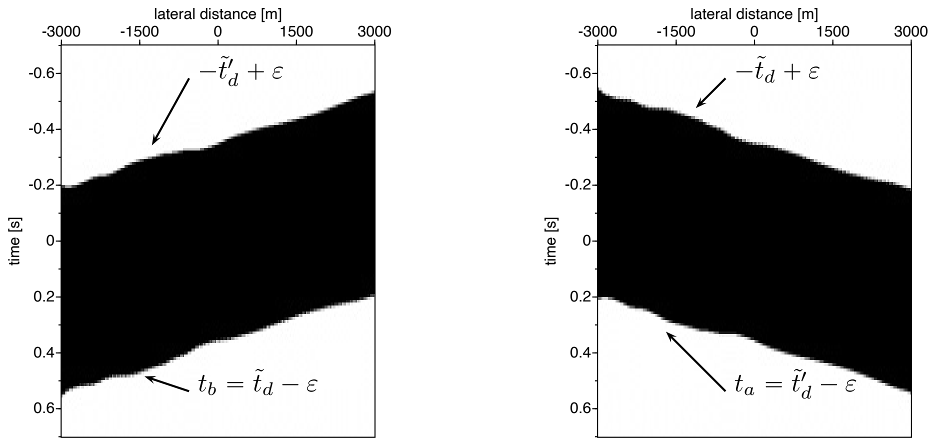

a) even iterations b) odd iterations

Figure 3.5: The time windows for dipping plane-waves for even (a) a
+5 degrees. The wavefields in the black area of the windows pa
zero.

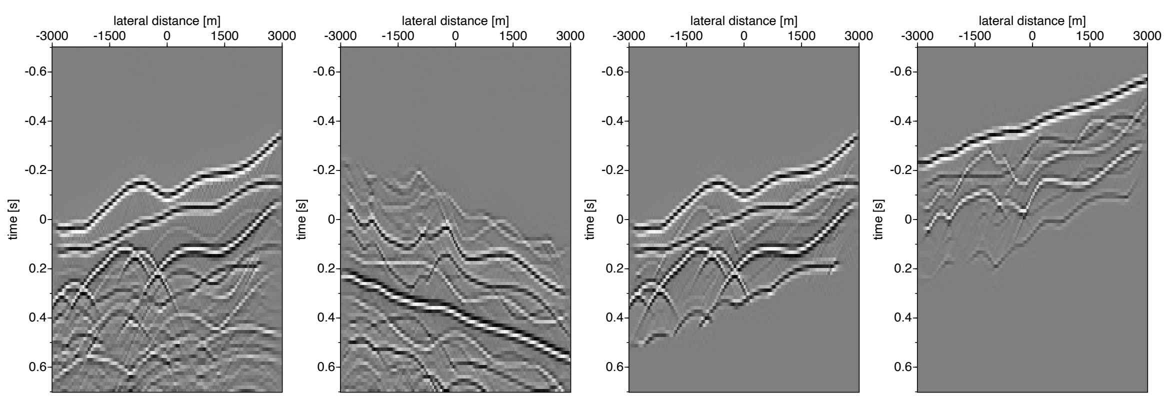

a) first iteration b) second iteration c) $\tilde{f}_1^-(\mathbf{x}_R, \mathbf{p}_A, t)$ d) $\tilde{f}_1^+(\mathbf{x}_R, \mathbf{p}_A, t)$

Figure 3.6: Basic plane-wave Marchenko results for a plane-wave wi
Note, that the results of the first iteration (a) is dipping i
(b) and the algorithm uses the time windows, designed 17 for di
and 18, to take this into account.

In the Marchenko algorithm the iterations are alternating be...
with R, or a correlation with R (Thorbecke et al., 2017). In the first step, correlation (16), the ... wavefield is shifted backward in time $\tilde{t}_d$, and in the second step the time convolution ... equation 15 the wavefield is shifted forward in time $\tilde{t}'_d$. In Figure 36 the result of the ... the first iteration (correlation) is shown. In Figure 36b the result of the second iterat... is shown. In Figure 36a we can see that the first event, that starts at ne... the undulation of the first reflector and has an opposite dip c... 37a. The result of the first iteration is muted in time with the window (with the window 35) ... mute $\tilde{G}^{-,+}(\mathbf{x}_R, \mathbf{p}_A, t)$, followed by time-reversal (equation 16). The result ... shown in Figure 36. In this second iteration the convolution step b... times corresponding to reflection times in the 37a. Note that the model ... that the arrival in Figure 36, just in time from the left at time 0.2 s dipp... is the same as the first arrival in $\tilde{t}_d$ 37a and 37b. The result of this second ... muted in time (with the window 35) to remove $\tilde{G}^{-,+}(\mathbf{x}_R, \mathbf{p}'_A, t)$ and the first arrival e... at $\tilde{f}^+_{1,d}(\mathbf{x}_R, \mathbf{p}_A, t)$, as indicated in 20. The odd iteration $\tilde{f}^-_1(\mathbf{x}_R, \mathbf{p}_A, t)$ are building ... $\tilde{G}^{-,+}(\mathbf{x}_R, \mathbf{p}_A, t)$ and the even iterations $\tilde{f}^+_1(\mathbf{x}_R, \mathbf{p}_A, t)$ are building $\tilde{G}^{-,-}(\mathbf{x}_R, \mathbf{p}'_A, t)$. Figure 36e and 36f show $\tilde{f}^+_1(\mathbf{x}_R, \mathbf{p}_A, t)$ and $\tilde{f}^-_1(\mathbf{x}_R, \mathbf{p}_A, t)$ respectively after 16 iterations.

In Figure 37 three plane-wave responses are shown with angles of -... Comparing these three plane-wave responses $\tilde{G}^{-,+}$ shows that each angle illum... ferent parts of the medium. This is clearly seen in the even... combining different plane-wave responses into one image a fu... using only a few (Meles et al., 2018). Plane-wave imaging, that suppres... can use the same strategies as point-source Marchenko, for e... der Neut et al. (2015), Staring et al. (2018) or Multi Dimensional Deconvolution (Ravasi et al., 2016; Almobarak, 2021) discusses different plane-wave imaging me... Marchenko Green's function plane-wave response is a comput...

Figure 38 shows horizontal plane-wave images from the Troll field ... was kindly provided by Equinor. This dataset is part of a ti... a small part of this data-set, with source and receiver posi... source spacing is 12.5 meter and traces are recorded with a t... pre-processed to remove free-surface multiples (Qu and Verschuur, 2020) and deconvo... The imaging is carried out according to Meles et al. (2018). In the standard ... imaging method, a forward modeled plane-wave response is co... smooth macro model of the data. This plane-wave depth respo... responses of the recorded data and integrated over the recei... This creates the plane-wave response of the data (Rietveld et al., 1992). This plane-wave res... of the data is correlated with the same modeled plane-wave re... condition $t = 0$ is used to construct the image for all depth levels. ... the left side panel of Figure 38 is called 'standard'.

To compute the Marchenko based image, the first arrivals of t... at each depth level is input to the plane-wave Marchenko algo... The $\tilde{G}^{-,+}$ is, similar to the standard imaging method, correlated with $\tilde{f}^+_{1,d}$ ... for each depth level, and $t = 0$ is the imaging condition to construct the image for all dep... horizontal plane-wave ($\mathbf{p}_A = (p = 0, x_{3,A})$) at one depth level $x_{3,A}$ the imaging condition is ... by

$$\tilde{I}(\mathbf{x}_R, \mathbf{p}_A) = \int_t \tilde{f}^+_{1,d}(\mathbf{x}_R, \mathbf{p}_A, t)\tilde{G}^{-,+}(\mathbf{x}_R, \mathbf{p}_A, t)dt. \quad (19)$$

The advantage of using $\tilde{G}^{-,+}$ is that this field does not contain downgoing ... layers above the focal/imaging depth. The Marchenko method ... and downgoing parts in the Greens functions by applying the ... data. Alternative strategies to compute an image without i... Thorbecke et al. (2021). To illustrate the working of the internal multip... on reflection data in Figure 39 ... Staring et al. (2018) ... source-... Marchenko redatuming and imaging on field data using an adap... of that paper shows internal multiples that are first predict...

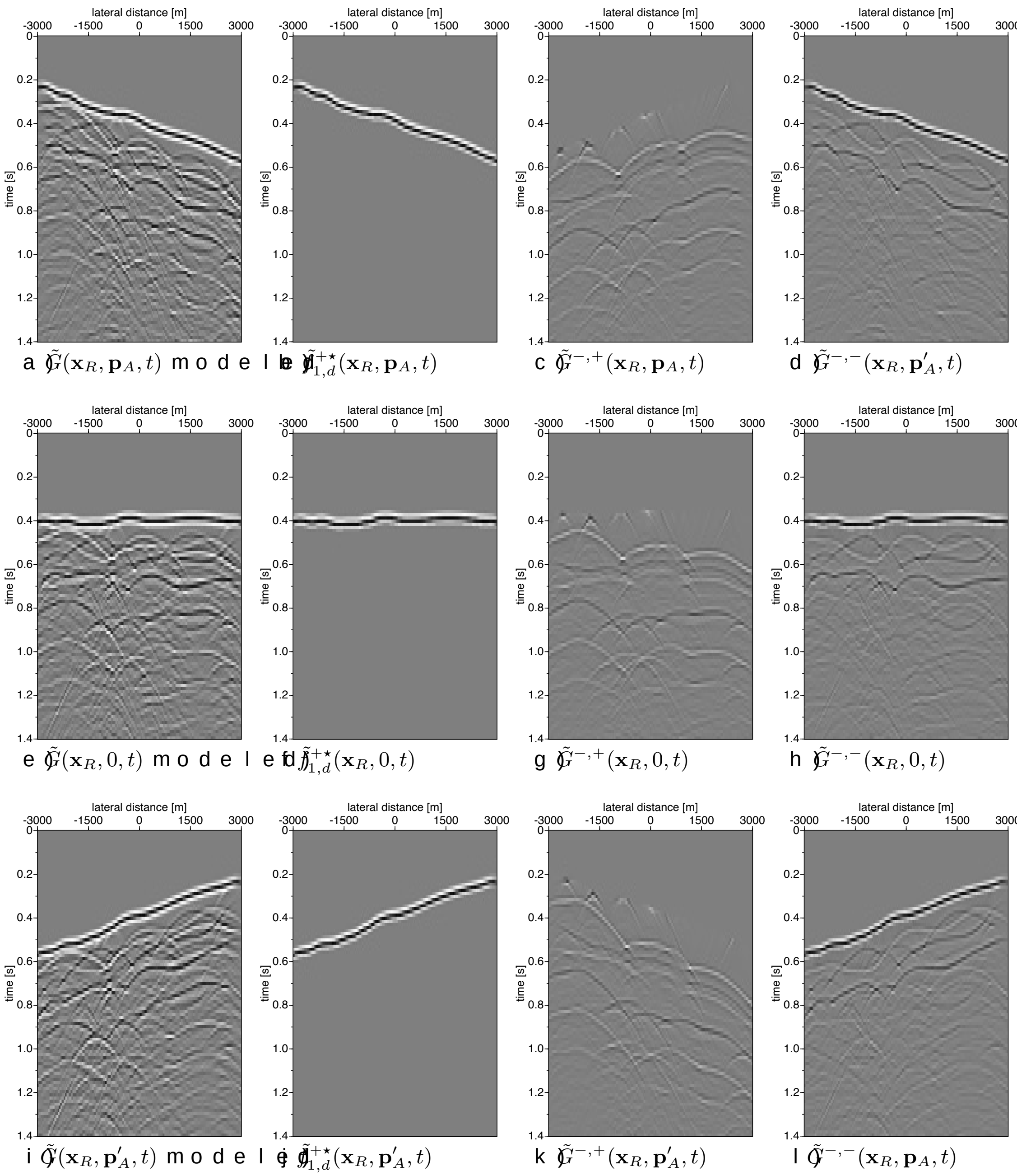

a) $\tilde{G}(\mathbf{x}_R, \mathbf{p}_A, t)$ modeled b) $\tilde{f}^{+\star}_{1,d}(\mathbf{x}_R, \mathbf{p}_A, t)$ c) $\tilde{G}^{-,+}(\mathbf{x}_R, \mathbf{p}_A, t)$ d) $\tilde{G}^{-,-}(\mathbf{x}_R, \mathbf{p}'_A, t)$

e) $\tilde{G}(\mathbf{x}_R, 0, t)$ modeled f) $\tilde{f}^{+\star}_{1,d}(\mathbf{x}_R, 0, t)$ g) $\tilde{G}^{-,+}(\mathbf{x}_R, 0, t)$ h) $\tilde{G}^{-,-}(\mathbf{x}_R, 0, t)$

i) $\tilde{G}(\mathbf{x}_R, \mathbf{p}'_A, t)$ modeled j) $\tilde{f}^{+\star}_{1,d}(\mathbf{x}_R, \mathbf{p}'_A, t)$ k) $\tilde{G}^{-,+}(\mathbf{x}_R, \mathbf{p}'_A, t)$ l) $\tilde{G}^{-,-}(\mathbf{x}_R, \mathbf{p}_A, t)$

Figure 3.7: Marchenko computed plane-wave responses for angles at
Note the diference in illumination in the decomposed Green’
plane-wave. An addition to Figure 3.4 of the Marchenko computed up-
Green’s function gives the forward modeled response in a.

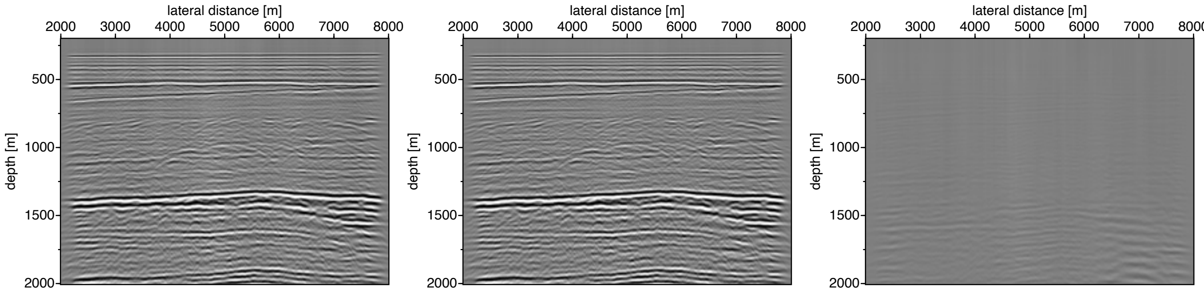

a) Standard at 0 degrees b) Marchenko at 0 degrees c) difference

Figure 38: Plane-wave images of the Troll feld data-set for a ho
imaging (left) and Marchenko based imaging (middle). All im
factor.

The middle picture of Figure 38 shows the Marchenko-created image. The difer
image and the Marchenko-based image is shown in Figure 38c. From this difference plot it
that the Marchenko method predicts and removes internal mul
multiple removal on this dataset is shown in van IJsseldijk et al. (2023) that Marchenko multip
on this dataset improves the confdence of the efects of smal

The plane-wave Marchenko method is a straightforward extens
A counter-intuitive aspect of the plane-wave method is that
Green's functions have opposite dipping angles. This is ta
separate the Green's function from the focusing function. I
function for a specifc dip angle, one would have to run the
angles. In this paper, the use of these time windows is illus
The plane-wave Marchenko method can give a computational ad
Specially for imaging applications with 3-dimensional dat
that case only a few plane-wave migrations are needed to com

The authors thank Equinor (formerly Statoil A.S.) for provi
This research was funded by the European Research Council (E
2020 research and innovation program (grant agreement no. 7

- Name of the code/library: OpenSource code for Finite Dif cessing utilities
- Contact: j.w.thorbecke@tudelft.nl
- Hardware requirements: tested on x86_64 and aarch64 proc
- Program language: C and Fortran
- Software required: C compiler, Fortran compiler, GNU Mak display and generation of the fgures is done with Seismic Un
- Program size: 147 MB

The source codes are available for downloading at the links: https://gitlab.com/gebhrk ics
The scripts to reproduce the results in this manuscript can b
The README in that directory explains all the steps to repro
the reproduction of the measured data example please contac
data if we can share the data.

To model a plane-wave with a tilt in the finite-difference code of Thorbecke and Draganov (2011) a ray-parameter value p [s/m] is defined by a chosen velocity and a p... depth-level. The plane-wave is triggered at all grid-points ... depth-level in the finite-difference grid. To simulate a dip ... defines the dipping plane-wave (eq. 22) as a time-delay t_p = p * distance from the rotation point, which is a linear function of the distance from the rotation point. The rotation point, $t=0$, of the ... is chosen at the center ($\mathbf{x}_c$) of the plane-wave.

$$\mathbf{p} = sin(\alpha)/c_p, \tag{20}$$

$$\mathbf{x}_p = (\mathbf{x} - \mathbf{x}_c) * dx, \tag{21}$$

$$t_p(\mathbf{x}) = \mathbf{x}_p * \mathbf{p}. \tag{22}$$

where α is the dip angle, c_p is the propagation velocity of the medium, and $\mathbf{x_c} = (x_{1,c}, x_{2,c})$ are the horizontal coordinates of the central location of the plane... in the definition of x_p, we ensure that the center of the plane-wave source ... of $t=0$ Brackenhoff (2016) et al.

In a homogenous model a plane-wave, modeled with these time... a plane-wave on a slanted line with an angle α in a medium with velocity $c = c_p$. In Figure 39 and 39 four snapshots are shown of a propagating plane-w... and a propagation velocity of 1500 m/s. The snapshots of the ... x-position -3000 and 0, have a negative time delay, $t=0$ is at ... the shot that is initiated first (at negative time) is positioned ... -3000 m in Figure 39 (a) and has a time-delay of -0.1742 s. To account for ... the modeling of dipping plane-waves in the finite-difference code of Thorbecke and Draganov (2011) ... is adapted. To model a negative angle the shot that is initi... sample in Figure (most right position 39 to 39) with +3000 m in Figure ... -0.1742 s.

An alternative implementation of a dipping plane-wave is ac... grid-point that also varies in depth. All sources are active at $t=0$ without any time-delays between 39 to 39 the sources. Figure shows snapshots of this impl... disadvantage of this implementation is that in solving the ... a defined angle α in depth, the ray-parameter p of $\tilde{G}^-(\mathbf{p}, A)$ and $\tilde{G}^{+,+}(-\mathbf{p}, A)$ are not ... more to ... since p is position dependent.

In the use of tilted plane-waves time-shifted sources play ... understand the effects of a time-shift in the regular Marchenko ... 40a to 40e the standard Marchenko results are shown for a focal point at 900 meter depth. In Figure 40 the forward modeled operator is shifted +0... hence the time-reverse of that, $f^+_{1,d}$, is shifted -0.3 seconds backward ... The Marchenko results in Figure 40 to 40 show that the solution of the Marchenko ... change; the same fields are computed, f_1^-, f_1^+ and G^- are shifted backward in time and G^+ is shifted forward in time.

To compute the time-shifted Marchenko results the time-windows in the Marchenko equations, to separate the focal- from the Green's function ... that for even and odd iterations different time-windows hav... constant-time shift of 0.3 seconds.

The results of the time-shifted Marchenko can of course also ... to be careful. For example $G^{-,+}$ can be back-propagated into the medium to b... depth, but before back-propagating the time-shifted respo... back to the origin of $t=0$ of $f^+_{1,d}$, otherwise $G^{+,+}$ will not focus at the focal depth of $f^+_{1,d}$.

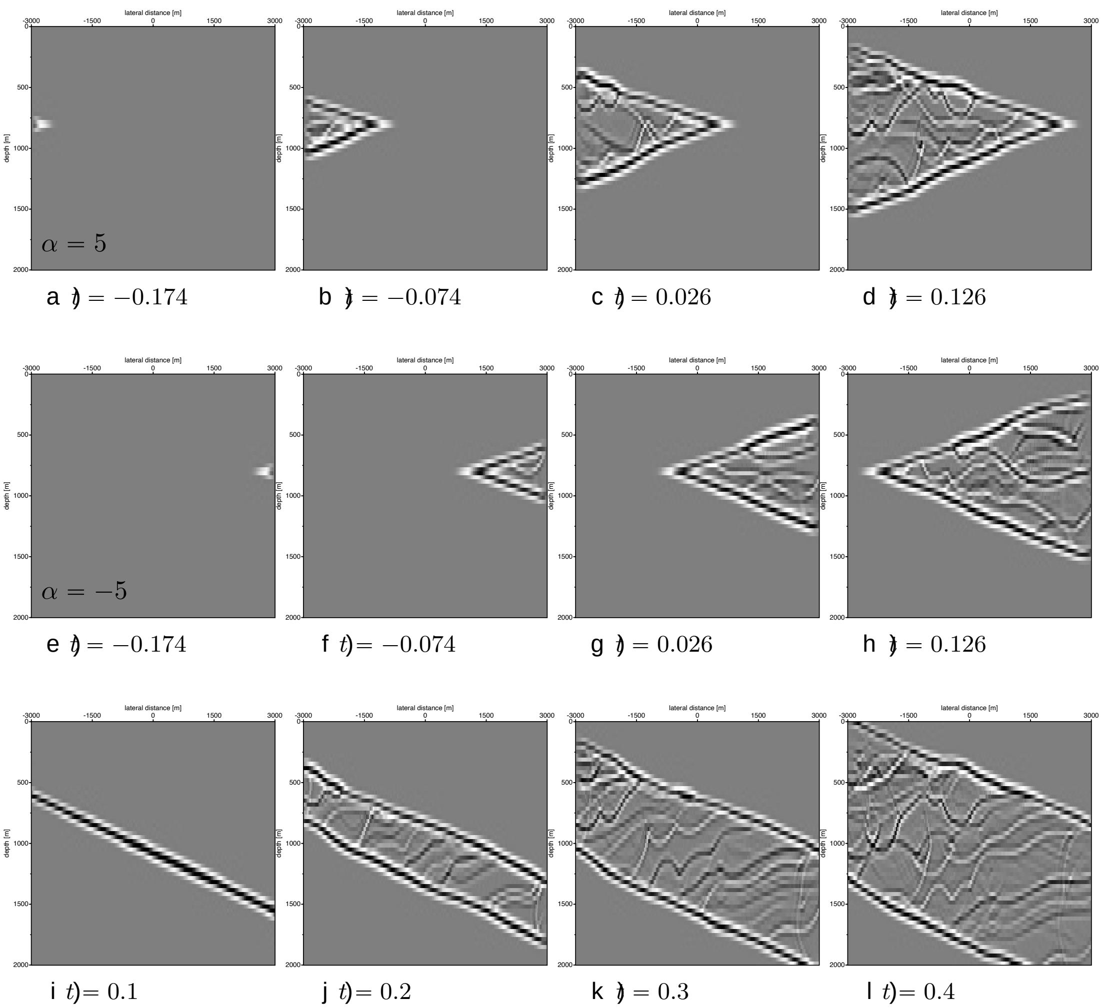

Figure 39: Time snapshots for diferent implementations to model a
the time-delayed implementation at time instances -0.174, -
+5 degrees. Pictures e-h show the time-delayed implementat
of -5 degrees. Pictures i to l show a titled grid position imp

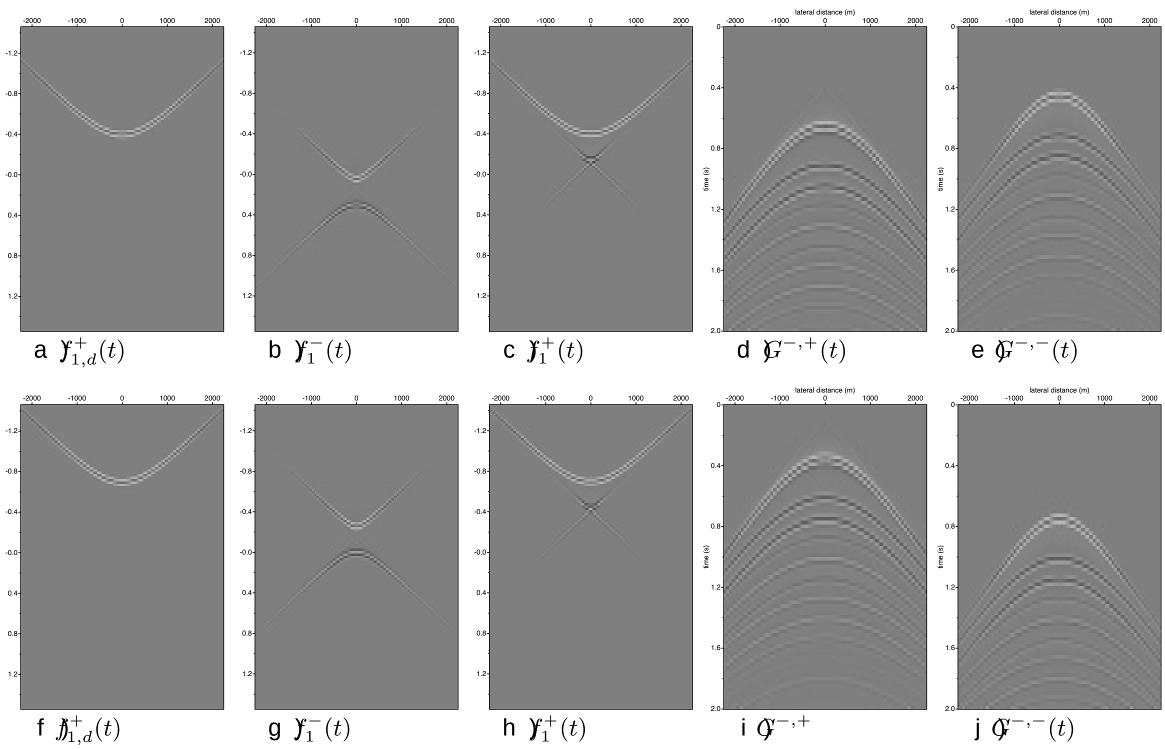

Figure 40: Standard and time-shifted Marchenko results for a fo
model of Figure 30. The applied shift is +0.3 s. forward $(f^+_{1,d})^*$ in time on the

m a r c h e n k o 3 D

Short instructions to install t

Summary how to reproduce the examples in t

Template to create your own Mak

File with system specifc setting and can be adap

Controls the compilation and linking of the p

Library for FFT transformation routine

where you can fnd this ma

Directory for the include fle fron

Directory where the FFT libra

Directory for the binaries compiled and l

This directory contains all source code

The bash-script to generate the FFigurres from in

and Dragoman (2010)

Bash-script which demonstrate the pos

Source code for programs to generate models, wavelet

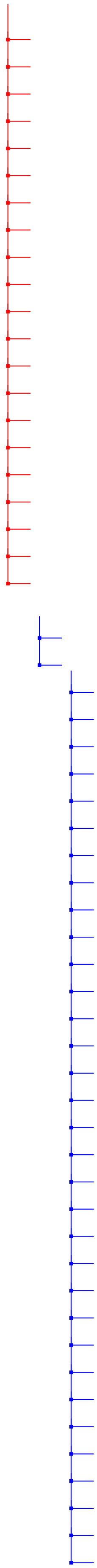

Executable for basic operations (shift, e
Executable to extends the edges of a fle with frs
Executable for auto-, cross-correlation, deconv
Executable for elastic acoustic fnite-di
Executable for the calculation of 2D Greens fu
Executable for building gridded s
Executable to generate w

Include fle for the FFT l

Library which contains the objects o

controls the compilation and linking o
header fle which defnes structure
header fle from SU for reading in pro
adjusted segy header fle, which defn
original segy header fr
Kernel of acoustic FD using 2'nd o
Kernel of acoustic FD using 4'th o
Kernel of acoustic FD using 6'th o
Routine which adds source amplitude(s)

converts ascii to arithmet
random number generat
computes, or read from fle, the s
function for self-documenta
Kernel of elastic FD using 4'th o
main FD modeling program, conta
fle handling routines to op
generate a Gaussian distribution o
stores energy felds (beams) in arrays
reads gridded model fle to compute min/max
reads in all parameters to set up
stores the wavefeld at the rece
reads source wavelet fle and computes maximur
functions to get parameters from the co
inserts a character string after the fler
reads gridded model fles and computes medium p
calculates the receiver positions base
computes interpolation based on t
tapers the wavefeld to suppress unwanted r
functions to print out verbose, error and w
Kernel of visco-acoustic FD using 4'
Kernel of visco-elastic FD using 4'
function used to calculate wa
writes the receiver array(s) t
writes gridded wavefeld(s) at a desire
writes the source and receiver positi
writes an 2D array to a SU

Almobarak, Mohammed, 2021, Plane-wave Marchenko imaging me
University of Technology.

Behura, J., K. Wapenaar and R. Snieder, 2014, Autofocus imag
scattering theory: Geophysics, 79, (3), A19–A26.

Brackenhof, J., 2016, Rescaling of incorrect source strengt
TU Delft Repository, Delft University of Technology.

Brackenhof, J., Thorbecke, J., and Wapenaar, K., 2019, Virt
- considerations for practical applications: Journal of G (11),
802–821.

Brackenhof, J., Thorbecke, J., Meles, G., Koehne, V., Bar
Marchenko applications: Implementation and examples: Geo, 85–56.

Broggini, F., K. Wapenaar, J. van der Neut and R. Snieder, 20
and application to imaging with multidimensional deconvo
Solid Earth, Vol., p. 425–441.

Broggini, F., R. Snieder, and K. Wapenaar, 2014, Data-driv
multidimensional deconvolution: Numerical examples fron
Geophysics, (3), WA107–WA115.

Cohen, J. K. and J. W. Stockwell, 2016, CWP/SU: Seismic Un*
software package for seismic research and processing: Cen
of Mines.

Costa Filho, C. A. da, M. Ravasi, A. Curtis, and G.A. Meles,
retrieval through single-sided Marchenko inverse scatter, 063201.

Costa Filho, C. A. da, G.A. Meles, A. Curtis, M. Ravasi and A
Marchenko focusing functions: 79th Annual International M
tists and Engineers, Expanded Abstracts, Tu P9 15.

Dukalski, M.S., and K. de Vos, 2017, Marchenko inversion in a
related multiples: Geophysical Journal International, (2), 760–776.

Jia, X., Guitton, A. and Snieder, R., 2018, A practical imp
with a Gulf of Mexico dataset: Geophysics, (5), S409–S419.

Lomas, A., and A. Curtis, 2019, An introduction to Marchenko (2),
F35–F45.

Lomas, A., S. Singh, and A. Curtis, 2020, Imaging vertical s
vertical seismic-profile data: Geophysics, (2), S103–S113.

Matias, M.A., R. Pestana, and J. van der Neut, 2018 Marchenk
tion: Geophysical Prospecting, (9), 1653–1666.

Meles, G.A., K. Löer, M. Ravasi, A. Curtis and C.A. da Costa F
and removal using Marchenko autofocusing and seismic inte (1), A7–A11.

Meles, G.A., C.A. da Costa Filho and A. Curtis, 2017, Synthe
from multiply-scattered data: 79th Annual International M
tists and Engineers, Expanded Abstracts, Tu P4 11.

Meles, G.A., K. Wapenaar, and J. Thorbecke, 2018, Virtual p
tuming: Geophysical Journal International, (1), 508–519.

Meles, G.A., L. Zhang, J. Thorbecke, K. Wapenaar and E. Slob
plane-wave responses: Geophysical Prospecting, 1834–1846.

Mildner, C., F. Broggini, K. de Vos and J.O.A. Robertsson,
trum Estimation Using Marchenko Focusing Functions: 79th
Expanded Abstracts, We B2 01.

Mildner C., F. Broggini, K de Vos, and J.O.A. Robertsson, 2
using Marchenko focusing functions: Geophysics, (6), Q73–Q83.

Pereira, R., Ramzy, M., Griscenco, P., Huard, B., Huang, H.,
multiple attenuation for OBN data with overburden/target
Meeting, Society of Exploration Geophysicists, Expanded A

Qu, S. and Verschuur, D.J. 2020, Simultaneous joint migrati
version of time-lapse seismic data sets: Geophysical Prosp, p. 1167–1188.

Ravasi, M., I Vasconcelos, A. Kritski, A. Curtis, C.A. da C
oriented Marchenko imaging of a North Sea field: Geophysica (1), 99–104.

Ravasi, M., 2017, Rayleigh-Marchenko redatuming for targe
physics, (6), S439–S452.

Ravasi, M., and I. Vasconcelos, 2020, PyLops - A linear-oper
optimization: SoftwareX, 100361.

Rietveld, W., G. Berkhout, and K. Wapenaar, C., 1992, Optim
reservoirs: Geophysics, (10), 1334–1345.

Singh, S., R. Snieder, J. Behura, J. van der Neut, K. Wapenaa
Imaging with primaries, internal multiples, and free-surf (5), S165–S174.

Singh, S., J. van der Neut, K. Wapenaar and R. Snieder, 2016,
receivers and virtual sources in the subsurface: 86th Ann
Abstracts, p. 5166–5171.

Singh, S., R. Snieder, J. van der Neut, J. Thorbecke, E. Slob
free-surface multiples in Marchenko imaging: Geophysics, (1), R19–R30.

Slob, E., K. Wapenaar, F. Broggini and R. Snieder, 2014, Seis
with Marchenko-type equations: Geophysics, (2), S63–S76.

Slob, E., 2016, Green's function retrieval and Marchenko i
Physical Review Letters, (16), 164301.

Sripanich, Y., Vasconcelos, I., and Wapenaar, K., 2019, Velo
and depth-imaging domains for media with mild lateral hete (5), Q57–Q72

Staring, M., J. van der Neut and K. Wapenaar, 2016, An inter
redatuming including free-surface multiples: 86th Annual
stracts p. 5172–5176.

Staring, M., R. Pereira, H. Douma, J. van der Neut, and K. Wap
method for source-receiver Marchenko redatuming on feld d
SEG, Expanded Abstracts, p. 4808–4812.

Staring, M., R. Pereira, H. Douma, J. van der Neut, and K. Wap
redatuming on feld data using an adaptive double-focusing (6), S570–S590.

Thomsen, H., 2016, Investigating the robustness of Green's
and Seismic Interferometry: MSc Thesis, ETH Zürich.

Thorbecke, J. and D. Draganov, 2011, Finite-diference mode
Geophysics (6), H1–H18.

Thorbecke, J., J. van der Neut and K. Wapenaar, 2013, Green
equations: A sensitivity analysis: 83th Annual Internat
SPMI 6.3.

Thorbecke, J., E. Slob, J. Brackenhof, J. van der Neut, and K
Marchenko method: Geophysics, (6), WB29–WB45.

Thorbecke, J., and J. Brackenhof, 2020, OpenSource code for
https://github.com/JanThorbecke/OpenSource, doi 10.528

Thorbecke, J. and L. Zhang and K. Wapenaar and E. Slob, 2021
multiple elimination algorithm: Geophysics, (2), F9–F23.

van IJsseldijk, J., J. van der Neut, J. Thorbecke, and K. Wap
traveltime changes in a reservoir using primaries and inte
zone isolation: Geophysics, accepted, 2023

van IJsseldijk, J., J. Brackenhof, J. Thorbecke, and K. Wape
Marchenko method on the Troll feld: under review for Geophy

Van der Neut, J., J. Thorbecke, K. Wapenaar and E. Slob, 201
Marchenko equation: 77th Annual International Meeting, EA

Van der Neut, J., I. Vasconcelos and K. Wapenaar, 2015b, On
substitution of the coupled Marchenko equations: Geophys (2), 792–
813.

Van der Neut, J., K. Wapenaar, J. Thorbecke, E. Slob and I V
adaptive Marchenko imaging: The Leading Edge, Vol. 818–822.

Van der Neut, J., and K. Wapenaar, 2016, Adaptive overburden
Marchenko equations: Geophysics, (5), T265–T284.

van der Neut, J., Johnson, J.L., van Wijk, K., Singh, S., Slob
equation for acoustic inverse source problems: J. Acoust.

Verschuur, E., A. Berkhout, and K. Wapenaar, 1992, Adaptiv
Geophysics, (9), 1166–1177.

Wapenaar, K., F. Broggini and R. Snieder, 2012, Creating a vi
data: heuristic derivation and stationary-phase analysis
(2), p. 1020–1024.

Wapenaar, K., F. Broggini, E. Slob and R. Snieder, 2013, Th
inverse scattering, data-driven focusing, Green's functi
Review Letters, Vol. 110 (8), 084301.

Wapenaar, K., 2014, Single-sided Marchenko focusing of comp
E, (6), 063202.

Wapenaar, K., J. Thorbecke, J. van der Neut, F. Broggini, E. S
retrieval from refection data, in absence of a receiver at
the Acoustical Society of America, (5), 2847–2861.

Wapenaar, K., J. Thorbecke, J. van der Neut, F. Broggini, E.
imaging: Geophysics, (3), WA39–WA57.

Wapenaar, K., J. Thorbecke, and J. van der Neut, 2016a, A sin
representation for holographic imaging, inverse scatteri
Green's function retrieval: Geophysical Journal Internat, p. 531–535.

Wapenaar, K., J. Thorbecke, J. van der Neut, E. Slob and R. S
responses, Part II: Data-driven single-sided (6), 1430–1451: Ge

Wapenaar, K., and van IJsseldijk, J., 2020, Discrete represe
sampled data: Geophysics, (2), A1–A5.

Wapenaar, K., Brackenhof, J., Dukalski, M., Meles, G., Rein
J., van der Neut, J., and Zhang, L., 2021, Marchenko redatu
and their mutual relations: Geophysics, Vol. (5), WC117–WC140.

Zhang, L., and M. Staring, 2018, Marchenko scheme based int
acoustic wavefeld: Journal of Applied Geophysics, (9), 429–433.

Zhang, L., and E. Slob, 2019, Free-surface and internal mult
subtraction: Geophysics, (1), A7–A11.

Zhang, L., J. Thorbecke, K. Wapenaar, and E. Slob, 2019, Tran
retrieval in data domain and consequences on imaging: Geo (4), Q27–Q36.

Zhang, L., and E. Slob, 2020a, A feld data example of Marchen
(2), S65–S70.

Zhang, L., and E. Slob, 2020b, A fast algorithm for multiple
in primary refections: Geophysical Journal International (1), 371–377.

Zhang, L., and E. Slob, 2020c, Marchenko multiple eliminat
Journal International, (2), 1138–1144.